Monthly Notices of the ROYAL ASTRONOMICAL SOCIETY
MNRAS **445,** 2–28 (2014) doi:10.1093/mnras/stu1681

The clustering of Galaxies in the SDSS-III Baryon Oscillation Spectroscopic Survey: potential systematics in fitting of baryon acoustic feature

Mariana Vargas-Magaña,[1⋆] Shirley Ho,[1] Xiaoying Xu,[1] Ariel G. Sánchez,[2] Ross O'Connell,[1] Daniel J. Eisenstein,[3] Antonio J. Cuesta,[4] Will J. Percival,[5] Ashley J. Ross,[5] Eric Aubourg,[6] Joel R. Brownstein,[7] Stéphanie Escoffier,[8] David Kirkby,[9] Marc Manera,[5,10] Donald P. Schneider,[11,12] Jeremy L. Tinker[13] and Benjamin A. Weaver[13]

[1]*Department of Physics, Carnegie Mellon University, 5000 Forbes Avenue, Pittsburgh, PA 15213, USA*
[2]*Max-Planck-Institut für extraterrestrische Physik, Postfach 1312, Giessenbachstr., D-85748 Garching, Germany*
[3]*Harvard–Smithsonian Center for Astrophysics, 60 Garden St, Cambridge, MA 02138, USA*
[4]*Institut de Ciències del Cosmos, Universitat de Barcelona, IEEC-UB, Martí Franquès 1, E-08028 Barcelona, Spain*
[5]*Institute of Cosmology & Gravitation, Dennis Sciama Building, University of Portsmouth, Portsmouth, PO1 3FX, UK*
[6]*APC, Astroparticule et Cosmologie, Université Paris Diderot, CNRS/IN2P3, CEA/Irfu, Observatoire de Paris, Sorbonne Paris Cité, 10, rue Alice Domon & Léonie Duquet, F-75205 Paris Cedex 13, France*
[7]*Department of Physics and Astronomy, University of Utah, 115 S 1400 E, Salt Lake City, UT 84112, USA*
[8]*CPPM, Aix-Marseille Université, CNRS/IN2P3, F-13288 Marseille, France*
[9]*Department of Physics and Astronomy, UC Irvine, 4129 Frederick Reines Hall, Irvine, CA 92697, USA*
[10]*Department of Physics & Astronomy, University College London,Gower Street, London WC1E 6BT, UK*
[11]*Department of Astronomy and Astrophysics, The Pennsylvania State University, University Park, PA 16802, USA*
[12]*Institute for Gravitation and the Cosmos, The Pennsylvania State University, University Park, PA 16802, USA*
[13]*Center for Cosmology and Particle Physics, New York University, New York, NY 10003, USA*

Accepted 2014 August 15. Received 2014 August 11; in original form 2013 December 18

ABSTRACT

Extraction of the Baryon Acoustic Oscillations (BAO) to per cent level accuracy is challenging and demands an understanding of many potential systematics to an accuracy well below 1 per cent, in order to ensure that they do not combine significantly when compared to statistical error of the BAO measurement. Baryon Oscillation Spectroscopic Survey (BOSS) Data Release 11 (DR11) reaches a distance measurement with ∼1 per cent statistical error and this prompts an extensive search for all possible sub-per cent level systematic errors which could previously be safely ignored. In this paper, we analyse the potential systematics in BAO fitting methodology using mocks and data from BOSS DR10 and DR11. We demonstrate the robustness of the fiducial multipole fitting methodology to be at 0.1–0.2 per cent level with a wide range of tests in mock galaxy catalogues pre- and post-reconstruction. We also find the DR10 and DR11 data from BOSS to be robust against changes in methodology at a similar level. This systematic error budget is incorporated into the BOSS DR10 and DR11 BAO measurements. Of the wide range of changes we have investigated, we find that when fitting post-reconstructed data or mocks, the only change which has an effect >0.1 per cent on the best-fitting values of distance measurements is varying the order of the polynomials to describe the broad-band terms (∼0.2 per cent). Finally, we compare an alternative methodology denoted as Clustering Wedges with Multipoles, and find that it is consistent with the standard approach.

Key words: large-scale structure of Universe.

1 INTRODUCTION

The Baryon Acoustic Oscillations (BAO) method has proven to be a powerful geometrical probe of the expansion history of the

⋆E-mail: mmagana@andrew.cmu.edu

Universe. The BAO provide a characteristic scale that can be used as a standard ruler. This is done by measuring its apparent size at a given redshift and comparing it with the physical size we know from first principles. Measurement of this standard ruler at different redshifts enables us to map the expansion history of the Universe (Eisenstein & Hu 1998; Meiksin, White & Peacock 1999; Eisenstein, Seo & White 2007).

Furthermore, measuring the BAO feature along the line of sight (LOS) and perpendicular to the LOS independently constrains the Hubble parameter $H(z)$ and the angular diameter distance $D_{\rm A}(z)$ at redshift z. Because of the low signal-to-noise ratio of the first large-scale surveys, most of the previous studies have focused on the spherically averaged analysis yielding measurements of the spherically averaged distance $D_{\rm V}(z) = ((1+z)^2 D_{\rm A}(z)^2 (cz/H(z))^{1/3}$, which has a strong degeneracy between $D_{\rm A}(z)$ and $H(z)$. Two-dimensional analysis breaks the degeneracy between $D_{\rm A}(z)$ and $H(z)$ as it measures the clustering in different directions (i.e. along the LOS and perpendicular to the LOS; Alcock & Paczynski 1979).

Early work on anisotropic clustering was performed with Sloan Digital Sky Survey II (SDSS-II) data. However, given the relatively low redshift of this sample, the constraints were similar to those from isotropic analysis, as at redshift $z \to 0$ distances are degenerate. Different methodologies for fitting BAO have been explored over the last few years. For example, Okumura et al. (2008) proposed fitting the radial and transverse correlation functions, and Padmanabhan & White (2009) proposed fitting the multipoles directly. More recently, Kazin, Sanchez & Blanton (2012) suggested splitting the full correlation function based on the angle of the pair to the LOS, resulting in a correlation function in each of two angular Clustering Wedges.

Based on the multipole methodology, Xu et al. (2012) studied the fitting procedure focusing on monopole and isotropic shifts. In Xu et al. (2013), this methodology was extended to the anisotropic clustering, including the effect of reconstruction on the anisotropic BAO signal as well as the application to SDSS-Data Release 7 (DR7; Abazajian et al. 2009) for cosmological constraints. With subsequent surveys such as SDSS-III Baryon Oscillation Spectroscopic Survey (BOSS; Dawson et al. 2012), for Data Release 9 (DR9; Ahn et al. 2013) analysis (Anderson et al. 2013), two different fitting methods have been applied (Kazin et al. 2012, 2013; Xu et al. 2013), producing consistent cosmological constraints on $D_{\rm A}(z)$ and $H(z)$.

Since the survey volume and the precision of the BAO measurement have increased, we extend previous studies by Xu et al. (2013) on multipole fitting. In particular, BOSS has doubled its survey volume from DR9 to Data Release 11 (DR11, to be publicly released with the final BOSS data set), requiring much higher precision and understanding of the systematic error as the statistical error shrinks. In particular, we analyse mock galaxy catalogues and data from BOSS Data Release 10 (DR10; Ahn et al. 2013) and DR11 and determine the effects of various choices in the fitting methodology on the final fitting result. We can then determine the systematic error budget from fitting methodologies included in the BOSS DR10 and DR11 BAO measurements in Anderson et al. (2014).

The layout of this paper is as follows. We introduce the anisotropic analysis techniques in Section 2. In Section 3, we describe the methodology used in the correlation function analysis, the covariance matrix estimation, the simulations, and the reconstruction procedure. In Section 4, we present the fiducial fitting procedure, and in Section 5, we describe the systematic tests performed on the fitting of the BAO anisotropic clustering signal. In Section 6, we present the results of our systematic tests using BOSS DR10 and DR11, CMASS mock galaxy catalogues. In Section 7, we compare the fitting results with results using other methodologies. In Section 8, we explore the consequences of systematics in fitting to the BOSS DR11 CMASS data before and after the application of reconstruction. Finally, we conclude and discuss our results in Section 9.

2 ANISOTROPIC CLUSTERING METHODS

2.1 Parametrization

Angularly averaged clustering analysis assumes that the clustering is isotropic and the BAO feature is shifted in an isotropic manner if we consider an incorrect cosmology. Any deviation from the true cosmology is parametrized by an isotropic shift α:

$$\alpha = \frac{(D_{\rm V}/r_{\rm s})}{(D_{\rm V}/r_{\rm s})_{\rm fid}}, \tag{1}$$

where the spherically averaged distance $D_{\rm V}$ is quoted relative to the sound horizon $r_{\rm s}$ at the drag epoch, and the suffix fid denotes the value at the fiducial cosmology. The angularly averaged analysis, extensively used in galaxy-clustering analyses, has provided important constraints in $D_{\rm V}$. However, as the clustering of galaxies is not isotropic, to optimize the extraction of information from BAO we must perform an anisotropic analysis. There are two sources of anisotropies: Redshift Space Distortions (RSD) and the anisotropies generated from assuming an incorrect cosmology.

The anisotropies arising from RSD can be separated by scale. At small scales, peculiar velocities generate the Finger-of-God (FoG) effect; at large scales, the coherent flows towards overdense regions generate the Kaiser Effect (Kaiser 1987). Both cases uniquely affect the LOS separations generating a smooth change with scale. The second source of anisotropy arises from assuming an incorrect cosmology via the Alcock–Paczynski test (AP). As $D_{\rm A}(z)$ and $H(z)$ depend differently on cosmology, computing incorrect separations generate artificial anisotropies in the clustering along the LOS and in perpendicular directions (Xu et al. 2013).

To distinguish anisotropy due to RSD from the AP effect due to a wrongly assumed cosmological model, we consider simple RSD models. We present in the fitting model section the details of the model for RSD. Even if simple models are not sufficiently accurate to model the RSD, any residual from inadequate matching with the models and broad-band shape data could be compensated by additional marginalization terms.

For analysing the anisotropic BAO signal, we need a model with a parametrization of the anisotropic signal. There are in the literature different ways of parametrizing the anisotropy in the BAO signal. In Xu et al. (2013) and Anderson et al. (2013), the anisotropic signal is parametrized by α for the isotropic dilation (equation 1) and ϵ for the anisotropic warping between true and fiducial cosmology,

$$\epsilon = \left[\frac{H^{\rm fid}(z) D_{\rm A}^{\rm fid}(z)}{H(z) D_{\rm A}(z)}\right]^{1/3} - 1, \tag{2}$$

where the suffix fid denotes the value of $D_{\rm A}(z)$, $H(z)$ and $r_{\rm s}$ at the fiducial cosmology. Since we include in the model the anisotropy produced by RSD, ϵ parametrizes the amount of AP anisotropy.

An alternative parametrization considers the shift parallel to the LOS ($\alpha_{||}$) and the shift perpendicular to the LOS ($\alpha_{\perp}$),

$$\alpha_{\perp} = \frac{D_{\rm A}(z) r_{\rm s}^{\rm fid}}{D_{\rm A}^{\rm fid}(z) r_{\rm s}}$$
$$\alpha_{||} = \frac{H(z)^{\rm fid} r_{\rm s}^{\rm fid}}{H(z) r_{\rm s}}. \quad (3)$$

2.2 Clustering estimators

Measuring both $D_{\rm A}(z)$ and $H(z)$ requires an estimator of the 2D correlation function $\xi(s, \mu)$, where s is the separation between two galaxies and μ the cosine of the angle between s and the LOS. Working with the full 2D correlation function is not practical in the case of galaxy-clustering, as we estimate our covariance matrix directly from the sample covariance of mock catalogues. To calculate the covariance matrix for a full 2D correlation function requires a much larger number of mock catalogues. We therefore compress our 2D correlation function into a small number of angular moments and use these for our analysis.

In particular, we describe the following two clustering estimators: Multipoles (Xu et al. 2013) and Clustering Wedges (Kazin et al. 2013). As Kazin et al. (2013) has discussed the systematics of fitting using Clustering Wedges, this paper will concentrate on the Multipoles technique (Xu et al. 2013) but will include comparisons with the Clustering Wedges method.

2.2.1 *Multipoles*

The formalism for the 2D correlation function in terms of the Multipole analysis is detailed in Xu et al. (2013) and Anderson et al. (2013). We briefly summarize the methodology as a reminder to the readers.

We start with the Legendre moments of the 2D correlation function

$$\xi_l(r) = \frac{2l+1}{2} \int_{-1}^{+1} {\rm d}\mu \xi(r, \mu) L_{\ell}(\mu), \quad (4)$$

where $L_{\ell}(\mu)$ is the ℓth Legendre polynomial.

For the multipole analysis, we focus only on the monopole and quadrupole.[1] We refer the readers to Anderson et al. (2013) for more details.

2.2.2 *Clustering Wedges*

We briefly review the alternate clustering estimator: Clustering Wedges (Kazin et al. 2012):

$$\xi_{\Delta_\mu}(r) = \frac{1}{\Delta\mu} \int_{\mu_{\rm min}}^{\mu_{\rm min}+\Delta\mu} {\rm d}\mu \xi(r, \mu). \quad (5)$$

In our analysis of the comparison between the Clustering Wedges and the Multipoles, we choose $\Delta\mu = 0.5$ such that we have a basis composed of a 'radial' component $\xi_{||}(s) \equiv \xi(s, \mu > 0.5)$, and a 'transverse' component $\xi_{\perp}(s) \equiv \xi(s, \mu < 0.5)$. A full description of the method and systematics tests can be found in Kazin et al. (2013).

[1] The multipole analysis focuses on the monopole and quadrupole; even if the higher order multipoles also provide information, their influence is quite negligible.

3 ANALYSIS

3.1 Fiducial cosmology

Throughout we assume a fiducial Λ cold dark matter (ΛCDM) cosmology with $\Omega_{\rm M} = 0.274$, $\Omega_{\rm b} = 0.0457$, $h = 0.7$ and $n_{\rm s} = 0.95$, matching that used in Anderson et al. (2012, 2013). The angular diameter distance to $z = 0.57$ for our fiducial cosmology is $D_{\rm A}(0.57) = 1359.72$ Mpc, while the Hubble parameter is $H(0.57) = 93.56$ kms^{-1}Mpc^{-1}. The sound horizon for this cosmology is $r_{\rm s} = 153.19$ Mpc, where we adopt the conventions in Eisenstein & Hu (1998).

3.2 Measuring correlation function

In anisotropic clustering analysis, we compute the 2D correlation function decomposing the separation r between two galaxies into the parallel $r_{||}$ and perpendicular $r_{\perp}$ direction to the LOS,

$$r^2 = r_{||}^2 + r_{\perp}^2. \quad (6)$$

We denote the angle between the galaxy pair separation and the LOS direction as θ and define μ as

$$\mu = \cos\theta = \frac{r_{||}}{r}. \quad (7)$$

The 2D correlation function $\xi(r, \mu)$ (for the pre-reconstructed case) is computed using Landy–Szalay (Landy & Szalay 1993) estimator:

$$\xi(r, \mu) = \frac{{\rm DD}(r, \mu) - 2 \times {\rm RD}(r, \mu) + {\rm RR}(r, \mu)}{{\rm RR}(r, \mu)}, \quad (8)$$

where ${\rm DD}(r, \mu)$, ${\rm RR}(r, \mu)$, and ${\rm RD}(r, \mu)$ are the number of pairs of galaxies which are separated by a radial separation r and angular separation μ from data–data samples, random–random and data–random samples, respectively. The correlation function is computed in bins of $\Delta r = 4.8\,h^{-1}$ Mpc and $\Delta\mu = 0.01$.

3.3 Data

We use data included in DR10 and DR11 of the SDSS (York et al. 2000). Together, SDSS I-II (Abazajian et al. 2009), and III (Eisenstein et al. 2011) used a drift-scanning mosaic CCD camera (Gunn et al. 1998) to image over one third of the sky (14 055 deg^2) in five photometric bandpasses (Fukugita et al. 1996; Smith et al. 2002; Doi et al. 2010) to a limiting magnitude of $r \simeq 22.5$ using the dedicated 2.5-m Sloan Telescope (Gunn et al. 2006) located at Apache Point Observatory in New Mexico. The imaging data were processed through a series of pipelines that perform astrometric calibration (Pier et al. 2003), photometric reduction (Lupton et al. 2001), and photometric calibration. All of the imaging data were re-processed as part of SDSS Data Release 8 (Aihara et al. 2011).

BOSS is designed to obtain spectra and redshifts for 1.35 million galaxies over an extragalactic footprint covering 10 000 deg^2. These galaxies are selected from the SDSS DR8 imaging and are being observed together with 200 000 quasars and approximately 100 000 ancillary targets. The targets are assigned to tiles of diameter 3° using a tiling algorithm that is adaptive to the density of targets on the sky (Blanton et al. 2003). Spectra are obtained using the double-armed BOSS spectrographs (Smee et al. 2013). Each observation is performed in a series of 900-s exposures, integrating until a minimum signal-to-noise ratio is achieved for the faint galaxy targets. This requirement ensures a homogeneous data set with a redshift completeness of more than 97 per cent over the full survey footprint. Redshifts are extracted from the spectra using

the methods described in Bolton et al. (2012). A summary of the survey design appears in Eisenstein et al. (2011), a full description is provided in Dawson et al. (2012).

We use the CMASS sample of galaxies DR10/DR11. The CMASS sample is designed to be approximately stellar mass limited above $z = 0.45$. The CMASS sample consists of 501 844 (DR10) and 690 826 (DR11) galaxies covering 6267 and 8498 deg^2. The redshift range is $0.43 < z < 0.70$, and the median redshift $z = 0.57$.

3.4 Simulations

In this paper, we use the SDSS III-BOSS PTHalos mock galaxy catalogues (Manera et al. 2013) exclusively to test the systematics of BAO fitting and to generate the sample covariance matrices. Inspired by the methodology in Scoccimarro & Sheth (2002), the mocks are based on Second Order Lagrangian Perturbation Theory (2LPT) for the density fields. The PTHalos mock galaxy catalogues were generated at $z = 0.55$ in boxes of size $L = 2400\ h^{-1}$ Mpc using 1280^3 dark matter particles. The haloes were found using a friends-of-friends algorithm with an appropriate linking length and masses calibrated with N-body simulations. For populating the haloes with galaxies, the Halo Occupation Distribution prescription was used, previously calibrated to match the observed clustering at small scales [30,80] h^{-1} Mpc following White et al. (2011). The angular and radial masks from DR10/DR11 were applied to subsample the galaxies from their original boxes. The mocks include RSD, but do not include other systematic corrections such as stellar correlation or evolution with redshift. A full description of the PTHalos galaxy mocks can be found in Manera et al. (2013).

3.5 Covariance

The sample covariance is computed with the 600 mocks as follows:

$$C_{i,j} = \frac{1}{n_s - 1} \Sigma_{m=1}^{n_s} \left(\bar{\xi}_{[2s]_i} - \xi^m_{[2s]_i}\right) \left(\bar{\xi}_{[2s]_j} - \xi^m_{[2s]_j}\right), \quad (9)$$

where, $\xi_{2s} = [\xi_0, \xi_2]$.

Unless otherwise noted, we rescale the inverse covariance matrix following (Hartlap, Simon & Schneider 2007):

$$\mathbf{C}^{-1} = \mathbf{C}_s^{-1} \frac{n_s - n_b - 2}{n_s - 1}, \quad (10)$$

where n_s is the number of simulations and n_b is the number of bins of parameters we are estimating.[2] This correction arises from the fact that the inverse of the sample covariance matrix computed from a finite number of mocks is a biased estimator of the inverse covariance matrix. A recent analysis of the covariance corrections extends this discussion and provides a prescription to propagate the correction to the inferred parameters (Percival et al. 2014). Section 5.7 in this paper is devoted to summarizing the corrections applied to the covariance and the uncertainties inferred along with their consequences on the final anisotropic fits.

3.6 Reconstruction

We include in this analysis the effect of reconstruction of the density field in the correlation function fitting procedure. The reconstruction algorithm has proved to be effective in correcting the effects of non-linear evolution, thus increasing the statistical sensitivity of measurements (Noh, White & Padmanabhan 2009; Padmanabhan et al. 2012)

The main idea of reconstruction is to use information encoded in the density field to estimate the displacement field, use this displacement field to reverse the peculiar motion of the particles, and partially remove the effect of non-linear growth of structure. This is possible because the non-linear evolution of the density field is dominated by the infall velocities and these bulk flows are approached by the same structures observed in the density field. The algorithm used here is described in Padmanabhan et al. (2012). The Lagrangian displacement field is calculated to first order using the Zeldovich approximation applied to the Gaussian-smoothed galaxy overdensity field. The displacement field is estimated using the finite difference method in configuration space.

The effects of reconstruction on the correlation functions are the sharpening of the peak in the monopole and a decrease in amplitude of the quadrupole. At large scales, the quadrupole approaches zero. If reconstruction were perfect, the quadrupole would go to zero and the isotropy in the two-point correlation would be restored for a correct cosmology.

4 FITTING METHODOLOGY

In this section, we will describe the various components of our anisotropic clustering fitting methodology in detail. In particular, we describe the model of the correlation function and various model parameter selection and priors included in the fitting procedure.

4.1 Model for the correlation function

In order to extract cosmological information from the BOSS data, a careful modelling of the correlation function is required. We start with a non-linear power spectrum template in 2D:

$$P(k, \mu) = (1 + \beta\mu^2)^2 F(k, \mu, \Sigma_s) P_{NL}(k, \mu), \quad (11)$$

where the term $(1 + \beta\mu^2)$ corresponds to the Kaiser model (Kaiser 1987) for large-scale RSD, which produces anisotropy in an otherwise isotropic 2D correlation function. $F(k, \mu, \Sigma_s)$ is the streaming model for the FoG effect(Peacock & Dodds 1994) given by

$$F(k, \mu, \Sigma_s) = \frac{1}{(1 + k^2\mu^2\Sigma_s^2)}. \quad (12)$$

where Σ_s is the streaming scale, which we set to $1.4\,h^{-1}$ Mpc, and $P_{NL}(k)$ is the non-linear power spectrum.

In this work, we consider two templates for the non-linear power spectrum $P_{NL}(k)$: the 'De-Wiggled' power spectrum P_{dw} (Anderson et al. 2012, 2013; Xu et al. 2012, 2013) and a template *inspired* by Renormalized Perturbation Theory (RPT), P_{pt}, also used in several galaxy-clustering analyses (Kazin et al. 2010, 2012; Anderson et al. 2013). We will describe these two templates in more detail in Sections 4.1.1 and 4.1.2.

We decompose the full 2D power spectrum into its Legendre moments:

$$P_\ell(k) = \frac{2\ell + 1}{2} \int_{-1}^{1} P(k, \mu) L_\ell(\mu) \mathrm{d}\mu, \quad (13)$$

which can then be transformed to configuration space using

$$\xi_\ell(r) = i^\ell \int \frac{k^3\, \mathrm{d}\ln(k)}{2\pi^2} P_l\, j_\ell(kr), \quad (14)$$

[2] For example, in power spectrum, this quantity would be the number of the bins in the power spectra.

where, $j_\ell(kr)$ is the ℓth spherical Bessel function and $L_\ell(\mu)$ is the ℓth Legendre polynomial.

4.1.1 De-Wiggled template

The De-Wiggled template is a non-linear power spectrum prescription widely used in clustering analysis (Blake et al. 2007; Anderson et al. 2012, 2013; Xu et al. 2012, 2013). This phenomenological prescription takes a linear power spectrum template to which we add the non-linear growth of structure. The De-Wiggled power spectrum is defined as

$$P_{\rm dw}(k,\mu) = [P_{\rm lin}(k) - P_{\rm nw}(k)] \times \exp\left[-(k^2\mu^2\Sigma_{||}^2 + k^2(1-\mu^2)\Sigma_{\perp}^2)/2\right] + P_{\rm nw}, \quad (15)$$

where $P_{\rm lin}(k)$ is the linear theory power spectrum and $P_{\rm nw}(k)$ is a power spectrum without the acoustic oscillations (Eisenstein & Hu 1998). $\Sigma_{||}$ and $\Sigma_{\perp}$ are the radial and transverse components of the standard Gaussian damping of BAO $\Sigma_{\rm NL}$, where

$$\Sigma_{\rm NL}^2 = (\Sigma_{||}^2 + \Sigma_{\perp}^2)/2, \quad (16)$$

and $\Sigma_{\rm NL}$ models the degradation of signal due to non-linear structure growth (Eisenstein et al. 2007).

4.1.2 RPT inspired template

Several BAO galaxy-clustering analyses (Beutler et al. 2011; Kazin et al. 2012; Sánchez et al. 2014) considered, instead of the De-Wiggled template, a template inspired by RPT. The main argument for this choice is that an RPT template provides an unbiased measurement of the dark energy equation of state (Crocce & Scoccimarro 2008; Sanchez, Baugh & Angulo 2008).

However, the template described here is only 'inspired by RPT', but its form is not the functional form one would obtain from RPT. The RPT-inspired template is given by Kazin et al. (2013):

$$P_{\rm pt}(k) = P_{\rm lin}(k)e^{-k^2\sigma_v^2} + A_{\rm MC}P_{\rm MC}(k), \quad (17)$$

where $P_{\rm MC}$ is given by

$$P_{\rm MC} = \frac{1}{4\pi^3}\int {\rm d}q|F(k-q,q)|^2 P_{\rm lin}(|k-q|)P_{\rm lin}(q). \quad (18)$$

$P_{\rm pt}(k)$ was used in Anderson et al. (2014). It was previously used by Kazin et al. (2013) in the analysis of the CMASS DR9 multipoles and Clustering Wedges and is described in detail in Sánchez et al. (2014). The parameter σ_v accounts for the damping of the BAO feature by non-linear evolution, while the parameter $A_{\rm MC}$ accounts for the induced coupling between Fourier modes.

We fit to the mocks mean with σ_v and $A_{\rm MC}$ as free parameters and use the value of the best-fits pre-reconstruction and post-reconstruction. In particular, σ_v is fixed to 4.85 h^{-1} Mpc and $A_{\rm MC}$ is fixed to 1.7 pre-reconstruction. For the post-reconstruction template, we expect a significantly sharpened peak, thus the value of σ_v is set to 1.9 h^{-1} Mpc; which corresponds to the linear power spectrum. The ideal scenario suggests that post-reconstruction $A_{\rm MC} = 0$, but Kazin et al. (2013) indicates that this choice induces a bias and the term $A_{\rm MC}$ is set to 0.05 post-reconstruction.

4.2 Overall fitting methodology

We now take moments of the model correlation function as described in equation (14) and synthesize the 2D correlation function by

$$\xi(r,\mu) = \sum_{\ell=0}^{\ell_{\rm max}} \xi_\ell(r)L_\ell(\mu). \quad (19)$$

In this work, we truncate this sum at $\ell_{\rm max} = 4$.

We now need to map the 2D correlation function to the data, i.e. mapping the observed $\xi(r,\mu)$ for each $(r,\mu)_{\rm fid}$ pair to their true $\xi(r,\mu)_{\rm true}$. This transformation can be compactly written by working in the transverse ($r_\perp$) and radial ($r_\parallel$) separations defined by equations (6) and (7). We have $r_\perp = \alpha_\perp r_{\perp,{\rm obs}}$ and $r_{||} = \alpha_{||}r_{||,{\rm obs}}$. We now compute $\xi_{\rm obs}(r,\mu)$ from the data and project it into multipole basis for comparison to the model $\xi^{\rm obs}_{0,2}(r)$.

Finally, we must include nuisance parameters to absorb the imperfect modelling of our broad-band model due to mismatches in cosmology, uncertain theoretical modelling, or potential smooth systematic effects. In particular, the multipole fits are performed simultaneously over the monopole and quadrupole for 10 total parameters with 4 non-linear parameters ($\log(B_0^2), \beta, \alpha, \epsilon$) and 6 linear nuisance parameters ($A_{l,i}(r)$):

$$\xi_0(r) = B_0^2\xi_0^t(r,\alpha,\epsilon) + A_0(r)$$
$$\xi_2(r) = \xi_2^t(r,\alpha,\epsilon) + A_2(r). \quad (20)$$

The monopole $\xi_0^t(r)$ and quadrupole $\xi_2^t(r)$ templates are estimated in a fiducial cosmology following the model described in Section 4.1. The α parameter measures the position of the peak of the data relative to the model, and ϵ measures the degree to which the peak is anisotropic.

The nuisance terms A_l are included for marginalizing the broad-band effects :

$$A_l(r) = \frac{a_{l,1}}{r^2} + \frac{a_{l,2}}{r} + a_{l,3}; l = 0, 2. \quad (21)$$

The quantity B_0^2 is a bias-like term that adjusts the amplitude of the monopole template ξ_0^t. Before fitting, B_0 is inferred from the multiplicative offset between the model and the measured correlation function at $r = 50\,h^{-1}Mpc$. This offset is then used to normalize the monopole and quadrupole. This procedure ensures $B_0 \sim 1$ and β is allowed to vary as it effectively allows the amplitude of the quadruple to change. Fits are performed over $\log(B_0^2)$ using a Gaussian prior with standard deviation of 0.4 to prevent unphysical negative values.

The best-fitting values of α and ϵ are obtained from minimizing the χ^2 given by

$$\chi^2(p) = (m(p) - \boldsymbol{d})^{\rm T}\mathbf{C}^{-1}(m(p) - \boldsymbol{d}), \quad (22)$$

where $m(p)$ corresponds to the model vector for the ξ_0 and ξ_2 given the parameters p, $\boldsymbol{d}$ is the data respective vector and $\mathbf{C}$ is the covariance described in the Section 3.5.

4.3 Fiducial fitting methodology model parameters

Since we will be investigating the effects of changing each of the model parameters, assumptions, and prior choices in our fitting methodology, we list them here explicitly for the convenience of the reader.

In our fiducial fitting methodology, we use the following model.

(i) De-Wiggled template.

(ii) α–ϵ parametrization.
(iii) 8 h^{-1} Mpc binning. The binning scheme of 8 h^{-1} Mpc binning differs from the 4 h^{-1} Mpc binning of previous analyses in Xu et al. (2012, 2013). This choice is based on the recent work on covariance matrix systematics performed by Percival et al. (2014).
(iv) Fitting range, [46, 200] h^{-1} Mpc, corresponding to 20 bins for each multipole.
(v) Nuisance terms: three-term $A_l(r)$.

We apply the following priors on various model parameters and further discuss the motivation for each prior in Section 5.4.

(i) Prior on $\log(B_0^2)$ centred on 1, with standard deviation of 0.4 to prevent B_0 wandering too far from 1.
(ii) Prior on β centred at 0.4, with a standard deviation of 0.2. This prior serves to limit the model, avoiding unphysical values of β. The central value is set to zero after reconstruction as we expect reconstruction to remove large-scale RSD.[3]
(iii) Prior on $1 + \epsilon$ centred at zero, 15 per cent top hat prior (10 per cent Gaussian prior), which prevents ϵ from taking unrealistic values. The cosmological implications of this prior were also tested in Xu et al. (2013); they estimated that ϵ distribution is nearly Gaussian with standard deviation 0.026.

We also fix the following parameter values.

(i) Streaming scale from equation (12): $\Sigma_s = 1.4\,h^{-1}$ Mpc.
(ii) Non-linear damping before reconstruction: $\Sigma_\perp = 6\,h^{-1}$ Mpc and $\Sigma_{||} = 11\,h^{-1}$ Mpc.
(iii) Non-linear damping pre-reconstruction.: $\Sigma_\perp = \Sigma_{||} = 3\,h^{-1}$ Mpc. The $\Sigma_{\perp,||}$ values used in pre and post-reconstruction were all fit from the average of the mocks in DR9 and we do not expect them to change drastically for DR10/DR11.

4.4 Uncertainty estimation

To estimate the errors, we calculate the probability distribution $p(\alpha, \epsilon)$ in a grid (α, ϵ). For each grid point (α, ϵ), we fit the remaining parameters using the best fit from χ^2. Assuming the likelihood is Gaussian $p(\alpha, \epsilon) \propto \exp(-\chi(p)^2/2)$ and using the corresponding normalization:

$$p(\alpha) = \int p(\alpha, \epsilon)\mathrm{d}\epsilon$$
$$p(\epsilon) = \int p(\alpha, \epsilon)\mathrm{d}\alpha. \quad (23)$$

Under the hypothesis of Gaussian posteriors, we can take the widths of the distributions σ_α and σ_ϵ as the measurements of the errors, given by the following expressions:

$$\sigma_\alpha = \int p_\alpha(\alpha - \langle\alpha\rangle)^2\mathrm{d}\alpha$$
$$\sigma_\epsilon = \int p_\epsilon(\alpha - \langle\alpha\rangle)^2\mathrm{d}\epsilon, \quad (24)$$

where $\langle x\rangle$ is the mean of the distribution $p(x)$:

$$\langle x\rangle = \int p(x)\mathrm{x}\mathrm{d}\mathrm{x}. \quad (25)$$

[3] The central value of β in this analysis $\beta = f/b \sim \Omega_\mathrm{m}^{0.55}/b = 0.4$, where b is the galaxy bias. is chosen to be different from fiducial case of Anderson et al. (2013) which adopted a value of $\beta_c = 0.6$.

We calculate the covariance between α and ϵ:

$$C_{\alpha,\epsilon} = \iint p(\alpha, \epsilon)(\alpha - \langle\alpha\rangle)(\epsilon - \langle\epsilon\rangle)\mathrm{d}\alpha\mathrm{d}\epsilon, \quad (26)$$

and the correlation coefficient $\rho_{\alpha,\epsilon}$:

$$\rho_{\alpha,\epsilon} = \frac{C_{\alpha,\epsilon}}{\sigma_\alpha\sigma_\epsilon}. \quad (27)$$

The fiducial parameters for the error (σ) estimation are as follows.

(i) The ranges for the error estimation are: $\alpha = [0.7, 1.3]$ and $\epsilon = [-0.3, 0.3]$.
(ii) The spacing in grids are: $\Delta_\alpha = 0.6/121 \sim 0.005$ and $\Delta_\epsilon = 0.6/61 \sim 0.01$.
(iii) A Gaussian prior on $\log(\alpha)$ with a width 0.15 is applied in the likelihood surface to suppress unphysical downturns in the χ^2 distribution at small α. We have adopted a slightly different methodology in the calculation of the best-fitting parameter uncertainties than in Anderson et al. (2014); our approach is detailed in Section 6.

5 $\xi(r)$ SYSTEMATICS ON MULTIPOLES FITTING

Given our fiducial case, we explore the robustness of the fitting method to different choices in the methodology. The choices explored are in an order similar to that described in Section 4.3, with the addition of two items at the end of the list:

(i) Model Templates and Parametrization of Anisotropic Clustering (Section 5.1)
(ii) Fitting range and bin sizes (Section 5.2)
(iii) Nuisance Terms Model (Section 5.3)
(iv) Priors on various parameters: $\log(B_0^2)$, β, ϵ, α (Section 5.4)
(v) Streaming models (Section 5.5)
(vi) Non-linear damping model parameters (Section 5.6)
(vii) Covariance matrix corrections (Section 5.7)
(viii) Grid sizes in likelihood surfaces (Section 5.8).

In this section, we describe the tests performed, as well as the predicted behaviour in terms of variations of α, ϵ, and their respective errors.

5.1 Model templates and parametrization of anisotropic clustering

There are multiple ways to define a theoretical correlation function, especially when considering non-linear correlation function in redshift space for galaxies. In this paper, we consider two templates: the de-wiggled template defined in Section 4.1.1 and the RPT-inspired template defined in Section 4.1.2.

There are also multiple ways to parametrize anisotropic clustering. In this paper, we concentrate on the multipoles only, and even within the multipoles, we can have two parameterizations of the anisotropic clustering, one with α–ϵ, one with $\alpha_{||} - \alpha_\perp$, both described in Section 2.1.

5.2 Fitting range and bin size

The choice of fitting ranges can be influenced by two factors, one based on our confidence in our theoretical templates, and whether the broad-band polynomial terms can remove the effects of the uncertainty in our theoretical templates. In Anderson et al. (2013), an optimal range for fitting was found to be [50, 200] h^{-1} Mpc when we fit for anisotropic clustering signals, while for isotropic

clustering signals, the optimal range was [30, 200] h^{-1} Mpc. We test these two different scenarios in our analysis.

The choice of bin sizes must be tested given our signal has a width of $\approx 10\,h^{-1}$ Mpc. Bins that are too large can miss the peak entirely, while bins that are too small dilute the signal. Xu et al. (2012) tested the effect of various bin sizes on the isotropic clustering and no significant differences were found when they fit with either 4 or $7\,h^{-1}$ Mpc bin sizes.

Percival et al. (2014) also examined bin size choices in the isotropic correlation function and power spectrum. They tested different bin sizes and found that the optimal choice was achieved with an 8 h^{-1} Mpc bin. We used this as our fiducial binning as in Anderson et al. (2014). This testing seeks to verify the validity of the wider bin size. We compare the $8h^{-1}$ Mpc fiducial results with the $4\,h^{-1}$ Mpc bin size used in Xu et al. (2012, 2013).

5.3 Nuisance terms model

In order to remove broad-band effects that are difficult to model, the fiducial methodology adds second-order polynomials (denoted nuisance terms $A_\ell(r)$) to the theoretical monopole and quadrupole as described in equation (20). We test variations from this choice by varying the order of the polynomials used (Xu et al. 2012, 2013). In principle, given the same type of broad-band features, either from mis-modelling of non-linearities, or observational systematics, the polynomial order should not affect the fitting results. However, if we expect different types of observational systematics (such is the case of Lyman α forest for example), the order of polynomials may need to change.

5.4 Priors

Xu et al. (2013) have shown that variations in parameters B_0 and β affect mostly the shape of quadrupole, and do not influence the BAO position. The only parameters which can shift the BAO position are α and ϵ. However, the structures in the derivatives of α and ϵ are partially degenerate with other parameters (B_0, β), thus the roles of these priors are to limit the models from exploring these degeneracies.

We test the effect of each prior on the best-fitting values and errors. We compare the results against the extreme cases when we place no priors and when all priors are applied. In the following subsections, we comment on what we expect when each prior is used individually and the related degeneracies.

5.4.1 *Prior on* B_0

B_0 is a bias-like term that adjusts the amplitude of the model to fit the data. The prior on $\log(B_0^2)$ should not significantly affect α; it should, however, have some effect on ϵ, σ_α and σ_ϵ because ϵ and B_0 are slightly degenerate. The ϵ dependence arises in three places: the derivative of the monopole, the quadrupole, and its derivative. The quadrupole does not have a strong BAO feature, thus the dominant information when we marginalize the shape is produced by the derivative of the monopole. Fig. 3 of Xu et al. (2013), demonstrates that there is a clear degeneracy between ϵ and B_0 for this term.

In the case of σ_α, we expect this prior to provide tighter constraints for extreme α values. Without the prior the fitter is allowed to set the normalization B_0^2 of the monopole to any value that produces the smallest χ^2, including completely unphysical values or even negative ones. However, if we have the prior, then the normalization of the model will be limited to being close to the central value of the prior (1.0), which is a reasonable assumption (i.e. we are assuming that the model should resemble the data substantially). The prior penalizes values of B_0^2 that are substantially different from 1.0, so the minimum χ^2 occurs closer to $B_0^2 = 1$. This new minimum χ^2 will, by definition, be larger than the global minimum without the prior, so the χ^2 versus α curve will be deeper and hence σ_α should become smaller.

5.4.2 *Prior on* β

The β parameter modulates the amplitude of the quadrupole, but this parameter is degenerate with ϵ. Because of this degeneracy the prior on β should change the value of ϵ, especially if ϵ is large. Additionally, the β prior and the $\log(B_0)$ prior have similar effects. One suppresses extreme tails in α and the other suppresses tails in ϵ. Without any prior on β, the fitter could push ϵ to an extreme value with lower χ^2. Thus, by imposing a prior one effectively forces χ^2 to be larger at the tails, thus producing a smaller p and price a narrower likelihood surface, i.e. smaller σ_ϵ.

5.4.3 *Prior on* ϵ

The prior on ϵ is basically a top-hat prior, so it will limit all values of ϵ to be between -0.15 and 0.15. The prior is not exactly a top-hat; the edges are tapered with a Gaussian to make the likelihood surfaces more smooth. If ϵ is beyond this range before the prior is applied, then after the prior is applied, it will equal to ± 0.15. This restriction also decreases σ_ϵ in the cases where ϵ is poorly measured. Outside the tophat, χ^2 quickly approaches infinity.

5.4.4 *Prior on* α

The prior on α is *different* from those on the other parameters. This prior is *only* applied to the likelihood surface, so it does not actually affect the best-fitting values of α or ϵ. If the likelihood surface is highly irregular (non-Gaussian), it will tighten the constraints on the error on α (see fig. 6 of Xu et al. 2013).

5.5 Streaming models

We explored the effect of changing the streaming model $F(k, \mu, \Sigma_s)$ by testing three streaming models:

(i) $\frac{1}{(1+k^2\mu^2\Sigma_s^2)^2}$ (fiducial)
(ii) $\exp[\frac{1}{1+(k\mu\Sigma_s)^2}]$ (exp)
(iii) $\exp(-(k\mu\Sigma_s)^2/2)$ (Gaussian).

We choose the first model as our fiducial one. Additionally, we investigated the effects of changing the value of Σ_s. Variations in Σ_s would broaden the BAO peak in the monopole, while in the quadrupole the effects of Σ_s are partially degenerate with Σ_{NL}. Changes in Σ_s affects the crest–trough contrast and can even eliminate the trough when $\Sigma_s = 0$. Effects are stronger on small scales, since the FoG is much stronger at small scales. We tested the effect of using a larger Σ_s than the fiducial case, $\Sigma_s = 1.4 \rightarrow 3.0$ both pre- and post-reconstruction.

5.6 Non-linear damping model parameters

The $\Sigma_{\rm NL}$ parameter models the smearing of the BAO due to the non-linear structure growth as defined in equation (16). Varying the parameters $\Sigma_{||,\perp}$ changes the structure of the peaks and troughs and reduces the crest–trough contrast. Using isotropic values for $\Sigma_{||,\perp}$ eliminates the trough-feature at the BAO scale in the quadrupole. Thus, with large values of $\Sigma_{||,\perp}$ and also by adjusting the isotropic/anisotropic values, we can significantly change the results of the fitting.

In this paper, we test the effects of changing $\Sigma_{||}$ and $\Sigma_{\perp}$. We tested two cases: pre-reconstruction, where we changed anisotropic values, $\Sigma_{||} = 11$ Mpch^{-1} and $\Sigma_{\perp} = 6$ Mpch^{-1} to isotropic values, $\Sigma_{||} = \Sigma_{\perp} = 8$ Mpc h^{-1}, and post-reconstruction, where we changed the isotropic fiducial values, $\Sigma_{||} = \Sigma_{\perp} = 3$ Mpch^{-1} to anisotropic values $\Sigma_{||} = 4$ Mpch^{-1} and $\Sigma_{\perp} = 2$ Mpc h^{-1}.

5.7 Covariance matrix corrections

In this work, we adopt the covariance matrix correction as suggested in Percival et al. (2014) as an additional systematic in the fitting procedure. This approach includes the corrections introduced due to the specificity of BOSS mocks. We begin by describing the two different kinds of corrections applied.

5.7.1 *Covariance corrections and their propagation*

Percival et al. (2014) extended previous work (Taylor, Joachimi & Kitching 2013; Dodelson & Schneider 2013) on the contribution of covariance matrix errors to the parameter errors. Percival et al. (2014) suggested the following corrections in particular.

To correct the bias caused by the limited number of mocks, a correction factor must be applied to the inverse covariance matrix

$$\Psi^t = (1 - D)\mathbf{C}^{-1}, \tag{28}$$

where

$$D = \frac{n_{\rm b} + 1}{n_{\rm s} - 1}. \tag{29}$$

This factor accounts for the skewness of the inverse Wishart distribution that describes $L(\Psi|\Psi_t)$.

Percival et al. (2014) also provided the correction needed to propagate errors in the covariance matrix through to parameter errors. Given a measurement of the sample variance (from mocks), we need to multiply the sample variance by m_1, given by

$$m_1 = \frac{1 + B(n_{\rm b} - n_p)}{1 + A + B(n_p + 1)}, \tag{30}$$

where

$$\begin{aligned} A &= \frac{2}{(n_{\rm s} - n_{\rm b} - 1)(n_{\rm s} - n_{\rm b} - 4)} \\ B &= \frac{(n_{\rm s} - n_{\rm b} - 2)}{(n_{\rm s} - n_{\rm b} - 1)(n_{\rm s} - n_{\rm b} - 4)}, \end{aligned} \tag{31}$$

where $n_{\rm b}$ is the number of data measurements such as band powers in $P(k)$, $n_{\rm s}$ is the number of simulations used to calculate the sample variance and n_p is the number of parameters p to be fitted. This correction produces an unbiased estimate of the full variance of parameter p.

5.7.2 *Covariance corrections in SDSS-III/BOSS mocks*

The mock galaxy catalogues used in Anderson et al. (2013) were generated by sampling from a single density field, although we separate them into the Northern Galactic Cap (NGC) and Southern Galactic Cap (SGC) to match the BOSS observations. There is therefore an overlap between the mocks in North and South as they are drawn from the same box. This overlapped region was relatively small for DR9, but for DR10 (DR11), there is 75 (100) per cent overlap in the area covered by the SGC.

To construct two sets of independent mocks, Anderson et al. (2013) used a set of NGC mocks different from the SGC mocks. However, there is still a correlation between them. The sample covariance matrix is defined as follows:

$$\begin{aligned} C_{i,j} = \frac{1}{2}\Bigg[&\frac{1}{299}\sum_{m<300}(\xi_i - \bar{\xi})(\xi_j - \bar{\xi}) \\ &+ \frac{1}{299}\sum_{m>300}(\xi_i - \bar{\xi})(\xi_j - \bar{\xi})\Bigg]. \end{aligned} \tag{32}$$

A correlation coefficient is defined as the inverse of the effective volume:

$$r = \frac{2V_{\rm overlap}}{V_{\rm NGC} + V_{\rm SGC}}, \tag{33}$$

producing a value of $r = 0.33$ for DR10 and $r = 0.49$ for DR11. We propagate this correlation coefficient to covariance errors by rescaling the terms A, B and D, by a factor $(1 + r^2)/2$.

For clarity in our analysis, we single out the covariance corrections, as they only change the covariance matrix we applied in the fitting. We perform the fitting robustness tests without considering any corrections of the covariance matrix for the overlapping regions. To measure the error derived from not considering this correction on the tests performed, we applied the corrections for the overlapping regions to our fiducial methodology and compared with the fiducial case without corrections. The measured error should be included in the total error budget.

In the fiducial methodology, a correction has been applied to achieve unbiased estimates of the covariance matrix. We retain this correction so that the methodology is closest to Xu et al. (2013), unless otherwise specified.

5.8 Grid sizes in likelihood surfaces

To estimate errors, we calculate likelihood surfaces on a grid (Section 4). Exploring the grids is time consuming as the investigations we performed require fitting a large number of mock galaxy correction functions. Thus, there is a trade-off between the width of the grids and the number of tests to be performed for this work.

In the ideal case, as the error on α is expected to be $\sim$1 per cent in current analysis, the optimal width for α grid would be $\Delta_\alpha = 0.001$, producing 10 grid points sampled within 1 per cent. However, this binning requires a huge amount of time and using this grid would restrict the number of tests performed. Thus, we tested the effect of using smaller grid widths such as 0.0025 and 0.005. Smaller grids should work if the likelihood surface is smooth. The wider grid, 0.005, may be too coarse for α, but for ϵ, where the error is closer to 0.005, might be sufficient. We study the effect of grid size on σ_α, σ_ϵ using various $\Delta\alpha$ and $\Delta\epsilon$ values (0.001, 0.0025, 0.005). We also vary the range on α explored by examining within the following limits: [0.7, 1.3] and [0.8, 1.2] and in ϵ, [−0.3, 0.3] and [−0.2, 0.2].

6 RESULTS FROM THE MOCKS

In this section, we present results of applying various robustness tests described in Section 5 to the full set of mock galaxy catalogues from BOSS as described in Section 3.4. We analyse the choices which have a significant impact on the results. We apply our robustness tests on both DR10 and DR11 mock galaxy catalogues, focusing on DR11 results. We also concentrate on $\alpha-\epsilon$ parametrization.

6.1 Fiducial results

Fig. 1 shows the average monopole and quadrupole of the simulations and their corresponding fits using our fiducial methodology pre- and post-reconstruction for DR11. There is a perfect match at large scales to the fitting template, especially in the monopole. Post-reconstruction, there is a residual quadrupole generated by the not perfect reconstruction. We also observe the sharpening of the baryonic acoustic feature on the reconstructed monopole and a quadrupole consistent with zero at large scales. This suggests that reconstruction does indeed undo the smearing of the peak generated by the non-linear evolution and partially restores the isotropy of the two-point correlation function. The distribution of the best-fitting values in the $\alpha-\epsilon$ parametrization are presented in Fig. 2 pre-[black] and post-reconstruction[red]. The labels indicate the mean and standard error on the mean.

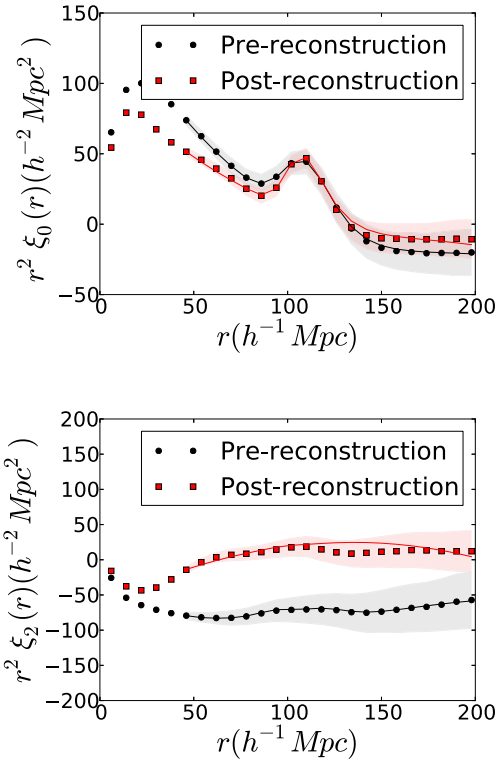

Figure 1. Mean monopole [top] and quadrupole [bottom] of all mock galaxy catalogues of DR11 pre-reconstruction [black dots] and post-reconstruction [red squares]. The shaded regions show the 1σ error bars. The fits shown in figure are found by applying the fiducial fitting methodology. We can see that reconstruction sharpens the peak in the monopole and decreases the large-scale anisotropy in the quadrupole generated by the RSD, which is to be expected. The fits show a good match on large scales for monopole and quadrupole, pre- and post-reconstruction.

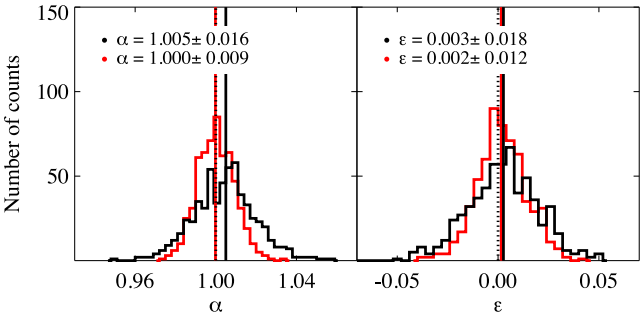

Figure 2. Histograms of α [left], ϵ [right] for fiducial case pre-reconstruction [black] and post-reconstruction [red]. The legend indicates the median and rms of the distributions. We can see that reconstruction narrows the distribution of both α and ϵ, which is to be expected. The histograms show the fiducial fitting methodology do not produce a significantly biased parameters; we measure $b_\alpha = 0.5$ per cent and $b_\epsilon = 0.3$ per cent pre-reconstruction. Post-reconstruction they reduce to b_α less than 0.1 per cent and $b_\epsilon = 0.2$ per cent. In all cases, the biases are within the rms dispersion.

Since our analysis assumes the same cosmology as the input of simulations, we expect to achieve a distribution of α and ϵ centre around 1 and 0. For ease of discussion, we first define the fitting bias as

$$b_\alpha = [\tilde{\alpha} - 1] \times 100$$
$$b_\epsilon = [\tilde{\epsilon} - 0] \times 100. \quad (34)$$

Pre-reconstruction, we expect about 0.5 per cent shift from 1 due to non-linear structure growth, even if we do not expect the 2LPT mocks to capture all the non-linearities. When we apply the fiducial methodology, we find $b_\alpha = 0.5$ per cent and $b_\epsilon = 0.3$ per cent pre-reconstruction. These values reduce to b_α less than 0.1 per cent and $b_\epsilon = 0.2$ per cent with reconstruction. As expected, reconstruction reduces the bias in both α and ϵ and also decreases the dispersion of the best-fitting values significantly. The bias on α and ϵ, however, are both within the rms dispersion of the mocks. This result suggests that the fiducial fitting methodology does not produce a significantly biased result.

6.2 Potential systematics on the fitting results

6.2.1 The effects of methodology change on best-fitting parameters

Tables 1 and 2 presents the results of the anisotropic fit when we apply various changes in the methodology for DR11 pre- and post-reconstruction. The tables include the median variation in α, $\widetilde{\Delta\alpha}$, and median variation in ϵ, $\widetilde{\Delta\epsilon}$. The variation is defined as the difference of the test case compared to the fiducial case,

$$\Delta_{\rm var} = \alpha_{\rm fid} - \alpha_{\rm var}, \quad (35)$$

where fid denotes the fiducial case and var refers to the different variations we apply to the fiducial methodology. The 16th, 86th percentiles of the distribution of $\Delta\alpha$ and $\Delta\epsilon$ are also listed in the tables to quantify the dispersion of the best-fitting values. The dispersion plots in α and ϵ for the methodology tests listed in these tables are displayed in Figs 3 and 4. Each panel corresponds to the dispersion plot when we apply one of the methodology tests compared with the fiducial methodology. The legends of the plot indicate the median variation and the 16th and 84th percentiles of the median variation.

We first consider the effects when we fit the pre-reconstruction mock catalogues. We observe some dispersion in $\Delta\alpha$ in five

Table 1. Fitting results with numerous variations of our fiducial fitting methodology for DR11 mock galaxy catalogues pre-reconstruction without covariance corrections for the overlapping mock regions. Each methodology test has been described earlier in Section 5; we clarify some of the less obvious ones here: '$P_{\rm pt}(k)$ floating' refers to using RPT-inspired $P_{\rm pt}(k)$ template with β floating and '$P_{\rm pt}(k)$ fixed' to the $P_{\rm pt}(k)$ template with β fixed to 0.4 for pre-reconstructed and $\beta = 0$ post-reconstruction, 'exp' and 'Gaussian' refer to various FoG models as described in Section 5.5. The first line shows the median and 16th and 84th percentiles for α, ϵ, $\alpha_{||,\perp}$. The remaining lines list the median bias and median variations $\Delta v = v_i - v_f$ with their corresponding 16th and 84th percentiles. The median bias $\widetilde{b}$, median variations $\widetilde{\Delta v}$, and percentiles are multiplied by 100.

Model	$\widetilde{\alpha}$	–	$\widetilde{\epsilon}$	–	$\widetilde{\alpha_\parallel}$	–	$\widetilde{\alpha_\perp}$	–
				DR11 Pre-reconstruction				
Fiducial	$1.0049^{+0.0142}_{-0.0156}$	–	$0.0027^{+0.0166}_{-0.0181}$	–	$1.0107^{+0.0404}_{-0.0413}$	–	$1.0018^{+0.021}_{-0.020}$	–
Model	$\widetilde{b_\alpha}$	$\widetilde{\Delta\alpha}$	$\widetilde{b_\epsilon}$	$\widetilde{\Delta\epsilon}$	$\widetilde{b_\parallel}$	$\widetilde{\Delta\alpha_\parallel}$	$\widetilde{b_\perp}$	$\widetilde{\Delta\alpha_\perp}$
$r_{\rm bin} \to 4{\rm Mpc}\,h^{-1}$	$0.46^{+1.24}_{-1.46}$	$0.03^{+0.40}_{-0.48}$	$-0.27^{+1.59}_{-1.70}$	$0.02^{+0.47}_{-0.47}$	$1.14^{+3.61}_{-4.24}$	$0.09^{+0.89}_{-0.99}$	$0.11^{+1.99}_{-1.73}$	$-0.03^{+0.68}_{-0.66}$
$30 < r < 200{\rm Mpc}\,h^{-1}$	$0.17^{+1.42}_{-1.46}$	$-0.26^{+0.24}_{-0.28}$	$-0.09^{+1.71}_{-1.76}$	$-0.15^{+0.15}_{-0.19}$	$0.39^{+4.07}_{-3.90}$	$-0.58^{+0.54}_{-0.65}$	$0.03^{+2.19}_{-1.97}$	$-0.08^{+0.11}_{-0.17}$
Two−term $A_\ell(r)$	$0.49^{+1.49}_{-1.48}$	$0.05^{+0.12}_{-0.11}$	$-0.31^{+1.66}_{-1.66}$	$0.03^{+0.31}_{-0.23}$	$1.15^{+4.11}_{-3.75}$	$0.10^{+0.73}_{-0.51}$	$0.17^{+2.11}_{-2.03}$	$-0.02^{+0.21}_{-0.23}$
Four−term $A_\ell(r)$	$0.47^{+1.44}_{-1.57}$	$-0.05^{+0.16}_{-0.13}$	$-0.27^{+1.64}_{-1.89}$	$-0.03^{+0.24}_{-0.23}$	$0.96^{+4.02}_{-4.18}$	$-0.11^{+0.58}_{-0.55}$	$0.13^{+2.16}_{-2.04}$	$-0.01^{+0.17}_{-0.17}$
Fixed $\beta = 0.4$	$0.48^{+1.42}_{-1.57}$	$-3{\rm e}{-3}^{+0.01}_{-0.02}$	$-0.26^{+1.65}_{-1.83}$	$4{\rm e}{-3}^{+0.05}_{-0.07}$	$1.01^{+4.08}_{-4.02}$	$0.01^{+0.10}_{-0.15}$	$0.16^{+2.17}_{-1.99}$	$-4{\rm e}{-3}^{+0.07}_{-0.07}$
$\Sigma_\parallel = \Sigma_\perp = 8\,{\rm Mpc}\,h^{-1}$	$0.49^{+1.51}_{-1.52}$	$0.05^{+0.22}_{-0.21}$	$0.05^{+1.75}_{-1.92}$	$-0.33^{+0.28}_{-0.25}$	$0.62^{+3.88}_{-4.46}$	$-0.62^{+0.68}_{-0.64}$	$0.54^{+2.12}_{-1.96}$	$0.39^{+0.24}_{-0.30}$
$\Sigma_{\rm s} \to 3.0\,{\rm Mpc}\,h^{-1}$	$0.53^{+1.40}_{-1.53}$	$0.03^{+0.04}_{-0.04}$	$-0.33^{+1.70}_{-1.83}$	$0.07^{+0.06}_{-0.06}$	$1.20^{+4.18}_{-4.16}$	$0.18^{+0.16}_{-0.15}$	$0.13^{+2.13}_{-2.03}$	$-0.04^{+0.04}_{-0.03}$
No priors	$0.54^{+1.52}_{-1.55}$	$0.02^{+0.13}_{-0.06}$	$-0.27^{+1.73}_{-1.79}$	$-0.01^{+0.21}_{-0.20}$	$1.19^{+3.97}_{-4.23}$	$-0.02^{+0.50}_{-0.37}$	$0.21^{+2.24}_{-2.02}$	$0.02^{+0.25}_{-0.17}$
Only $\log(B_0^2)$ prior	$0.54^{+1.42}_{-1.54}$	$0.01^{+0.06}_{-0.02}$	$-0.25^{+1.70}_{-1.78}$	$-0.01^{+0.18}_{-0.18}$	$1.12^{+3.98}_{-4.23}$	$-0.02^{+0.37}_{-0.31}$	$0.17^{+2.21}_{-2.00}$	$0.01^{+0.22}_{-0.18}$
Only with β prior	$0.50^{+1.49}_{-1.56}$	$3{\rm e}-3^{+0.01}_{-0.05}$	$-0.28^{+1.68}_{-1.78}$	$0.00^{+0.04}_{-0.04}$	$1.12^{+4.03}_{-4.15}$	$0.01^{+0.16}_{-0.11}$	$0.19^{+2.20}_{-2.00}$	$0.01^{+0.07}_{-0.03}$
$P_{\rm pt}(k)$ floating β	$-0.04^{+1.47}_{-1.52}$	$-0.54^{+0.16}_{-0.15}$	$-0.21^{+1.82}_{-1.89}$	$-0.04^{+0.21}_{-0.18}$	$0.57^{+4.12}_{-4.29}$	$-0.64^{+0.47}_{-0.35}$	$-0.35^{+2.19}_{-2.02}$	$-0.51^{+0.24}_{-0.21}$
$P_{\rm pt}(k)$ fixed $\beta = 0.4$	$-0.07^{+1.48}_{-1.51}$	$-0.55^{+0.16}_{-0.15}$	$-0.20^{+1.80}_{-1.85}$	$-0.06^{+0.20}_{-0.20}$	$0.53^{+4.08}_{-4.42}$	$-0.67^{+0.46}_{-0.44}$	$-0.33^{+2.16}_{-2.04}$	$-0.49^{+0.25}_{-0.21}$
FoG model → exp	$0.49^{+1.42}_{-1.56}$	$-4{\rm e}{-3}^{+6{\rm e}-3}_{-6{\rm e}-3}$	$-0.25^{+1.66}_{-1.80}$	$-0.01^{+0.01}_{-0.01}$	$1.06^{+4.03}_{-4.12}$	$-0.02^{+0.02}_{-0.02}$	$0.18^{+2.12}_{-2.03}$	$0.01^{+0.01}_{-0.01}$
FoG model → Gauss	$0.49^{+1.42}_{-1.56}$	$0.3{\rm e}-4^{+2{\rm e}-4}_{-2{\rm e}-4}$	$-0.27^{+1.66}_{-1.81}$	$1{\rm e}{-4}^{+2{\rm e}-4}_{-3{\rm e}-4}$	$1.07^{+4.04}_{-4.13}$	$3{\rm e}{-4}^{+7{\rm e}-4}_{-8{\rm e}-4}$	$0.18^{+2.13}_{-2.03}$	$-1{\rm e}{-4}^{+1{\rm e}-4}_{-1{\rm e}-4}$

Table 2. Fitting results of mocks numerous variations of our fiducial fitting methodology for DR11 mock galaxy catalogues post-reconstruction without covariance corrections for the overlapping mock regions. Each methodology test has been described earlier in Section 5; we clarify some of the less obvious ones here: '$P_{\rm pt}(k)$ floating' refers to using RPT-inspired $P_{\rm pt}(k)$ template with β floating and '$P_{\rm pt}$ fixed' to the $P_{\rm pt}(k)$ template with β fixed to 0.4 for pre-reconstructed and $\beta = 0$ post-reconstruction, 'exp' and 'Gaussian' refer to various FoG models as described in Section 5.5. The first line shows the median and 16th and 84th percentiles for α, ϵ, $\alpha_{||,\perp}$. The remaining lines lists the median bias and median variations $\Delta v = v_i - v_f$ with their corresponding 16th and 84th percentiles. The median bias $\widetilde{b}$, median variations $\widetilde{\Delta v}$, and percentiles are multiplied by 100.

Model	$\widetilde{\alpha}$	–	$\widetilde{\epsilon}$	–	$\widetilde{\alpha_\parallel}$	–	$\widetilde{\alpha_\perp}$	–
				DR11 Post-reconstruction				
Fiducial	$0.9998^{+0.0094}_{-0.0084}$	–	$0.0016^{+0.0124}_{-0.0116}$	–	$1.0029^{+0.0272}_{-0.0247}$	–	$0.9991^{+0.0136}_{-0.0159}$	–
Model	$\widetilde{b_\alpha}$	$\widetilde{\Delta\alpha}$	$\widetilde{b_\epsilon}$	$\widetilde{\Delta\epsilon}$	$\widetilde{b_\parallel}$	$\widetilde{\Delta\alpha_\parallel}$	$\widetilde{b_\perp}$	$\widetilde{\Delta\alpha_\perp}$
$r_{\rm bin} \to 4\,{\rm Mpc}\,h^{-1}$	$0.03^{+0.80}_{-0.84}$	$0.03^{+0.31}_{-0.36}$	$-0.09^{+1.22}_{-1.01}$	$-0.03^{+0.37}_{-0.34}$	$0.23^{+2.61}_{-2.36}$	$-0.03^{+0.74}_{-0.71}$	$-0.11^{+1.36}_{-1.36}$	$0.05^{+0.48}_{-0.54}$
$30 < r < 200\,{\rm Mpc}\,h^{-1}$	$0.06^{+0.83}_{-0.85}$	$0.06^{+0.14}_{-0.12}$	$-0.27^{+1.25}_{-1.09}$	$0.10^{+0.15}_{-0.11}$	$0.60^{+2.62}_{-2.29}$	$0.26^{+0.41}_{-0.32}$	$-0.17^{+1.37}_{-1.48}$	$-0.05^{+0.09}_{-0.09}$
Two−term $A_\ell(r)$	$0.07^{+0.87}_{-0.88}$	$0.05^{+0.07}_{-0.07}$	$-0.47^{+1.23}_{-1.03}$	$0.31^{+0.16}_{-0.13}$	$1.05^{+2.61}_{-2.32}$	$0.68^{+0.35}_{-0.26}$	$-0.39^{+1.29}_{-1.47}$	$-0.26^{+0.13}_{-0.19}$
Four−term $A_\ell(r)$	$-0.08^{+0.92}_{-0.83}$	$-0.05^{+0.06}_{-0.08}$	$1{\rm e}{-4}^{+1.25}_{-1.17}$	$-0.15^{+0.11}_{-0.13}$	$-0.05^{+2.71}_{-2.48}$	$-0.35^{+0.27}_{-0.32}$	$0.02^{+1.33}_{-1.58}$	$0.10^{+0.08}_{-0.07}$
Fixed $\beta = 0.0$	$-0.04^{+0.95}_{-0.84}$	$-4{\rm e}-3^{+0.01}_{-0.03}$	$-0.18^{+1.24}_{-1.14}$	$0.02^{+0.09}_{-0.10}$	$0.36^{+2.63}_{-2.52}$	$0.04^{+0.16}_{-0.19}$	$-0.15^{+1.41}_{-1.54}$	$-0.02^{+0.10}_{-0.11}$
$\Sigma_\parallel = 4$, $\Sigma_\perp = 2({\rm Mpc}\,h^{-1})$	$-0.02^{+0.93}_{-0.85}$	$-2{\rm e}-3^{+0.03}_{-0.03}$	$-0.21^{+1.21}_{-1.13}$	$0.05^{+0.05}_{-0.05}$	$0.37^{+2.66}_{-2.43}$	$0.09^{+0.10}_{-0.10}$	$-0.14^{+1.37}_{-1.56}$	$-0.05^{+0.05}_{-0.06}$
$\Sigma_{\rm s} \to 3.0\,{\rm Mpc}\,h^{-1}$	$2{\rm e}-3^{+0.92}_{-0.83}$	$0.02^{+0.04}_{-0.04}$	$-0.24^{+1.26}_{-1.15}$	$0.09^{+0.08}_{-0.07}$	$0.49^{+2.69}_{-2.50}$	$0.20^{+0.19}_{-0.19}$	$-0.15^{+1.39}_{-1.59}$	$-0.06^{+0.05}_{-0.05}$
No prior	$-0.01^{+0.95}_{-0.86}$	$1{\rm e}-3^{+0.048}_{-0.019}$	$-0.13^{+1.30}_{-1.16}$	$-0.04^{+0.14}_{-0.15}$	$0.28^{+2.72}_{-2.60}$	$-0.08^{+0.28}_{-0.26}$	$-0.05^{+1.41}_{-1.60}$	$0.03^{+0.18}_{-0.14}$
Only $\log(B_0^2)$ prior	$-0.01^{+0.94}_{-0.85}$	$0.01^{+0.04}_{-0.01}$	$-0.13^{+1.28}_{-1.14}$	$-0.03^{+0.13}_{-0.13}$	$0.32^{+2.67}_{-2.58}$	$-0.05^{+0.26}_{-0.23}$	$-0.04^{+1.39}_{-1.61}$	$0.03^{+0.16}_{-0.12}$
Only β prior	$-0.03^{+0.94}_{-0.85}$	$-0.01^{+0.01}_{-0.01}$	$-0.15^{+1.25}_{-1.14}$	$-2{\rm e}-3^{+0.02}_{-0.03}$	$0.28^{+2.73}_{-2.49}$	$-0.01^{+0.03}_{-0.07}$	$-0.09^{+1.40}_{-1.60}$	$1{\rm e}-3^{+0.02}_{-0.02}$
$P_{\rm pt}(k)$ with floating β	$0.01^{+0.94}_{-0.87}$	$0.03^{+0.03}_{-0.03}$	$-0.11^{+1.26}_{-1.11}$	$-0.03^{+0.05}_{-0.05}$	$0.29^{+2.68}_{-2.47}$	$-0.04^{+0.13}_{-0.11}$	$-0.02^{+1.30}_{-1.55}$	$0.06^{+0.05}_{-0.05}$
$P_{\rm pt}(k)$ with $\beta = 0.0$	$-2{\rm e}-3^{+0.94}_{-0.86}$	$0.02^{+0.03}_{-0.03}$	$-0.14^{+1.22}_{-1.14}$	$-0.01^{+0.09}_{-0.10}$	$0.33^{+2.58}_{-2.55}$	$4{\rm e}-3^{+0.169}_{-0.216}$	$-0.08^{+1.40}_{-1.50}$	$0.04^{+0.10}_{-0.11}$

cases: changing the bin size to smaller bins produces a 0.5 per cent dispersion, changing the fitting range to [30, 200] produces a 0.3 per cent dispersion, using higher order polynomials for modelling the broad-band terms, using $P_{\rm pt}$ templates and changing the NL damping parameters produce a 0.2 per cent dispersion each. The remaining cases show a small dispersion of $\leq$0.1 per cent.

In the case of $\Delta\epsilon$, the largest dispersions are observed when we change the bin size, showing a 0.5 per cent dispersion. When we use lower order polynomials for the broad-band terms or when we vary

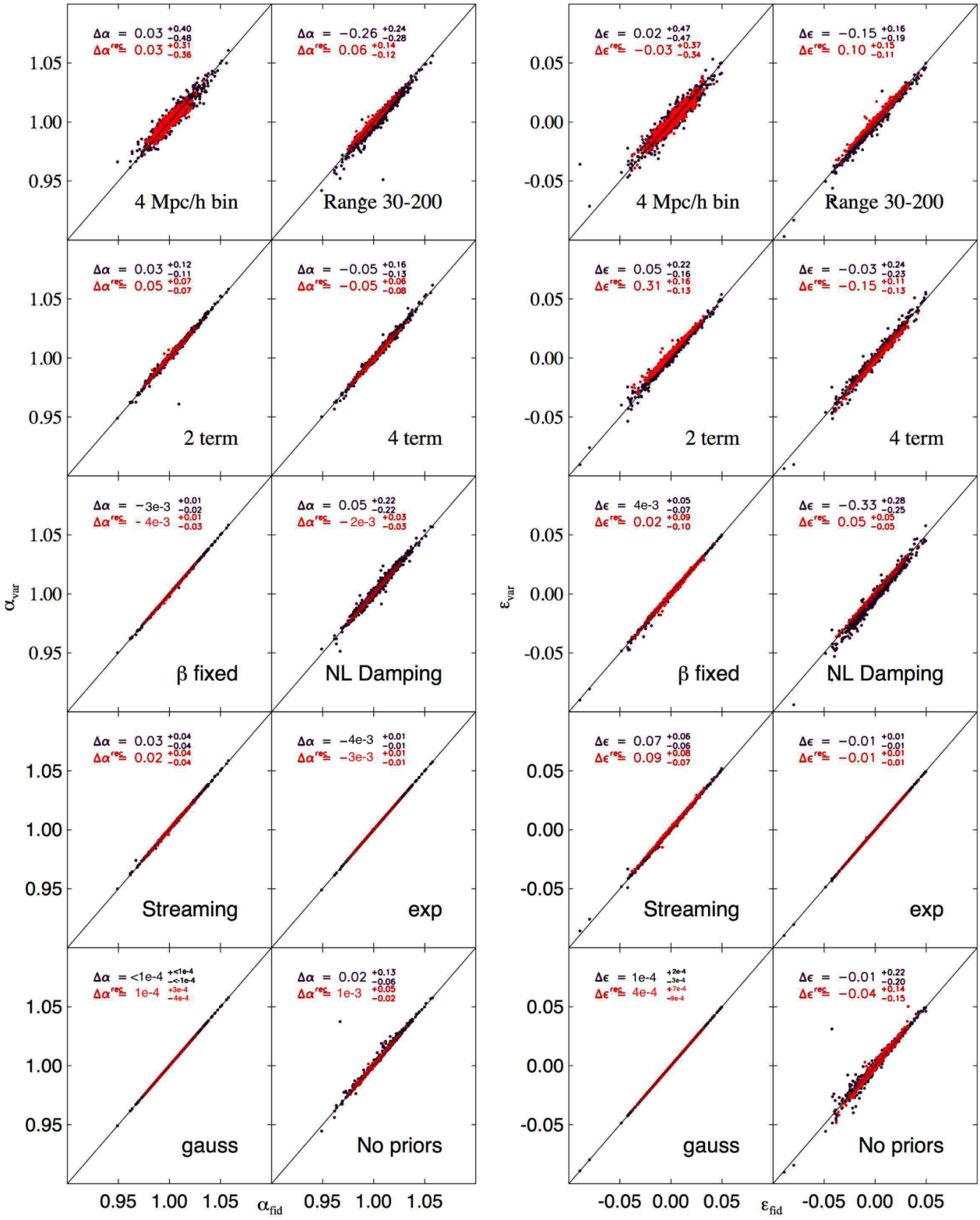

Figure 3. Dispersion plots of α [left] and ϵ [right] for the different cases enumerated in Tables 1 and 2 for DR11 pre and post-reconstructed mocks. The dispersion is between the fiducial fitting methodology and particular methodology/fitting parameter change. For example, in the upper left-most plot, the x-axis is α using fiducial model, while the y-axis is α using the fiducial model except with the β parameter fixed, instead of varying β; with a prior of width 0.2 centred around 0.35. 'NL Damping' denotes changing $\Sigma_{\parallel}$ and $\Sigma_{\perp} \rightarrow \Sigma_{\parallel} = \Sigma_{\perp} = 8\,h^{-1}$ Mpc for pre-reconstructed case and $\Sigma_{\parallel} = \Sigma_{\perp} \rightarrow \Sigma_{\parallel} = 4\,h^{-1}$ Mpc & $\Sigma_{\perp} = 2\,h^{-1}$ Mpc for post-reconstruction, '$P_{\rm pt}(k)$ floating' refers to using the RPT-inspired $P_{\rm pt}(k)$ template with β floating and '$P_{\rm pt}(k)$ fixed' to the $P_{\rm pt}(k)$ template with β fixed to 0.4 for pre-reconstruction and $\beta = 0$ post-reconstruction, 'exp' and 'Gaussian' refer to various FoG models as described in Section 5.5; 'Streaming' refers to changing the streaming value to $\Sigma_{\rm s} = 1.5 \rightarrow 3.0\,h^{-1}$ Mpc. Black denotes pre-reconstruction distributions, while red denotes post-reconstruction distributions. All quantities are multiplied by 100. We can see that the dispersion is fairly small for nearly all cases shown here.

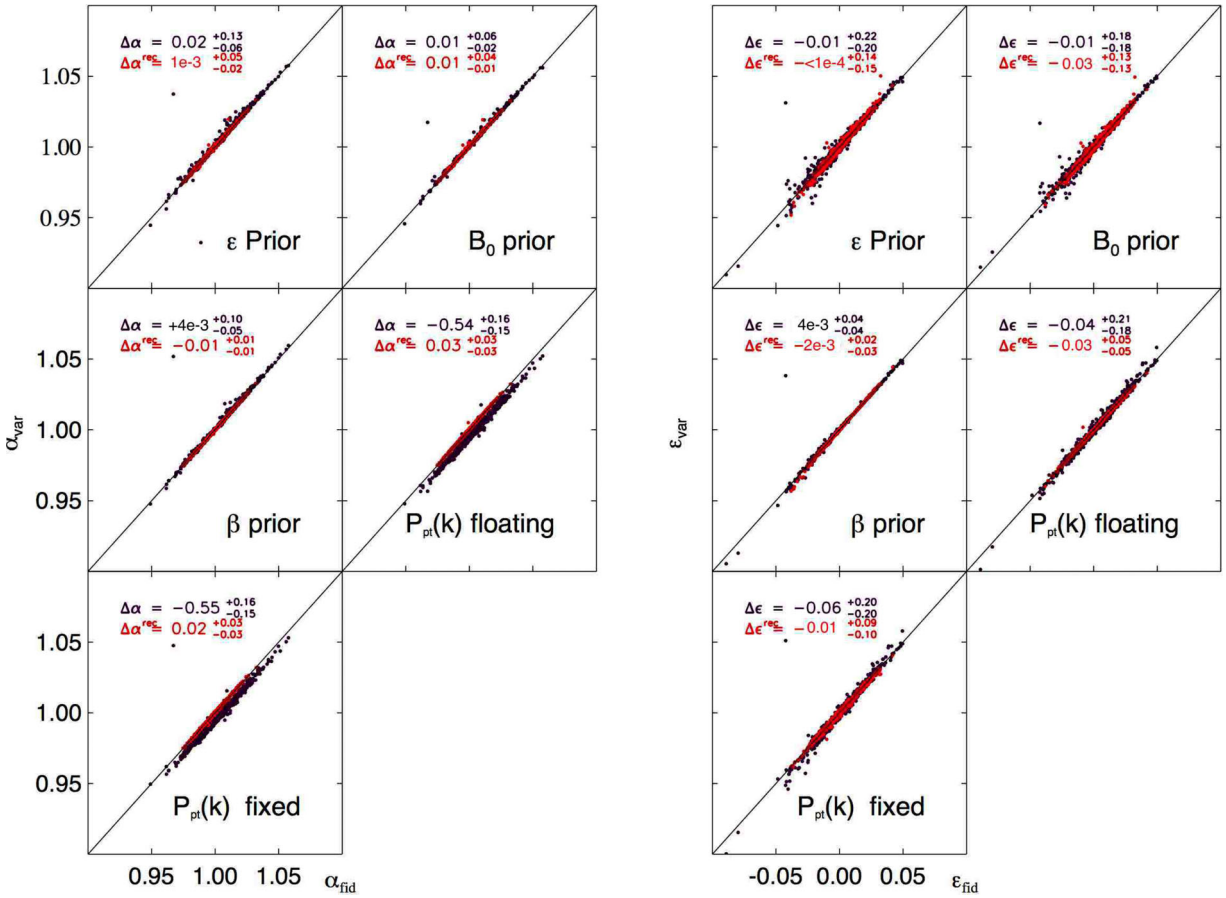

Figure 4. Continuation of Fig. 3. Dispersion plots α and ϵ for methodology tests enumerated in Tables 1 and 2. 'NL Damping' denotes changing $\Sigma_\parallel$ & $\Sigma_\perp \rightarrow \Sigma_\parallel = \Sigma_\perp = 8\,h^{-1}$ Mpc for pre-reconstructed case and $\Sigma_\parallel = \Sigma_\perp \rightarrow \Sigma_\parallel = 4\,h^{-1}$ Mpc *and* $\Sigma_\perp = 2\,h^{-1}$ Mpc for post-reconstruction, '$P_{\rm pt}(k)$ floating' refers to using RPT-inspired $P_{\rm pt}(k)$ template with β floating and '$P_{\rm pt}(k)$ fixed' with β fixed to 0.4 for pre-reconstructed and $\beta = 0$ post-reconstruction, 'exp' and 'Gaussian' refer to various FoG models as described in Section 5.5; 'Streaming' refers to changing the streaming value to $\Sigma_{\rm s} = 1.5 \rightarrow 3.0\,h^{-1}$ Mpc. Black denotes pre-reconstruction distributions, while red denotes post-reconstruction distributions. All quantities are multiplied by 100. We can see that the dispersion is fairly small for nearly all cases shown here.

the NL damping parameters both produce a dispersion 0.3 per cent and four cases show a 0.2 per cent dispersion: when using higher order polynomials for the broad-band terms, the cases eliminating priors, using $P_{\rm pt}$ templates and changing the range of the fit. The remaining cases show a small dispersion $\leq$0.1 per cent.

Post-reconstruction the dispersion is significantly reduced. With only one exception, the dispersion observed in $\Delta\alpha$ is $\leq$0.1 per cent. The exceptional case uses smaller bins, and has a dispersion of 0.3 per cent. The parameter $\Delta\epsilon$ also shows a small dispersion of $\leq$0.1 per cent, with the exception of three cases: using smaller bins shows a 0.4 per cent dispersion, using lower order polynomials for the broad-band terms yields a 0.3 per cent dispersion and the fitting range case yields a 0.15 per cent dispersion.

Table 1 demonstrates that biases in the best-fitting α values pre-reconstruction are $\leq$0.5 per cent for all robustness tests. Smaller biases in best-fitting α values are produced when we use the $P_{\rm pt}$ template or a larger fitting range. In the case of best-fitting ϵ values, systematic biases of $\sim$0.3 per cent are found in almost all cases. Smaller biases in best-fitting ϵ values are found when the fitting range is increased, when the$P_{\rm pt}(k)$ template with fixing/floating β is used, or when varying $\Sigma_{||,\perp}$. The fact that the $P_{\rm pt}(k)$ template produces a smaller bias pre-reconstruction is not surprising because these templates include a mode coupling term that is supposed to match the non-linear correlation function better than the de-wiggled template. This decrease in the bias associated with the $P_{\rm pt}(k)$ templates has been reported in previous works (Kazin et al. 2012; Sánchez et al. 2012). When we fit with reconstructed catalogues, observed biases in the best-fitting α values are all $\leq$0.1 per cent. The fitting range results suggest that there is a trade-off between obtaining a smaller bias between pre- and post-reconstruction cases when using the same range. In ϵ, the only three cases that produce a larger bias than the fiducial one (2 per cent) are those applying two-term polynomials, enlarging the fitting range and changing $\Sigma_{\rm s} \rightarrow 3.0$ Mpc h^{-1}.

We then turn to the differences each change in methodology can cause compared to the results of the fiducial fitting methodology. With a large array of robustness tests, our fiducial methodology shows maximum differences of 0.5 per cent in best-fitting α value and 0.3 per cent in best-fitting ϵ value pre-reconstruction. Post-reconstruction, the variations in α and ϵ are impressively small, $\Delta\alpha$, $\Delta\epsilon \leq 0.1$ per cent, except in the case of broad-band terms modelling, where a change to two− or four-term polynomials affects the ϵ post-reconstruction at the still relatively modest level of 0.2−0.3 per cent.

6.2.2 *Effects of methodology choices on best-fitting uncertainties*

Fig. 5 shows the distribution of σ_α and σ_ϵ from fitting the DR11 mock galaxy catalogues using the fiducial fitting methodology. The

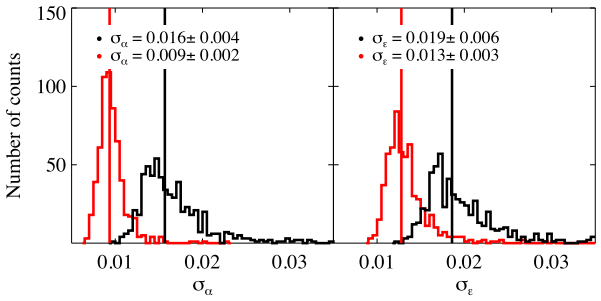

Figure 5. Histograms of σ_α [left], σ_ϵ [right] for fiducial fitting methodology pre-reconstruction [black] and post-reconstruction [red]. The legends indicate the median and rms of the distributions. We can see that reconstruction clearly reduces the errors on fitted parameters.

black [red] solid lines indicates the pre-[post-]reconstruction results. The median errors (and their quartiles) are $\widetilde{\sigma_\alpha} = 0.016^{+0.004}_{-0.002}$ and $\widetilde{\sigma_\epsilon} = 0.019^{+0.005}_{-0.002}$. When we apply the fiducial fitting methodology to reconstructed DR11 mock galaxy catalogues, $\widetilde{\sigma_\alpha} = 0.009^{+0.001}_{-0.001}$ and $\widetilde{\sigma_\epsilon} = 0.013^{+0.002}_{-0.001}$, respectively. The distributions of σ are highly skewed and the large tails extending to larger values of σ in the pre-reconstruction are significantly reduced post-reconstruction. From the 16th and 86th percentiles of the σ_α and σ_ϵ distributions, we observe that the σ_ϵ distribution appears to be more skewed.

We now move to analysing the dispersion and variations in the uncertainties of the best-fitting parameter when we modify the fiducial fitting methodology. We concentrate on Figs 6 and 7 for the following discussion. To summarize, we observe small dispersions in the uncertainties of the best-fitting parameters (both $\Delta\sigma_\alpha$ and $\Delta\sigma_\epsilon$) of $\leq$0.001 ($\sim$6 per cent), except when we change the fitting range or the priors applied in the methodology. A larger fitting range produces a dispersion of $\Delta\sigma_\epsilon$ at 0.002 ($\sim$ 11 per cent). We observe relatively large dispersions in $\Delta\sigma_\alpha$, $\Delta\sigma_\epsilon$ when certain priors are removed when fitting both pre- and post-reconstructed mock catalogues (Tables 3 and 4). Pre-reconstruction, the dispersion could be as high as 0.005 (31 per cent) for $\Delta\sigma_\alpha$ and 0.007 ($\sim$36 per cent) for $\Delta\sigma_\epsilon$. Post-reconstruction, the dispersion for the cases eliminating priors could reach values as high as 0.025 ($\sim$ 277 per cent) for $\Delta\sigma_\alpha$ and 0.029 ($\sim$223 per cent) for $\Delta\sigma_\epsilon$.

We summarize the results on the best-fitting uncertainties in Tables 3 and 4. There are large variations when we change our prior assumptions; this will be discussed in the following section devoted to the priors (Section 6.3.4). Here, we present only changes not related to prior assumptions in the fitting methodology. The results demonstrate that only few cases show variations in σ_α; different robustness tests affect mostly σ_ϵ. When fitting using DR11 pre-reconstructed mock galaxy catalogues, σ_α is only affected when we apply lower order polynomials for broad-band terms, and when the bin sizes are changed. In both cases, σ_α shows a variation of $0.001/0.016 \sim 6$ per cent. The quantity σ_ϵ displays ($\Delta\sigma_\epsilon = \pm 0.001$)

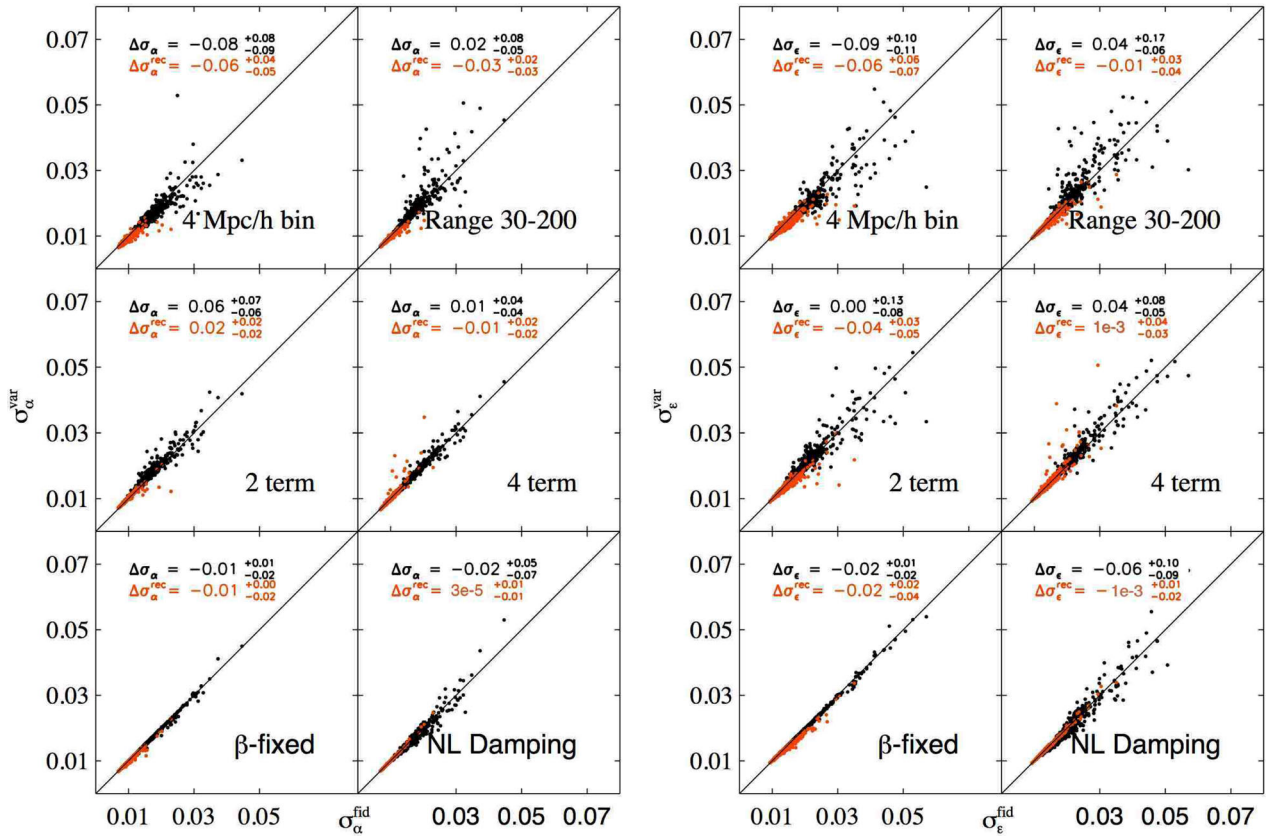

Figure 6. Dispersion plots of σ_α [left] and σ_ϵ [right] from various fitting methodologies to DR11 pre- and post-reconstructed mock galaxy catalogues. The fitting methodologies tested are listed in Tables 3 and 4. The dispersion is between the fiducial fitting methodology and the modified methodology. For example, for the upper left-most plot, the x-axis is σ_α using fiducial model, while the y-axis is σ_α applying fiducial methodology but with β parameter fixed instead of varying β with a prior. Black denotes pre-reconstruction distributions, while red denotes post-reconstruction distributions. All quantities are multiplied by 100. We can see that the dispersion is fairly small (though not as small as the dispersion observed for the fitted values of the measured parameters) for nearly all cases shown here.

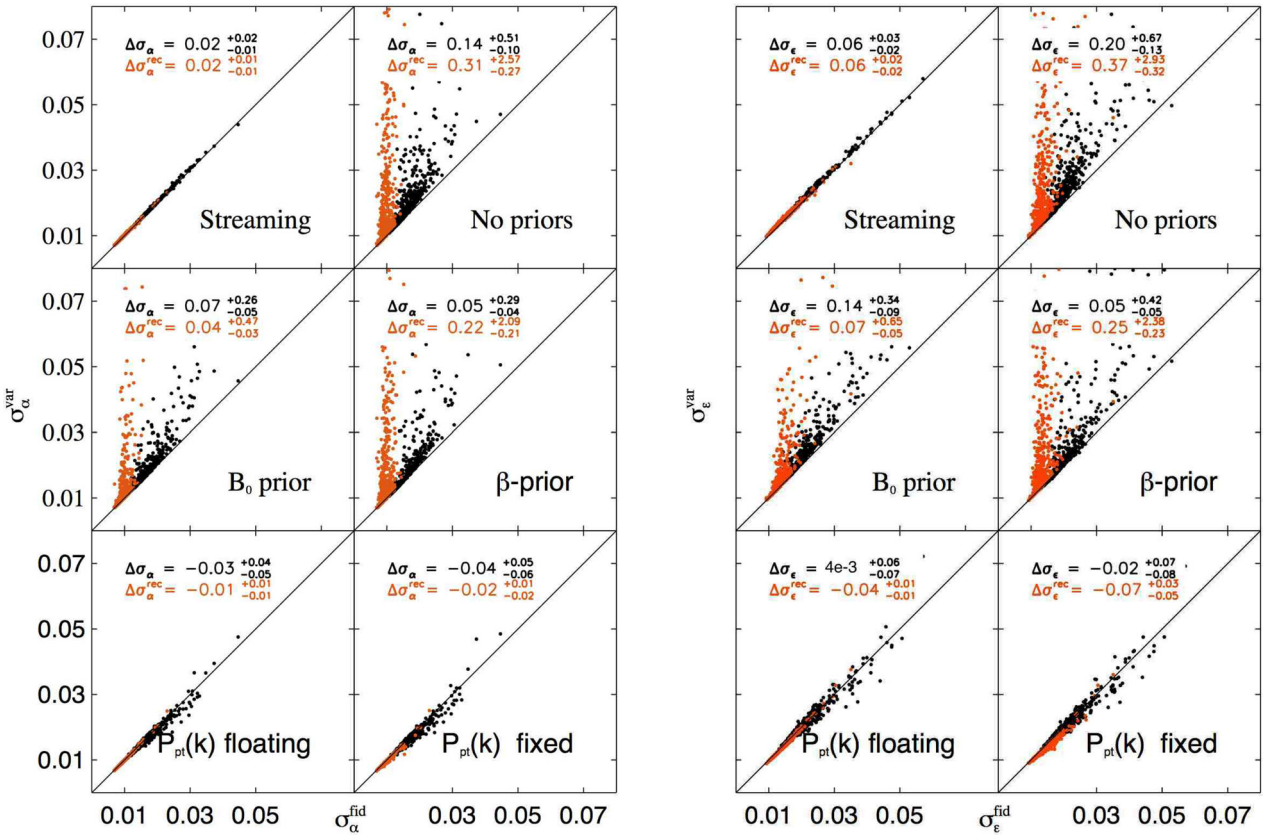

Figure 7. A continuation of Fig. 6. Dispersion plots of σ_α[left] and σ_ϵ [right] when we apply various fitting methodologies to DR11 pre- and post-reconstructed mock galaxy catalogues. The fitting methodologies tested are listed in Tables 3 and 4. Black denotes pre-reconstruction distributions, while red denotes post-reconstruction distributions. All quantities are multiplied by 100. We can see that the dispersion is fairly small (though not as small as the dispersion observed for the fitted values of the measured parameters) for cases not involving changing priors. The prior related cases tested here do not limit the integration range for the errors to a physically meaningful range, and will be discussed further in the text.

Table 3. The best-fitting errors with numerous variations of our fiducial fitting methodology for DR11 mock galaxy catalogues pre-reconstruction without covariance corrections for the overlapping mock regions. Each methodology test has been described earlier in Section 5; we clarify some of the less obvious ones here: '$P_{\rm pt}(k)$ floating' refers to using RPT-inspired $P_{\rm pt}(k)$ template with β floating and '$P_{\rm pt}(k)$ fixed' to the $P_{\rm pt}(k)$ template with β fixed to 0.4 for pre-reconstructed and $\beta = 0$ post-reconstruction, 'exp' and 'Gaussian' refers to various FoG models as described in Section 5.5. The columns list the median and 16th and 84th percentiles of the $\sigma_{\alpha,\epsilon,||,\perp}$ and variations $\Delta v = v_i - v_f$. Except for the fiducial case all quantities are multiplied by 100.

Model	$\widetilde{\sigma_\alpha}$	$\widetilde{\Delta\sigma_\alpha}$	$\widetilde{\sigma_\epsilon}$	$\widetilde{\Delta\sigma_\epsilon}$	$\widetilde{\sigma_{\alpha_\parallel}}$	$\widetilde{\Delta\sigma_{\alpha_\parallel}}$	$\widetilde{\sigma_{\alpha_\perp}}$	$\widetilde{\Delta\sigma_{\alpha_\perp}}$
				DR11 Pre-reconstruction				
Fiducial	$0.0157^{+0.0037}_{-0.0023}$	–	$0.0186^{+0.0051}_{-0.0024}$	–	$0.0438^{+0.0133}_{-0.0069}$	–	$0.0211^{+0.0038}_{-0.0022}$	–
$r_{\rm bin} \to 4{\rm Mpc}\,h^{-1}$	$1.49^{+0.36}_{-0.20}$	$-0.08^{+0.08}_{-0.09}$	$1.76^{+0.48}_{-0.21}$	$-0.09^{+0.10}_{-0.11}$	$4.23^{+1.27}_{-0.69}$	$-0.16^{+0.27}_{-0.33}$	$1.99^{+0.29}_{-0.21}$	$-0.13^{+0.08}_{-0.11}$
$30 < r < 200{\rm Mpc}\,h^{-1}$	$1.59^{+0.45}_{-0.24}$	$0.02^{+0.08}_{-0.05}$	$1.92^{+0.63}_{-0.26}$	$0.04^{+0.16}_{-0.06}$	$4.57^{+1.68}_{-0.78}$	$0.13^{+0.40}_{-0.21}$	$2.11^{+0.40}_{-0.24}$	$-0.01^{+0.05}_{-0.04}$
Two−term $A_\ell(r)$	$1.64^{+0.39}_{-0.24}$	$0.06^{+0.07}_{-0.06}$	$1.87^{+0.59}_{-0.25}$	$0.00^{+0.12}_{-0.08}$	$4.43^{+1.63}_{-0.89}$	$-0.04^{+0.40}_{-0.19}$	$2.15^{+0.48}_{-0.29}$	$0.02^{+0.19}_{-0.11}$
Four−term $A_\ell(r)$	$1.57^{+0.41}_{-0.23}$	$0.01^{+0.04}_{-0.04}$	$1.89^{+0.57}_{-0.24}$	$0.04^{+0.08}_{-0.05}$	$4.45^{+1.52}_{-0.71}$	$0.08^{+0.18}_{-0.11}$	$2.14^{+0.37}_{-0.24}$	$0.02^{+0.04}_{-0.03}$
Fixed $\beta = 0.4$	$1.56^{+0.37}_{-0.22}$	$-0.01^{+0.01}_{-0.02}$	$1.84^{+0.48}_{-0.24}$	$-0.02^{+0.01}_{-0.02}$	$4.35^{+1.34}_{-0.66}$	$-0.03^{+0.07}_{-0.09}$	$2.10^{+0.37}_{-0.22}$	$-0.02^{+0.04}_{-0.04}$
$\Sigma_\parallel = \Sigma_\perp = 8\,{\rm Mpc}\,h^{-1}$	$1.54^{+0.37}_{-0.21}$	$-0.02^{+0.05}_{-0.06}$	$1.79^{+0.59}_{-0.25}$	$-0.06^{+0.10}_{-0.09}$	$3.99^{+1.47}_{-0.73}$	$-0.38^{+0.25}_{-0.22}$	$2.30^{+0.39}_{-0.26}$	$0.17^{+0.09}_{-0.08}$
$\Sigma_{\rm s} \to 3.0\,{\rm Mpc}\,h^{-1}$	$1.59^{+0.38}_{-0.23}$	$0.02^{+0.02}_{-0.01}$	$1.92^{+0.52}_{-0.24}$	$0.06^{+0.03}_{-0.02}$	$4.57^{+1.38}_{-0.73}$	$0.17^{+0.07}_{-0.05}$	$2.13^{+0.39}_{-0.22}$	$0.02^{+0.01}_{-0.01}$
No priors	$1.77^{+0.84}_{-0.37}$	$0.14^{+0.51}_{-0.10}$	$2.14^{+1.16}_{-0.42}$	$0.20^{+0.67}_{-0.13}$	$4.90^{+3.04}_{-1.18}$	$0.43^{+1.74}_{-0.41}$	$2.29^{+0.75}_{-0.36}$	$0.16^{+0.42}_{-0.15}$
Only $\log(B_0^2)$ prior	$1.66^{+0.59}_{-0.27}$	$0.07^{+0.26}_{-0.05}$	$2.01^{+0.82}_{-0.31}$	$0.14^{+0.34}_{-0.09}$	$4.66^{+2.12}_{-1.02}$	$0.21^{+0.97}_{-0.25}$	$2.23^{+0.60}_{-0.33}$	$0.10^{+0.28}_{-0.13}$
Only β prior	$1.64^{+0.68}_{-0.29}$	$0.05^{+0.29}_{-0.04}$	$1.96^{+0.93}_{-0.32}$	$0.05^{+0.41}_{-0.05}$	$4.68^{+2.52}_{-0.94}$	$0.14^{+1.24}_{-0.12}$	$2.16^{+0.46}_{-0.25}$	$0.03^{+0.08}_{-0.02}$
$P_{\rm pt}(k)$ with floating β	$1.53^{+0.37}_{-0.21}$	$-0.03^{+0.04}_{-0.05}$	$1.86^{+0.54}_{-0.24}$	$4{\rm e}{-3}^{+0.06}_{-0.07}$	$4.20^{+1.39}_{-0.70}$	$-0.15^{+0.16}_{-0.18}$	$2.23^{+0.37}_{-0.25}$	$0.10^{+0.07}_{-0.07}$
$P_{\rm pt}(k)$ with $\beta = 0.0$	$1.51^{+0.37}_{-0.20}$	$-0.04^{+0.05}_{-0.06}$	$1.84^{+0.52}_{-0.24}$	$-0.02^{+0.07}_{-0.08}$	$4.15^{+1.30}_{-0.64}$	$-0.20^{+0.15}_{-0.23}$	$2.23^{+0.35}_{-0.25}$	$0.10^{+0.07}_{-0.08}$
FoG model → exp	$1.57^{+0.37}_{-0.23}$	$-3{\rm e}{-3}^{+1{\rm e}-3}_{-2{\rm e}-3}$	$1.85^{+0.52}_{-0.24}$	$-9{\rm e}{-3}^{+3{\rm e}-3}_{-4{\rm e}-3}$	$4.35^{+1.33}_{-0.69}$	$-0.02^{+0.01}_{-0.01}$	$2.11^{+0.38}_{-0.22}$	$-3{\rm e}{-3}^{+2{\rm e}-3}_{-1{\rm e}-3}$
FoG model → Gauss	$1.57^{+0.37}_{-0.23}$	$3{\rm e}{-4}^{+1{\rm e}-4}_{-2{\rm e}-4}$	$1.86^{+0.51}_{-0.24}$	$-9{\rm e}{-4}^{+3{\rm e}-4}_{-4{\rm e}-4}$	$4.38^{+1.33}_{-0.69}$	$2{\rm e}{-3}^{+7{\rm e}-4}_{-9{\rm e}-4}$	$2.11^{+0.38}_{-0.22}$	$-3{\rm e}{-4}^{+2{\rm e}-4}_{-1{\rm e}-4}$

Table 4. The best-fitting errors with numerous variations of our fiducial fitting methodology for DR11 mock galaxy catalogues post-reconstruction without covariance corrections for the overlapping mock regions. Each methodology tests has been described earlier in Section 5; we clarify some of the less obvious ones here: '$P_{\rm pt}(k)$ floating' refers to using RPT-inspired $P_{\rm pt}(k)$ template with β floating and '$P_{\rm pt}(k)$ fixed' to the $P_{\rm pt}(k)$ template with β fixed to 0.4 for pre-reconstructed and $\beta = 0$ post-reconstruction, 'exp' and 'Gaussian' refers to various FoG models as described in Section 5.5. The columns list the median and 16th and 84th percentiles of the $\sigma_{\alpha,\epsilon,||,\perp}$ and variations $\Delta v = v_i - v_f$. Except for the fiducial case all quantities are multiplied by 100.

Model	$\widetilde{\sigma_\alpha}$	$\widetilde{\Delta\sigma_\alpha}$	$\widetilde{\sigma_\epsilon}$	$\widetilde{\Delta\sigma_\epsilon}$	$\widetilde{\sigma_{\alpha_\parallel}}$	$\widetilde{\Delta\sigma_{\alpha_\parallel}}$	$\widetilde{\sigma_{\alpha_\perp}}$	$\widetilde{\Delta\sigma_{\alpha_\perp}}$
				DR11 Post-reconstruction				
Fiducial	$0.0093^{+0.0013}_{-0.0011}$	–	$0.0128^{+0.0024}_{-0.0014}$	–	$0.0280^{+0.0064}_{-0.0041}$	–	$0.0151^{+0.0021}_{-0.0015}$	–
$r_{\rm bin} \rightarrow 4\,{\rm Mpc}\,h^{-1}$	$0.87^{+0.12}_{-0.10}$	$-0.07^{+0.04}_{-0.05}$	$1.22^{+0.19}_{-0.13}$	$-0.06^{+0.06}_{-0.07}$	$2.67^{+0.57}_{-0.34}$	$-0.13^{+0.17}_{-0.21}$	$1.41^{+0.15}_{-0.12}$	$-0.10^{+0.06}_{-0.07}$
$30 < r < 200\,{\rm Mpc}\,h^{-1}$	$0.91^{+0.12}_{-0.09}$	$-0.03^{+0.02}_{-0.03}$	$1.26^{+0.21}_{-0.13}$	$-0.01^{+0.03}_{-0.04}$	$2.79^{+0.57}_{-0.37}$	$-3e{-}3^{+0.11}_{-0.13}$	$1.46^{+0.19}_{-0.14}$	$-0.04^{+0.03}_{-0.03}$
Two−term $A_\ell(r)$	$0.96^{+0.13}_{-0.11}$	$0.02^{+0.02}_{-0.02}$	$1.25^{+0.20}_{-0.14}$	$-0.04^{+0.03}_{-0.05}$	$2.80^{+0.58}_{-0.41}$	$-2e{-}3^{+0.08}_{-0.12}$	$1.44^{+0.18}_{-0.13}$	$-0.06^{+0.02}_{-0.04}$
Four−term $A_\ell(r)$	$0.92^{+0.14}_{-0.10}$	$-0.01^{+0.02}_{-0.02}$	$1.27^{+0.26}_{-0.14}$	$1e{-}3^{+0.04}_{-0.03}$	$2.77^{+0.69}_{-0.39}$	$-0.02^{+0.09}_{-0.09}$	$1.52^{+0.20}_{-0.15}$	$5e{-}3^{+0.02}_{-0.01}$
Fixed $\beta = 0.0$	$0.92^{+0.13}_{-0.10}$	$-0.01^{+0.00}_{-0.02}$	$1.26^{+0.20}_{-0.13}$	$-0.02^{+0.02}_{-0.04}$	$2.74^{+0.54}_{-0.32}$	$-0.04^{+0.09}_{-0.15}$	$1.48^{+0.19}_{-0.14}$	$-0.03^{+0.03}_{-0.03}$
$\Sigma_\parallel = 4$ & $\Sigma_\perp = 2$	$0.93^{+0.14}_{-0.10}$	$3e{-}5^{+0.01}_{-0.01}$	$1.28^{+0.22}_{-0.14}$	$-1e{-}3^{+0.01}_{-0.02}$	$2.84^{+0.62}_{-0.40}$	$0.03^{+0.03}_{-0.04}$	$1.48^{+0.21}_{-0.15}$	$-0.03^{+0.01}_{-0.01}$
$\Sigma_{\rm s} \rightarrow 3.0\,{\rm Mpc}\,h^{-1}$	$0.95^{+0.13}_{-0.11}$	$0.02^{+0.01}_{-0.01}$	$1.35^{+0.23}_{-0.15}$	$0.06^{+0.02}_{-0.02}$	$2.97^{+0.67}_{-0.42}$	$0.16^{+0.06}_{-0.05}$	$1.52^{+0.20}_{-0.15}$	$0.02^{+0.01}_{-0.01}$
No prior	$1.30^{+2.52}_{-0.39}$	$0.31^{+2.46}_{-0.27}$	$1.73^{+3.02}_{-0.49}$	$0.37^{+2.90}_{-0.32}$	$4.21^{+8.99}_{-1.65}$	$1.15^{+8.55}_{-1.09}$	$1.64^{+0.36}_{-0.23}$	$0.11^{+0.19}_{-0.06}$
Only $\log(B_0^2)$ prior	$1.00^{+0.52}_{-0.14}$	$0.04^{+0.47}_{-0.03}$	$1.38^{+0.77}_{-0.21}$	$0.07^{+0.65}_{-0.05}$	$3.04^{+2.35}_{-0.66}$	$0.15^{+2.02}_{-0.19}$	$1.59^{+0.26}_{-0.19}$	$0.06^{+0.09}_{-0.04}$
Only β prior	$1.21^{+2.10}_{-0.33}$	$0.22^{+2.02}_{-0.21}$	$1.62^{+2.49}_{-0.41}$	$0.25^{+2.33}_{-0.23}$	$3.86^{+7.64}_{-1.28}$	$0.86^{+6.95}_{-0.79}$	$1.55^{+0.28}_{-0.18}$	$0.02^{+0.11}_{-0.01}$
$P_{\rm pt}(k)$ with floating β	$0.86^{+0.12}_{-0.09}$	$-0.08^{+0.04}_{-0.04}$	$1.17^{+0.20}_{-0.12}$	$-0.11^{+0.07}_{-0.08}$	$2.57^{+0.57}_{-0.33}$	$-0.22^{+0.17}_{-0.21}$	$1.38^{+0.16}_{-0.11}$	$-0.13^{+0.06}_{-0.07}$
$P_{\rm pt}(k)$ with $\beta = 0.0$	$0.91^{+0.13}_{-0.10}$	$-0.02^{+0.01}_{-0.02}$	$1.20^{+0.20}_{-0.12}$	$-0.07^{+0.03}_{-0.05}$	$2.65^{+0.53}_{-0.33}$	$-0.14^{+0.10}_{-0.16}$	$1.45^{+0.20}_{-0.14}$	$-0.05^{+0.03}_{-0.03}$

5 per cent variation in three different cases: using smaller bins (when we bin monopoles and quadrupoles), changing the value of streaming parameter, or changing the non-linear damping parameters. The variations when fitting using DR11 pre-reconstructed mock galaxy catalogues do not produce variations in σ_α. In a few cases, a small variation of σ_ϵ at ∼7 per cent level ($\Delta\sigma_\epsilon = 0.001/0.013$) is seen: when we switch to using smaller bin size in binning the correlation function, when we change $\Sigma_{\rm s}$ and when we apply the $P_{\rm pt}(k)$ non-linear power spectrum template.

6.3 Discussion of individual robustness tests

We will now turn to the discussion of the results of individual robustness tests and their effects. These tests are listed in Section 5 in the same order as the following discussion.

6.3.1 Model templates

Table 1 shows that when changing from the 'De-Wiggled' template to the RPT-inspired template, the best-fitting values using pre-reconstructed DR11 mock galaxy catalogues change slightly, with variations are on the order of 0.5 per cent on α, and ≤0.1 per cent on ϵ. The best-fitting values are changed by ≤0.1 per cent when we use post-reconstructed mock catalogues (Table 2). The fitted uncertainties in both pre- and post-reconstructed catalogues are well within 0.1 per cent.

In addition, the best-fitting results are slightly biased (we compare measured α to 1 and ϵ to 0 as the input cosmology of the mock catalogues is known) and the'De-Wiggled' template produces biased best-fitting values in the opposite direction ($\widetilde{\alpha} = 1.0049, \widetilde{\epsilon} = 0.0027$) when compared with bias in best-fitting values ($\widetilde{\alpha} = 0.996, \widetilde{\epsilon} = -0.002$) using $P_{\rm pt}(k)$ template. This inverted trend generates quite different results in terms of $\alpha_{||}-\alpha_\perp$ parametrization. For the 'De-Wiggled' template, the bias in best-fitting $\alpha_{||}$ reaches 1.1 per cent but only shifts the best-fitting $\alpha_\perp$ 0.2 per cent, while using $P_{\rm pt}(k)$ template produces 0.6 per cent shift in $\alpha_{||}$ and −0.3 per cent shift in $\alpha_\perp$. After reconstruction, the templates have consistent results, the bias on the best-fitting α reduces to less than 0.1 per cent for both templates and ϵ has a slightly larger bias with 'De-Wiggled' template of 0.2 per cent compared to 0.1 per cent for the $P_{\rm pt}(k)$ template.

The information in Tables 3 and 4 demonstrates that changing the of non-linear power spectrum template does not significantly affect the uncertainties on the best-fitting parameters either pre- or post-reconstruction; the changes are well within ≤0.1 per cent for all cases.

6.3.2 Fitting range and bin sizes

Anderson et al. (2013), found that the optimal fitting range for anisotropic clustering in DR9 mock galaxy catalogue is [50, 200] h^{-1} Mpc, and that using [30, 200] h^{-1} Mpc produces a more biased measurement of α and ϵ. However, we find that fitting the DR11 pre-reconstructed mock galaxy catalogues using [30, 200] h^{-1} Mpc yields less biased best-fitting values. This result is unexpected since it is the opposite of the DR9 findings (Table 1). On the other hand, the differences between using one fitting range and another are consistently small in both the DR9 (Anderson et al. 2013) and the DR11 pre-reconstructed galaxy mock catalogues. Furthermore, once we apply reconstruction to the galaxy catalogues, the differences in best-fitting values between using different fitting ranges are well within 0.1 per cent (0.3 per cent) for DR11 (DR9) (see Table 2 for more details). Applying larger fitting ranges to the post-reconstructed galaxy catalogues produces a slight increase in the bias in the best-fitting values. In particular, the bias of the best-fitting α (ϵ) is 0.06 per cent (0.1 per cent). Tables 3 and 4 show that changing the fitting range does not affect the estimated uncertainties of any of the fitted parameters both pre- and post-reconstruction. Tables 1 and 2 demonstrate that using smaller bins has a negligible effect in the best-fitting values. The variations in the errors are also small; identical results are obtained when fitting either pre- or post-reconstruction mock catalogues.

Table 5. The median variations of the fitted values and the fitted errors from DR11 reconstructed mocks for different changes relative to the fiducial fitting methodology. The variation is defined as $\Delta v = v^i - v^{\rm fid}$, where $v = \alpha, \epsilon, \alpha_\parallel, \alpha_\perp, \sigma_{||}, \sigma_\perp$ and i denotes the modification in the methodology being tested. The median variations $\widetilde{\Delta v}$, and percentiles are multiplied by 100. Note that (RL) stands for calculating the errors by integrating over specific intervals in the likelihood surfaces in α–ϵ, $\alpha = [0.8, 1.2]$ and $\epsilon = [-0.15, 0.15]$.

Model	$\widetilde{\Delta\alpha}$	$\widetilde{\Delta\sigma_\alpha}$	$\widetilde{\Delta\epsilon}$	$\widetilde{\Delta\sigma_\epsilon}$	$\widetilde{\Delta\alpha_\parallel}$	$\widetilde{\Delta\sigma_{\alpha_\parallel}}$	$\widetilde{\Delta\alpha_\perp}$	$\widetilde{\Delta\sigma_{\alpha_\perp}}$
				DR11 Post-reconstruction				
Only α prior	$1e{-}3^{+0.05}_{-0.02}$	$0.31^{+2.46}_{-0.27}$	$-0.04^{+0.14}_{-0.15}$	$0.37^{+2.90}_{-0.32}$	$-0.08^{+0.28}_{-0.26}$	$1.15^{+8.55}_{-1.09}$	$0.03^{+0.18}_{-0.14}$	$0.11^{+0.19}_{-0.06}$
Only B_0 α priors	$0.01^{+0.04}_{-0.01}$	$0.04^{+0.47}_{-0.03}$	$-0.03^{+0.13}_{-0.13}$	$0.07^{+0.65}_{-0.05}$	$-0.05^{+0.26}_{-0.23}$	$0.15^{+2.02}_{-0.19}$	$0.03^{+0.16}_{-0.12}$	$0.06^{+0.09}_{-0.04}$
Only β α priors	$-0.01^{+0.01}_{-0.01}$	$0.22^{+2.02}_{-0.21}$	$-2e{-}3^{+0.02}_{-0.03}$	$0.25^{+2.33}_{-0.23}$	$-0.01^{+0.03}_{-0.07}$	$0.86^{+6.95}_{-0.79}$	$1e{-}3^{+0.02}_{-0.02}$	$0.02^{+0.11}_{-0.01}$
No priors	$1e{-}3^{+0.05}_{-0.02}$	$0.95^{+4.61}_{-0.87}$	$-0.04^{+0.14}_{-0.15}$	$1.05^{+5.46}_{-0.95}$	$-0.08^{+0.28}_{-0.26}$	$3.28^{+15.77}_{-3.05}$	$0.03^{+0.18}_{-0.14}$	$0.13^{+0.37}_{-0.08}$
Only B_0 prior	$0.01^{+0.04}_{-0.01}$	$0.07^{+0.91}_{-0.05}$	$-0.03^{+0.13}_{-0.13}$	$0.09^{+1.11}_{-0.08}$	$-0.05^{+0.26}_{-0.23}$	$0.24^{+3.48}_{-0.28}$	$0.03^{+0.16}_{-0.12}$	$0.07^{+0.12}_{-0.04}$
Only β prior	$-0.01^{+0.01}_{-0.01}$	$0.73^{+4.53}_{-0.68}$	$-2e{-}3^{+0.02}_{-0.03}$	$0.84^{+5.15}_{-0.77}$	$-0.01^{+0.03}_{-0.07}$	$2.67^{+15.15}_{-2.45}$	$1e{-}3^{+0.02}_{-0.02}$	$0.03^{+0.29}_{-0.02}$
No priors(RL)	$1e{-}3^{+0.05}_{-0.02}$	$0.03^{+0.10}_{-0.02}$	$-0.04^{+0.14}_{-0.15}$	$0.07^{+0.22}_{-0.05}$	$-0.08^{+0.28}_{-0.26}$	$0.11^{+0.72}_{-0.14}$	$0.03^{+0.18}_{-0.14}$	$0.07^{+0.10}_{-0.04}$
Only B_0 prior(RL)	$0.01^{+0.04}_{-0.01}$	$0.03^{+0.08}_{-0.02}$	$-0.03^{+0.13}_{-0.13}$	$0.05^{+0.16}_{-0.03}$	$-0.05^{+0.26}_{-0.23}$	$0.07^{+0.51}_{-0.13}$	$0.03^{+0.16}_{-0.12}$	$0.05^{+0.08}_{-0.03}$
Only β prior(RL)	$-0.01^{+0.01}_{-0.01}$	$2e{-}3^{+0.01}_{-0.00}$	$-2e{-}3^{+0.02}_{-0.03}$	$0.02^{+0.03}_{-0.01}$	$-0.01^{+0.03}_{-0.07}$	$0.03^{+0.07}_{-0.02}$	$1e{-}3^{+0.02}_{-0.02}$	$0.01^{+0.02}_{-0.01}$
β B_0	$<1e{-}4^{<+1e-4}_{<-1e-4}$	$0.01^{+0.20}_{-0.01}$	$<1e{-}4^{<+1e-4}_{<-1e-4}$	$0.01^{+0.25}_{-0.01}$	$<1e{-}4^{<+1e-4}_{<-1e-4}$	$0.03^{+0.85}_{-0.03}$	$<1e{-}4^{<+1e-4}_{<-1e-4}$	$1e{-}3^{+0.01}_{-1e-3}$
β ϵ B_0	$<1e{-}4^{<+1e-4}_{<-1e-4}$	$2e{-}3^{+2e-3}_{-1e-3}$	$<1e{-}4^{<+1e-4}_{<-1e-4}$	$<1e{-}4^{+1e-3}_{-0.00}$	$<1e{-}4^{<+1e-4}_{<-1e-4}$	$1e{-}3^{+5e-3}_{-1e-3}$	$<1e{-}4^{<+1e-4}_{<-1e-4}$	$1e{-}3^{+1e-3}_{-1e-3}$
Only ϵ	$1e{-}3^{+0.05}_{-0.02}$	$0.03^{+0.13}_{-0.02}$	$-0.04^{+0.14}_{-0.15}$	$0.07^{+0.24}_{-0.05}$	$-0.08^{+0.28}_{-0.26}$	$0.12^{+0.77}_{-0.15}$	$0.03^{+0.18}_{-0.14}$	$0.07^{+0.10}_{-0.04}$
ϵ B_0	$0.01^{+0.04}_{-0.01}$	$0.03^{+0.09}_{-0.02}$	$-0.03^{+0.13}_{-0.13}$	$0.05^{+0.17}_{-0.03}$	$-0.05^{+0.26}_{-0.23}$	$0.08^{+0.58}_{-0.13}$	$0.03^{+0.16}_{-0.12}$	$0.05^{+0.08}_{-0.03}$
ϵ β	$-0.01^{+0.01}_{-0.01}$	$2e{-}3^{+0.02}_{-5e-3}$	$-2e{-}3^{+0.02}_{-0.03}$	$0.02^{+0.04}_{-0.01}$	$-0.01^{+0.03}_{-0.07}$	$0.03^{+0.09}_{-0.02}$	$0.1e{-}3^{+0.02}_{-0.02}$	$0.01^{+0.02}_{-0.01}$

6.3.3 Nuisance terms model

The effects of the broad-band modelling are most prominent when one examines the best-fitting values on post-reconstruction mock galaxy catalogues as shown in Tables 1 and 2. The fiducial fitting methodology uses three terms, providing relatively unbiased best-fitting values of α and ϵ. For the pre-reconstructed galaxy catalogues, biases of best-fitting values are $\leq$0.5 per cent. For post-reconstructed galaxy catalogs, the best-fitting values are only biased by $\leq$0.2 per cent. Varying the number of terms included in the broad-band modelling produces little effect on the best-fitting values using pre-reconstructed mock galaxy catalogues. When we use post-reconstructed mock galaxy catalogues increasing the number of terms removes the bias of best-fitting ϵ completely, while decreasing the number of terms in the broad-band modelling to two-terms increases the bias of the best-fitting ϵ by 0.3 per cent.

6.3.4 Priors

Tables 1 and 2 show that the application of different priors has a large effect on uncertainties of the best-fitting values, especially on the uncertainties in the best-fitting ϵ. For example, applying the fiducial methodology to DR11 pre-reconstruction mock galaxy catalogues produces median variations of $\Delta\alpha \sim 0.001$, $\Delta\epsilon \leq 0.002$. These increase to $\Delta\alpha \sim 0.002$ and $\Delta\epsilon \leq 0.004$ when we apply the same methodology to post-reconstruction mock catalogues. In addition, a large dispersion is observed in σ_α and σ_ϵ among the results where we apply fitting to reconstructed mock galaxy catalogues. The large dispersion observed is also quite obvious in the dispersion plots in Figs 6 and 7 for DR11. The presence of 'column' structures in the dispersion plot indicates the large difference between some of the mocks.

In order to explore the origin of these large variations and dispersions, we expand our investigation into the priors-related cases using DR11 post-reconstructed mock catalogues. The results are listed in Table 5. In addition to test cases shown in previous Tables (No priors, only β, and only B_0), we add similar cases with an α prior (discussed in Sections 5 and 5.4.4) and ϵ prior (Sections 5 and 5.4.3). We also include the same test cases where a large fluctuation is observed, but we restrict our integration intervals in the likelihood surfaces when the uncertainties are calculated for the best-fitting parameters. We choose the range for our integration intervals by restricting ourselves to the fitting ranges, limiting α and ϵ to ranges which would not lead us outside our fitting range of [50,200] h^{-1} Mpc. These cases are denoted as 'Range Limited' (RL). The reason for these RL cases will be discussed later. When we apply β and B_0 prior without any α or ϵ prior, the fitting of DR11 post-reconstructed data produces 1.4 per cent rms for ϵ, compared to 1.3 per cent when we include the α and ϵ priors.

Given the strong dependence of our fit on the various priors, we examine the 2D $\Delta\chi^2$ surfaces of α and ϵ. Fig. 8 shows that the 2D likelihood surfaces are highly degenerate along the $\alpha = 1 + \epsilon$ direction. The long tail when we do not apply all of the priors corresponds to large variations in $\alpha_{||}$ and small variations in $\alpha_\perp$. The variations in $\alpha_{||}$ for the extreme cases are of order $(1.25)^3$. In other words, these cases correspond to places where the acoustic peak along the LOS has been shifted out of our [50–200] h^{-1} Mpc fitting range. The asymmetry towards small α, ϵ refers to the case when the peak shifts to larger apparent scale. One should not be surprised that when the data lacks a good acoustic peak along the LOS, the fitter can place one at a huge scale, beyond our fitted range of correlation function scales. This feature motivates placing a bound on ϵ, which is not a cosmological prior.

We propose to examine the effects of integrating over a range (with flat priors) in both α and ϵ to calculate uncertainties on these parameters. We adopt an integration interval of $\alpha = [0.8, 1.2]$ and $\epsilon = [-0.15, 0.15]$, which corresponds to a maximum dilation of $\sim$1.7. This forces the peak to be contained within our fitted domain. such cases are presented as 'RL' in Table 5. With the limited range of integration, the fitted uncertainties are extremely stable with or without the application of any other priors. Thus, we adopt these intervals as the standard integration intervals in all

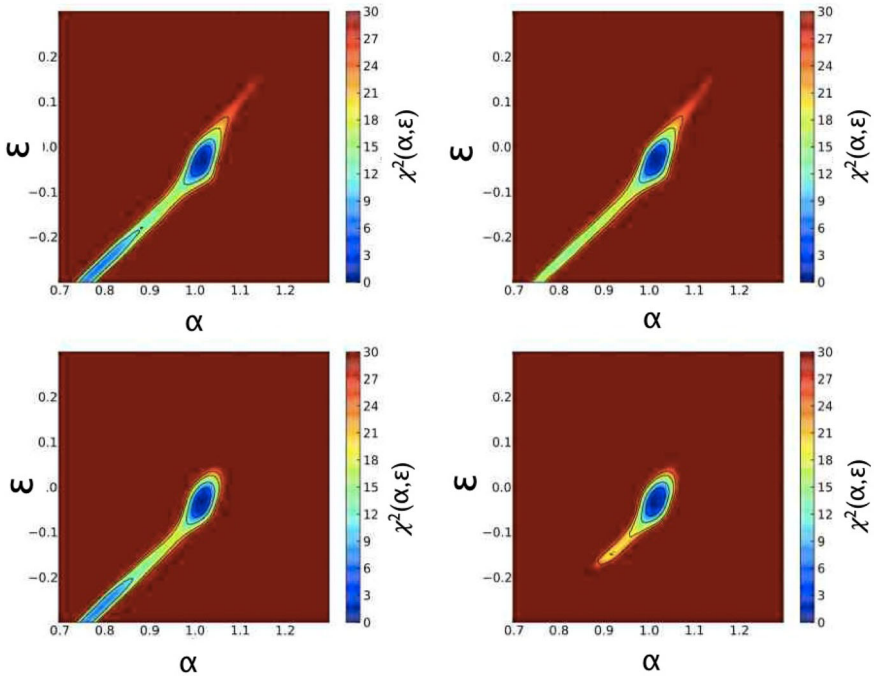

Figure 8. Contours plots of $\Delta\chi^2(\alpha,\epsilon)$. Top-left panel shows the $\Delta\chi^2(\alpha,\epsilon)$ when no priors are applied in the fitting methodology on DR11 post-reconstructed CMASS data set, the top-right panel applies only B_0 prior, the bottom-left panel applies only β prior, and the bottom right utilizes all priors.

uncertainties quoted in Anderson et al. (2014). This integration interval is merely used to set a quoted error; it does not change the likelihood surface and the full likelihood surface of the anisotropic fitting is used for all cosmological analysis in Anderson et al. (2014).

6.3.5 *Interdependence between* $\Sigma_{||,\perp}$, Σ_s *and* ϵ

We measure a variation of 0.3 per cent in the median of ϵ when the values of $\Sigma_{||\perp}$ and Σ_s are modified and measure a variation in ϵ around 0.1 per cent when we change $\Sigma_s = 1.5 \rightarrow 3.0$. Changes in Σ_{NL} values affect the quadrupole because we are not changing the overall value of Σ_{NL} just the relative contribution of the components ($\Sigma_{||,\perp}$). In particular, we change anisotropic values, $\Sigma_{||} = 11$ and $\Sigma_\perp = 6\,\mathrm{Mpc}\,h^{-1}$ to isotropic values and set $\Sigma_{||} = \Sigma_\perp = 8\,\mathrm{Mpc}\,h^{-1}$ post-reconstruction. Thus, the effect is best described as lowering the contrast in the crest–trough structure. For Σ_s, we increase the streaming value and thereby enhance the crest–trough structure. These parameters are degenerate, the results in Table 3 suggest that reducing this contrast in the structure of the quadrupole when fitting the pre-reconstructed mock catalogues decreases the observed biases in best-fitting parameters.

Results in Table 4 show that changes in values of $\Sigma_{||,\perp}$ do not have any effect on best-fitting values or fitted errors for the post-reconstructed mock catalogue analysis. The negligible effect post-reconstruction is not surprising as reconstruction is designed to eliminate most of the quadrupole at large scales. The residuals between our model of the non-linear correlation function that includes the RSD and the reconstructed correlation functions, should be smaller than pre-reconstruction correlation functions. The effect of a large Σ_s is not surprising either, as this large value of the streaming is unrealistic for reconstructed mocks, thus an artificial enhancement of the crest–trough structure should give a poorer match to the measured multipoles. The effects of the $\Sigma_{||,\perp,s}$ on the best-fitting values indicate that calibration of these parameters is important for improving the performance of the fitting methodology. The residual mismatch is compensated by systematic polynomials. However, as we explained in Section 6.3.3, the order of the polynomials introduces also extra variations in best-fitting values pre- and post-reconstruction. We leave the interplay between the broad-band terms and the non-linear damping and streaming parameters to a future study.

6.3.6 *Covariance matrix corrections*

This section presents the results including all covariance corrections described Section 5. We measure the systematic error introduced in the results by not applying the correction for the overlapping region in the mock generation. We quantify the effect in DR10 and DR11 to integrate this error into our previous results that do not consider this defect of the mocks. Table 6 presents the median and rms observed when including the correction factors A, B, C and r (described in Section 5) pre- and post-reconstruction for the two templates, 'De-Wiggled' and $P_{pt}(k)$. We do not include the m_1 factor. The final result should be still rescaled by $\sqrt{m_1}$ as shown by equation (30). This factor has a value of 1.0198 for DR10 and 1.0221 for DR11.

We do not find any variation in the best-fitting values of α and ϵ in all cases, which is to be expected since these corrections only change the covariance matrices. We do (as expected) observe variations on the uncertainties of best-fitting ϵ when we apply the covariance corrections to pre-reconstructed mock galaxy catalogues.

6.3.7 *Effect of grids sizes in the likelihood surface*

Table 7 summarizes the results for tests performed for the four different data sets varying the grid-size and fixing the range for the α and ϵ grid to [0.7, 1.3] and [−0.3, 0.3], respectively. Table 7 shows the σ_α and σ_ϵ as well as the mean α ($\langle\alpha\rangle$) and mean ϵ ($\langle\epsilon\rangle$) when varying the number of grid points in α (n_α), and, in ϵ (n_ϵ).

Table 6. A comparison of fitting results in DR11 mock galaxy catalogues including both covariance corrections and the correction for overlapping regions of mocks (CC) versus not including any of those corrections. The median bias $\widetilde{b}$, median errors $\widetilde{\Delta\sigma}$, and percentiles are multiplied by 100.

Model	$\widetilde{b_\alpha}$	$\widetilde{\sigma_\alpha}$	$\widetilde{b_\epsilon}$	$\widetilde{\sigma_\epsilon}$	$\widetilde{b_\parallel}$	$\widetilde{\sigma_{\alpha_\parallel}}$	$\widetilde{b_\perp}$	$\widetilde{\sigma_{\alpha_\perp}}$
Pre−reconstruction. NoCC	$0.49^{+1.42}_{-1.56}$	$1.57^{+0.37}_{-0.23}$	$0.27^{+1.66}_{-1.81}$	$1.86^{+0.51}_{-0.24}$	$1.07^{+4.04}_{-4.13}$	$4.38^{+1.33}_{-0.69}$	$0.18^{+2.13}_{-2.03}$	$2.11^{+0.38}_{-0.22}$
Pre−reconstruction CC	$0.51^{+1.41}_{-1.59}$	$1.44^{+0.34}_{-0.21}$	$0.26^{+1.65}_{-1.82}$	$1.69^{+0.44}_{-0.21}$	$1.08^{+4.02}_{-4.17}$	$3.97^{+1.19}_{-0.62}$	$0.17^{+2.13}_{-2.03}$	$1.93^{+0.33}_{-0.20}$
Post−reconstruction CC	$-0.02^{+0.94}_{-0.84}$	$0.86^{+0.12}_{-0.10}$	$0.15^{+1.25}_{-1.13}$	$1.17^{+0.22}_{-0.13}$	$0.29^{+2.72}_{-2.48}$	$2.57^{+0.58}_{-0.37}$	$-0.08^{+1.36}_{-1.59}$	$1.39^{+0.19}_{-0.14}$
Post−reconstruction. No CC	$-0.02^{+0.94}_{-0.84}$	$0.93^{+0.13}_{-0.11}$	$0.16^{+1.24}_{-1.16}$	$1.28^{+0.24}_{-0.14}$	$0.29^{+2.72}_{-2.47}$	$2.80^{+0.64}_{-0.41}$	$-0.09^{+1.36}_{-1.59}$	$1.51^{+0.21}_{-0.15}$

Table 7. Uncertainties on the best-fitting values when varying the bin size of the grids for a fixed interval of $\alpha = [0.8,1.2]$.

n_α/n_ϵ	σ_α	σ_ϵ	$\sigma_{\alpha,\epsilon}$	$\langle\alpha\rangle$	$\langle\epsilon\rangle$
DR10 Pre-reconstruction					
121/61	0.0229	0.0441	0.000 62	1.006	−0.027
241/121	0.0229	0.0440	0.000 61	1.006	−0.027
401/201	0.0229	0.0441	0.000 61	1.006	−0.027
DR10 Post-reconstruction					
121/61	0.0112	0.0233	0.000 54	1.018	−0.012
241/121	0.0112	0.0233	0.000 54	1.018	−0.012
401/201	0.0112	0.0233	0.000 54	1.018	−0.012
DR11 Pre-reconstruction					
121/61	0.0192	0.0360	0.000 47	1.021	−0.015
241/121	0.0192	0.0375	0.000 47	1.021	−0.015
401/201	0.0192	0.0376	0.000 47	1.021	−0.015
DR11 Post-reconstruction					
121/61	0.0108	0.0186	0.000 13	1.011	−0.036
241/121	0.0108	0.0186	0.000 13	1.011	−0.036
401/201	0.0108	0.0186	0.000 13	1.011	−0.036

We test three different $n_\alpha = (401, 241$ and $121)$, which correspond to $\Delta_\alpha = 0.0015, 0.0025$ and 0.005, and test three different $n_\epsilon = 61$, 121, 241, that correspond to $\Delta\epsilon = 0.01, 0.005, 0.0025$. The results show that variations on these parameters do not have any effect in the estimation of the best-fitting values or their respective uncertainties from the likelihood surfaces.

7 COMPARISON WITH OTHER METHODOLOGIES

We compare the methodology followed in this work with previously published methodologies. We describe first the methodologies explored in this section and then enumerate the main differences.

(i) *Multipoles-Gridded (hereafter Multip. Grid)*. This is our fiducial fitting methodology, which is described extensively in Section 4.3. We adopt the non-linear template RPT-inspired $P_{\rm pt}(k)$ described in Section 4.1.2, instead of the fiducial De-Wiggled template, to make a fair comparison with the others methodologies.

(ii) *Multipoles-MCMC (hereafter Multip. MCMC)*. This approach follows the multipoles-fitting methodology combined with a Monte Carlo Markov Chain sampling of the posterior in $\alpha_{||}$, $\alpha_\perp$, while marginalizing over all the remaining parameters. The template for the non-linear power spectrum is $P_{\rm pt}(k)$ as described in Section 4.1.2.

(iii) *Clustering Wedges (hereafter Wedges)*. Described previously in Section 2.2.2, the Wedges analysis consists of an alternative set of moments; for a detailed description, please refer to Kazin et al. (2012), Kazin et al. (2013). This methodology also samples the posterior using Multip. MCMC in the $\alpha_{||}-\alpha_\perp$ parametrization. The template for the non-linear power spectrum is also the RPT-inspired template, $P_{\rm pt}(k)$, described in Section 4.1.2.

The main differences between the methodologies listed above are as follows.

(i) The Multip. MCMC and the Wedges approaches have in common that the parametrization is in $\alpha_{||}$–$\alpha_\perp$ instead of α–ϵ of the Multip. Grid method.

(ii) The sampling of the posterior is generated with an MCMC instead of our grid approach.

(iii) Both Multip. MCMC and Wedges apply flat priors on $\alpha_{||}$ and $\alpha_\perp$, compared with a Gaussian prior on ϵ and α.

(iv) There is a difference in the model, Wedges and Mutlip. MCMC methodologies fix β and include a normalization factor in quadrupole, $rB_\perp$:

$$\begin{aligned}\xi_\perp(r) &= B_\perp\xi_{0,\perp}(r) + A_\perp(r)\\ \xi_{||}(r) &= rB_\perp\xi_{0,||}(r) + A_{||}(r).\end{aligned} \tag{36}$$

(v) There is a difference in the quoted values. We use the best-fitting values for Multip. Grid method whereas the mean values are adopted for Multip. MCMC and Wedges.[4] Regarding uncertainties, the values of σ for Multip. MCMC correspond to the symmetrized percentiles and for Multip.Grid method uses the rms from the likelihoods.

We fitted the 600 mocks using these three different methodologies and compare the fitted parameters and errors. For this test, we considered the full covariance matrix corrections. The tests were performed for DR10/DR11 in the pre- and post-reconstructed mocks, but for clarity we only quoted DR11 results. Also in this section, we use the $\alpha_{||,\perp}$ parametrization to compare the techniques, as the other two methodologies use this parametrization.

7.1 Results from the mocks

Table 8 shows the median and standard deviation of the best-fitting values and errors estimated with the results of the mocks for the three methodological choices. In the pre-reconstruction mocks, we found small variations in the bias between methodologies but there is no indication that one methodology is more biased with respect to the others. For DR11, the biases are $|b_{||}| \leq 0.6$ per cent and $|b_\perp| \leq 0.4$ per cent. For the post-reconstruction mocks, the three variations in methodology produce consistent results; the bias is less than 0.3 per cent for $\alpha_{||,\perp}$.

[4] For Multip. MCMC, the mean values and the best-fitting values are similar but not identical, between them, the mean values are the most robust estimator. The contrary happens for the Multip. Grid method; the best values are more robust and the mean values are poor estimates of the parameters for low signal to noise ratio BAO features.

Table 8. The fitting results on $\alpha_{||}$ and $\alpha_{\perp}$ and their respective errors when different anisotropic clustering fitting methodologies are used on different mock galaxy catalogues (DR10, DR11, pre- and post-reconstruction). We present median values since median values are more representative of the skewed σ distributions and slightly asymmetric $\alpha_{\parallel}$ pre-reconstruction distributions.The columns are the median values of the bias $b_{\alpha,\epsilon,||,\perp}$, median values of errors on $\alpha_{||}$, $\alpha_{\perp}$ ($\widetilde{\sigma_{\alpha_{||},\alpha_{\perp}}}$), the standard deviation of α, ϵ, $\alpha_{||}$, $\alpha_{\perp}$, ($S_{\alpha,\epsilon,\alpha_{||},\alpha_{\perp}}$), and finally the standard deviation of the errors $S_{\sigma_{\alpha_{||},\alpha_{\perp}}}$. The median bias, the median values of the errors $\widetilde{\Delta v}$, and the standard deviations are multiplied by 100.

Method	$\widetilde{b_{\alpha}}$	S_{α}	$\widetilde{b_{\epsilon}}$	S_{ϵ}	$\widetilde{b_{\alpha_{\parallel}}}$	$S_{\alpha_{\parallel}}$	$\widetilde{\sigma_{\alpha_{\parallel}}}$	$S_{\sigma_{\alpha_{\parallel}}}$	$\widetilde{b_{\alpha_{\perp}}}$	$S_{\alpha_{\perp}}$	$\widetilde{\sigma_{\alpha_{\perp}}}$	$S_{\sigma_{\alpha_{\perp}}}$
DR11 Post-reconstruction												
Multip. Grid	0.02	0.92	0.11	1.22	0.32	2.66	2.48	0.72	−0.01	1.49	1.37	0.18
Multip. MCMC	0.00	0.89	0.15	1.12	0.19	2.47	2.73	0.55	−0.11	1.39	1.48	0.22
Wedges	0.03	0.90	0.05	1.24	0.06	2.64	2.96	0.52	−0.07	1.53	1.61	0.26
DR11 Pre-reconstruction												
Multip. Grid	−0.05	1.55	0.22	1.89	0.58	4.43	3.84	1.50	−0.35	2.10	2.04	0.32
Multip. MCMC	−0.08	1.54	0.03	2.06	0.17	4.82	4.29	2.26	−0.18	2.15	2.22	0.47
Wedges	−0.09	1.52	−0.11	2.07	−0.35	4.75	4.66	1.37	0.07	2.22	2.30	0.86
DR10 Post-reconstruction												
Multip. Grid	0.15	1.26	0.04	1.53	0.28	3.38	3.17	1.25	0.04	1.92	1.73	0.28
Multip. MCMC	0.20	1.27	−0.00	1.50	0.05	3.46	3.30	2.21	0.13	1.82	1.85	0.38
Wedges	0.21	1.19	−0.15	1.53	−0.03	3.35	3.62	0.88	0.37	1.88	1.93	0.42
DR10 Pre-reconstruction												
Multip. Grid	−0.25	1.92	0.25	2.54	0.27	5.86	4.98	2.40	−0.31	2.69	2.60	0.73
Multip. MCMC	−0.10	2.07	−0.02	3.11	−0.25	7.52	5.04	4.09	−0.07	2.98	2.72	1.37
Wedges	−0.17	1.99	−0.23	2.94	−0.46	6.66	5.50	3.47	0.05	3.07	2.83	1.88

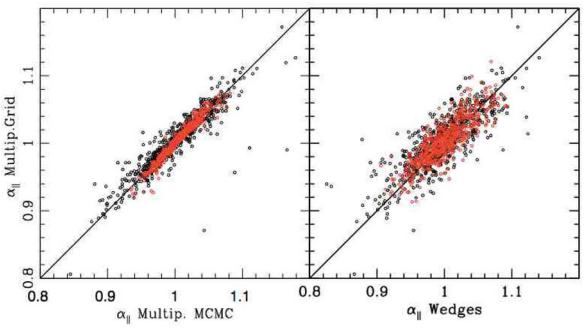

Figure 9. Dispersion plots of $\alpha_{||}$, pre [black] and post-reconstruction [red] using different methodologies. The left-hand panel compares multipoles using Multip. Grid and Multip. MCMC approaches, and right-hand panel compares Gid and Wedges.

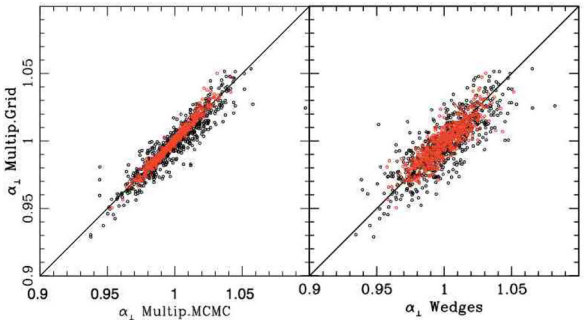

Figure 10. Dispersion plots of $\alpha_{\perp}$, pre- [black] and post-reconstruction [red] using different methodologies. The left-hand panel compares multipoles using Multip. Grid and Multip. MCMC, and right-hand panel compares Multip. Grid and Wedges.

The second observation is that the rms of α and the median and rms of σ are consist across the three methods. The agreement is even better post-reconstruction, but there are small differences in their values. In this section, we explore the small discrepancies observed between the three methodological choices.

Figs 9 and 10 show the dispersion plots of $\alpha_{||}$ and $\alpha_{\perp}$, pre- and post-reconstruction using different methodologies for DR11. The left-hand panel compares Multip. MCMC and Wedges, and right-hand panel compares Multip. MCMC and Multip. Grid methods. In general, the two dispersion plots show a good correspondence between different methodologies. There is, however, some dispersion in the parallel direction that decreases post-reconstruction.

To perform a quantitative comparison of the differences, we estimate the median variation, where we define the variation as

$$\Delta\alpha_{||,\perp} = \alpha_{||,\perp}^{\text{Method a}} - \alpha_{||,\perp}^{m}. \quad (37)$$

To quantify the dispersion we show the 16th and 84th percentiles of the variation. The comparisons discern the contributions of the discrepancy observed between the three methodological choices. Table 9 summarizes the median difference and dispersion observed between the methodologies in the fitted parameters and fitted errors.

7.1.1 *Comparison of Multip. MCMC and Multip. Grid approaches*

This section compares the two Multipoles approaches, MCMC and Grid. We first consider the results of fitting to the pre-reconstruction mock catalogues. Table 9, demonstrates that the median difference is small, $|\widetilde{\alpha_{||,\perp}}| \leq 0.003$. The observed dispersion is ∼0.013 in the parallel direction and 0.007 in the perpendicular direction. The dispersion of the Multip. MCMC-Multip.Grid is illustrated in the right-hand panels of Figs 9 and 10 for the parallel and perpendicular directions.

The post-reconstruction mocks possess smaller dispersion and median differences. The median difference is zero for both $\alpha_{||,\perp}$ and the dispersion is almost half of the value pre-reconstruction. The dispersion in $\alpha_{||}$ is only 0.004 and in $\alpha_{\perp}$ is 0.002. The smaller

Table 9. Dispersion observed between the different methodologies in the fitted parameters and fitted errors. We define the variation $\Delta\alpha_{||,\perp,\alpha,\epsilon} = \alpha^{\text{Method a}}_{||,\perp,\alpha,\epsilon} - \alpha^{\text{Method b}}_{||,\perp,\alpha,\epsilon}$. The columns show the median variation and the 16th and 84th percentiles. The median values $\widetilde{\Delta v}$, and percentiles are multiplied by 100

Model	$\widetilde{\Delta\alpha}$	$\widetilde{\Delta\epsilon}$	$\widetilde{\Delta\alpha_{\parallel}}$	$\widetilde{\Delta\sigma_{\alpha_{\parallel}}}$	$\widetilde{\Delta\alpha_{\perp}}$	$\widetilde{\Delta\sigma_{\alpha_{\perp}}}$
DR11 Post-reconstruction						
Multip. Grid-Multip.MCMC	$0.02^{+0.08}_{-0.07}$	$-0.02^{+0.21}_{-0.19}$	$-0.02^{+0.44}_{-0.38}$	$-0.22^{+0.35}_{-0.36}$	$0.04^{+0.21}_{-0.20}$	$-0.11^{+0.12}_{-0.13}$
Multip. Grid-Wedges	$0.02^{+0.18}_{-0.21}$	$0.14^{+0.69}_{-0.71}$	$0.27^{+1.32}_{-1.37}$	$-0.46^{+0.46}_{-0.39}$	$-0.11^{+0.75}_{-0.73}$	$-0.24^{+0.14}_{-0.18}$
Multip. MCMC-Wedges	$-0.01^{+0.16}_{-0.18}$	$0.12^{+0.70}_{-0.64}$	$0.23^{+1.31}_{-1.27}$	$-0.24^{+0.19}_{-0.17}$	$-0.15^{+0.69}_{-0.72}$	$-0.14^{+0.09}_{-0.10}$
DR11 Pre-reconstruction						
Multip. Grid-Multip.MCMC	$-0.02^{+0.40}_{-0.47}$	$0.16^{+0.60}_{-0.59}$	$0.32^{+1.17}_{-1.29}$	$-0.39^{+0.58}_{-0.59}$	$-0.17^{+0.70}_{-0.75}$	$-0.21^{+0.23}_{-0.24}$
Multip. Grid-Wedges	$-0.02^{+0.57}_{-0.47}$	$0.37^{+1.04}_{-1.31}$	$0.72^{+2.26}_{-2.61}$	$-0.77^{+0.75}_{-0.78}$	$-0.40^{+1.40}_{-1.13}$	$-0.28^{+0.26}_{-0.33}$
Multip. MCMC-Wedges	$0.06^{+0.28}_{-0.31}$	$0.18^{+1.00}_{-1.01}$	$0.38^{+1.99}_{-2.09}$	$-0.40^{+0.33}_{-0.35}$	$-0.14^{+0.98}_{-0.97}$	$-0.08^{+0.17}_{-0.20}$
DR10 Post-reconstruction						
Multip. Grid-Multip.MCMC	$-0.03^{+0.11}_{-0.15}$	$0.06^{+0.30}_{-0.26}$	$0.08^{+0.65}_{-0.52}$	$-0.10^{+0.65}_{-0.49}$	$-0.13^{+0.27}_{-0.25}$	$-0.12^{+0.18}_{-0.19}$
Multip. Grid-Wedges	$-0.06^{+0.26}_{-0.25}$	$0.20^{+0.87}_{-0.88}$	$0.32^{+1.70}_{-1.81}$	$-0.37^{+0.65}_{-0.66}$	$-0.21^{+0.84}_{-0.97}$	$-0.20^{+0.21}_{-0.26}$
Multip. MCMC-Wedges	$-0.01^{+0.21}_{-0.21}$	$0.15^{+0.79}_{-0.89}$	$0.27^{+1.56}_{-1.74}$	$-0.31^{+0.24}_{-0.28}$	$-0.16^{+0.88}_{-0.85}$	$-0.08^{+0.13}_{-0.15}$
DR10 Pre-reconstruction						
Multip. Grid-Multip.MCMC	$-0.07^{+0.79}_{-0.74}$	$0.18^{+1.00}_{-1.01}$	$0.28^{+2.30}_{-2.07}$	$-0.10^{+1.00}_{-0.89}$	$-0.32^{+1.25}_{-1.04}$	$-0.13^{+0.35}_{-0.40}$
Multip. Grid-Wedges	$0.02^{+0.81}_{-0.82}$	$0.35^{+1.44}_{-1.50}$	$0.74^{+2.92}_{-3.30}$	$-0.48^{+1.31}_{-1.08}$	$-0.37^{+1.56}_{-1.57}$	$-0.18^{+0.39}_{-0.50}$
Multip. MCMC-Wedges	$0.06^{+0.41}_{-0.34}$	$0.23^{+1.20}_{-1.25}$	$0.45^{+2.48}_{-2.41}$	$-0.38^{+0.54}_{-0.56}$	$-0.13^{+1.25}_{-1.20}$	$-0.06^{+0.26}_{-0.26}$

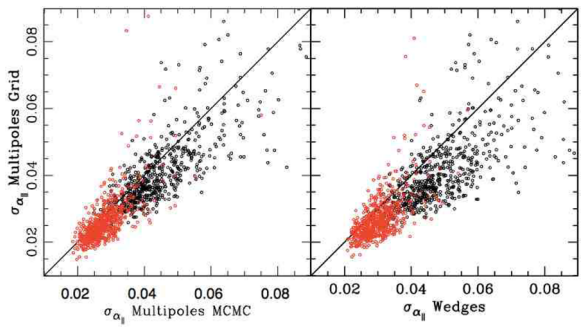

Figure 11. Dispersion plots of $\sigma_{||}$ pre- [black] and post-reconstruction [red] using different methodologies. The left-hand panel compares multipoles using Multip. MCMC approach and Multip. Grid, and the right-hand panel compares Multip. Grid and Wedges.

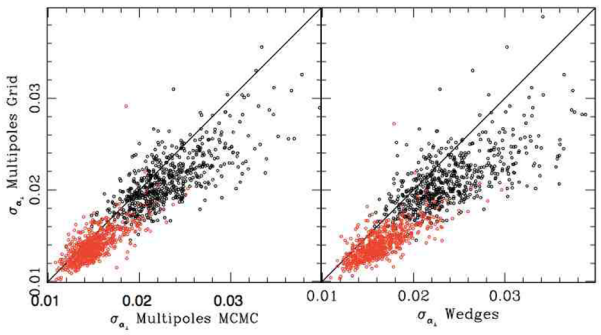

Figure 12. Dispersion plots of $\sigma_{\perp}$, pre [black] and post-reconstruction [red] using different methodologies. Left-hand panel compares multipoles using Multip. MCMC approach and Multip. Grid, and right-hand panel compare Multip. Grid and Wedges.

dispersion post-reconstruction is also clearly observed in the dispersion plots (see Figs 9 and 10).

Concerning the fitted errors, Figs 11 and 12 show the dispersion plots for $\sigma_{||}$[left], and $\sigma_{\perp}$[right] comparing Multip. MCMC and Multip.Grid results pre- and post-reconstruction for DR11. The figures demonstrate that the errors are well correlated for the two methodologies, although there is some level of dispersion. The dispersion is mostly observed in the parallel direction, and the dispersion decreases significantly post-reconstruction.

The actual values we obtained from the pre-reconstructed mocks are for the median variation $\widetilde{\Delta\sigma_{||}} = -0.004$ with 0.006 dispersion and $\widetilde{\Delta\sigma_{\perp}} = -0.002$ with ∼0.003 dispersion. Post-reconstruction, the mocks have smaller variations and dispersion levels. The median differences and dispersions are approximately half of the pre-reconstruction values, $\widetilde{\sigma_{||}} = -0.002$ with 0.004 dispersion and $\widetilde{\sigma_{\perp}} = -0.001$ with 0.001 dispersion.

To conclude, there is good agreement between the Multip. MCMC and Multip. Grid methodologies, although there remains a small level of scatter. The discrepancies could be explained by the slight differences in the implementations (and codes).

7.1.2 Comparing wedges and multipoles methodologies

We focus on the comparison between Multip. Grid and Wedges methodology. Table 9 shows that for DR11 pre-reconstruction the median difference is $\Delta\alpha_{||} = -0.007^{+0.023}_{-0.026}$ and $\Delta\alpha_{\perp} = +0.004^{+0.014}_{-0.011}$. If we compare this result with the row corresponding to Wedges-Multip. MCMC ($\Delta\alpha_{||} = -0.004^{+0.020}_{-0.021}$ and $\Delta\alpha_{\perp} = +0.001^{+0.010}_{-0.010}$), we observe the majority of the scatter is related to the difference in estimators used; however, the median difference is larger for Multip. Grid-Wedges compared to the Wedges-Multip. MCMC case. This indicates two sources of the discrepancy: the difference in estimators and the remaining methodological differences. In mocks post-reconstruction, the median differences and scatter are only determined by the difference in estimators, the

remaining methodological differences are not contributing to the dispersion or increasing the median difference.

For the uncertainties, the difference in estimator and the remaining methodological differences are contributing at the same level to the dispersion, but the median differences have closer values indicating that the difference in errors is primarily related to the difference in estimator. The post-reconstruction mocks have two contributions in the median difference and dispersion of the errors. The median variations of the errors in Wedges-Multip. Grid is two times higher than the with Wedges-Multip. MCMC, and the dispersion in Wedges-Multip. Grid is twice the scatter in Wedges-Multip. MCMC.

Summarizing, the median differences in the best-fitting values and in their errors between Wedges and Multip. Grid methods post-reconstruction are $\Delta\alpha_{||,\perp} \leq 0.003$ for the fitted parameters and $\Delta\sigma_{||,\perp} \leq 0.005$ for the errors. The small discrepancies could be explained by the way the priors impact the different estimators.

8 RESULTS WITH THE DATA

8.1 Robustness test on data

In this section, we present the results of applying the same robustness tests applied to the mocks to the DR11 CMASS data described in Section 3.3. For these tests, we apply all covariance corrections described in Section 5.7.

The results of the robustness test on data are summarized in Table 10 for DR11 post-reconstruction. The first line lists the best α and ϵ values as well as the corresponding $\alpha_{||}$ and $\alpha_{\perp}$ with their respective errors and the χ^2/d.o.f. of the fit for the fiducial case. The remaining lines of Table 10 present the difference between fitted values or errors with respect to the fiducial case $\Delta v = v - v^{\rm fid}$.

First, we consider variations in best-fitting α due to changes in the fitting methodology; the largest variations observed are at 0.2 per cent level when the range of fitting is changed, regardless of template used. Small variations at the 0.1 per cent level are observed in a few cases, such as when the order of the systematic polynomials is changed, when we eliminate all priors and when we fix the β for $P_{\rm pt}(k)$ template uniquely. All these cases agree with the behaviour observed when the robustness tests are applied to mock galaxy catalogues, as discussed in Section 6.

The variations in best-fitting value of ϵ are $\leq$0.3 per cent, with two exceptions. The changes are in agreement with the results of the mocks, as described in Section 6. The two exceptions show a variation of $\sim$0.7$-$0.8 per cent and occur when the lower order polynomials for the broad-band terms is used. This is a feature of both the De-Wiggled and $P_{\rm pt}(k)$ templates. Higher order polynomials produce a variation at 0.2 per cent level.

Since the best-fitting values of $\alpha_{\perp}$ and $\alpha_{||}$ are generated from α and ϵ, the variations observed in α and ϵ are also observed in $\alpha_{\perp}$ and $\alpha_{||}$. In particular, $\Delta\alpha_{||} \leq 0.4$ per cent and $\Delta\alpha_{\perp} \leq 0.3$ per cent, except for a few cases: (a) changing the fitting range produces variations at 0.7–1.8 per cent, (b) using the lower order polynomials produces variations at 1.5$-$1.7 per cent in $\alpha_{||}$, (c) using lower order polynomials, $\alpha_{\perp}$ shows variations at 0.7–0.8 per cent level, and (d) fitting without priors produces a 0.6 per cent variation in $\alpha_{\perp}$.

Now we turn our attention to the errors on the various fitted values. For all of the robustness tests $\Delta\sigma_{\alpha}$, $\Delta\sigma_{\epsilon} \leq 0.002$. For errors on $\alpha_{||}$ and $\alpha_{\perp}$, the variations are all within 0.3 per cent. All of these cases agreed with the behaviour observed when the robustness tests are applied to mock galaxy catalogues, as discussed in Section 6.

Finally, a fixed β parameter does not lead to much smaller error and does not change our central values of fitted parameters compared to the fiducial case.

Table 10. The results of the robustness test on CMASS post-reconstruction DR11 data. We show the best-fitting α and ϵ values as well as the corresponding $\alpha_{||}$ and $\alpha_{\perp}$ with their respective errors and the $\chi^2/d.o.f$ of the fit for the fiducial case (with De-Wiggled Template). The remaining lines of the table show the difference between the fitted value or error with respect to the fiducial case $\Delta v = v - v^{\rm fid}$. (RL) stands for calculating the errors by integrating over specific intervals in the likelihood surfaces in α–ϵ or $\alpha_{||}$–$\alpha_{\perp}$. The median variations $\widetilde{\Delta v}$ are multiplied by 100. The definitions of various rows are similar to those in earlier tables such as Table 1.

Model	α	σ_{α}	ϵ	σ_{ϵ}	$\alpha_{\|\|}$	$\sigma_{\alpha_{\|\|}}$	$\alpha_{\perp}$	$\sigma_{\alpha_{\perp}}$	χ^2/d.o.f.
DR11 Post-reconstruction									
Fiducial	1.0166	0.0089	−0.0324	0.0133	0.9518	0.0314	1.0507	0.0127	21./30
Model	$\Delta\alpha$	$\Delta\sigma_{\alpha}$	$\Delta\epsilon$	$\Delta\sigma_{\epsilon}$	$\Delta\alpha_{\|\|}$	$\Delta\sigma_{\alpha_{\|\|}}$	$\Delta\alpha_{\perp}$	$\Delta\sigma_{\alpha_{\perp}}$	χ^2/d.o.f.
Fitting $30 < r < 200\,h^{-1}$ Mpc	0.23	−0.09	0.30	−0.07	0.80	−0.26	−0.08	0.03	36./30
Two−term $A_0(r)$ & $A_2(r)$	0.09	0.04	0.82	−0.03	1.70	0.04	−0.79	−0.09	38./30
Four−term $A_0(r)$ & $A_2(r)$	−0.07	−0.02	−0.16	−0.05	−0.39	−0.16	0.10	0.02	16./30
Fixed $\beta = 0.0$	0.04	−0.05	−0.15	−0.08	−0.26	−0.22	0.20	−0.02	21./30
$\Sigma_{\|} = \Sigma_{\perp} = 8\,{\rm Mpc\,h^{-1}}$	0.01	0.02	0.06	0.02	0.12	0.08	−0.06	−0.03	20./30
$\Sigma_{\rm s} \rightarrow 3.0\,{\rm Mpc\,h^{-1}}$	0.02	0.05	0.12	0.05	0.26	0.17	−0.11	0.00	21./30
FoG model → exp	−0.00	−0.00	−0.02	−0.01	−0.05	−0.02	0.02	0.00	21./30
FoG model → gauss	0.00	0.00	0.00	0.00	0.00	0.00	−0.00	0.00	21./30
No prior(RL)	−0.08	0.14	0.05	0.20	0.03	0.56	−0.14	0.04	20./30
Only β prior(RL)	−0.05	0.03	−0.12	0.06	−0.29	0.15	0.08	0.02	21./30
Only $\log(B_0^2)$ prior(RL)	−0.03	0.09	0.17	0.12	0.30	0.35	−0.22	0.01	20./30
$P_{\rm pt}(k)$ floating β	0.02	−0.01	−0.01	−0.02	−0.01	−0.05	0.04	−0.01	20./30
$P_{\rm pt}(k)$ fitting $30 < r < 200\,h^{-1}$ Mpc	0.24	−0.10	0.26	−0.09	0.73	−0.30	−0.03	0.02	36./30
$P_{\rm pt}(k)$ two−term $A_{\ell}(r)$	0.08	0.02	0.72	−0.05	1.49	−0.02	−0.69	−0.11	37./30
$P_{\rm pt}(k)$ four−term $A_{\ell}(r)$	−0.06	−0.04	−0.18	−0.08	−0.40	−0.23	0.14	0.00	16./30
$P_{\rm pt}(k)$ fixed β	0.06	−0.07	−0.18	−0.10	−0.30	−0.28	0.26	−0.03	21./30
$P_{\rm pt}(k)$ only β prior(RL)	−0.02	0.01	−0.12	0.03	−0.25	0.08	0.11	0.01	20./30
$P_{\rm pt}(k)$ only B_0 prior(RL)	−0.00	0.06	0.17	0.08	0.33	0.25	−0.18	−0.01	20./30
$P_{\rm pt}(k)$ no priors(RL)	−0.04	0.11	0.07	0.15	0.09	0.44	−0.12	0.02	20./30

Table 11. CMASS fitting results using various data set (DR10, DR11, pre- and post-reconstruction) using different methodologies. A few notes: the isotropic fit quoted here is the single fit in correlation function with De-Wiggled template, thus it should be most comparable to Multip. Grid-DeW anisotropic fit. The Multip. Grid-DeW anisotropic fits are most likely to be similar to the isotropic fit, particularly post-reconstruction. All quoted errors includes only statistical errors, but not systematic errors.

Model	α	ϵ	$\rho_{\alpha,\epsilon}$	$\alpha_{\|\|}$	$\alpha_{\perp}$	$\rho_{\|\|,\perp}$	$\chi^2/d.o.f$
DR11 Post-reconstruction							
Consensus	**1.0186 ± 0.0104**	**−0.0252 ± 0.0142**	**0.390**	**0.9678 ± 0.0329**	**1.0449 ± 0.0145**	**−0.523**	
Multip. Grid DeW	1.0166 ± 0.0089	−0.0324 ± 0.013	0.512	0.9518 ± 0.031	1.0507 ± 0.013	−0.297	21./30
Multip. Grid-RPT	1.0168 ± 0.0088	−0.0326 ± 0.013	0.505	0.9517 ± 0.031	1.0511 ± 0.013	−0.304	21./30
Multip. MCMC	1.017 ± 0.010	−0.028 ± 0.012	0.363	0.962 ± 0.028	1.047 ± 0.013	−0.439	18/30
Wedges	1.019 ± 0.010	−0.018 ± 0.013	0.389	0.982 ± 0.0312	1.038 ± 0.014	−0.501	21./30
Isotropic	1.021 ± 0.009	–	–	–	–	–	16/17
DR11 Pre-reconstruction							
Multip. Grid-DeW	1.0245 ± 0.0142	−0.0101 ± 0.019	0.572	1.0039 ± 0.049	1.0350 ± 0.017	−0.144	33./30
Multip. Grid-RPT	1.0170 ± 0.0133	−0.0122 ± 0.019	0.495	0.9923 ± 0.046	1.0296 ± 0.018	−0.241	35./30
Multip. MCMC	1.015 ± 0.015	−0.016 ± 0.018	0.423	0.983 ± 0.044	1.033 ± 0.019	−0.406	31/30
Wedges	1.018 ± 0.015	−0.008 ± 0.018	0.236	1.001 ± 0.043	1.027 ± 0.021	−0.453	33/30
Isotropic	1.031 ± 0.013	–	–	–	–	–	14/17
DR10 Post-reconstruction							
Consensus	**1.0187 ± 0.0151**	**−0.0123 ± 0.0202**	**0.502**	**0.9937 ± 0.0495**	**1.0314 ± 0.0187**	**−0.501**	
Multip. Grid-DeW	1.0151 ± 0.0155	−0.0203 ± 0.023	0.669	0.9744 ± 0.057	1.0361 ± 0.019	−0.158	16./30
Multip. Grid-RPT	1.0155 ± 0.0157	−0.0203 ± 0.023	0.683	0.9747 ± 0.058	1.0365 ± 0.018	−0.136	16./30
Multip. MCMC	1.016 ± 0.015	−0.019 ± 0.018	0.484	0.979 ± 0.045	1.035 ± 0.018	−0.445	16/30
Wedges	1.020 ± 0.015	−0.006 ± 0.019	0.513	1.009 ± 0.049	1.027 ± 0.018	-0.474	17/30
Isotropic	1.022 ± 0.013	–	–	–	–	–	14/17
DR10 Pre-reconstruction							
Multip. Grid-DeW	1.0123 ± 0.0177	−0.0215 ± 0.026	0.555	0.9693 ± 0.063	1.0345 ± 0.023	−0.233	35./30
Multip. Grid-RPT	1.0043 ± 0.0162	−0.0244 ± 0.025	0.439	0.9560 ± 0.057	1.0294 ± 0.024	−0.344	36./30
Multip. MCMC	1.000 ± 0.018	−0.023 ± 0.022	0.388	0.955 ± 0.051	1.024 ± 0.024	−0.458	32/30
Wedges	1.004 ± 0.018	−0.015 ± 0.022	0.104	0.975 ± 0.049	1.020 ± 0.028	−0.482	30/30
Isotropic	1.022 ± 0.017	–	–	–	–	–	16/17

8.2 Data results with different methodologies

We apply different methodologies to the data and summarize the results in Table 11. We test four different methodologies, namely Multip. Grid with two templates (De-Wiggled and $P_{\rm pt}$ templates), Multip. MCMC and Wedges. We also include the results of the isotropic fitting in order to compare the isotropic and anisotropic fitting results. The isotropic results are described in Anderson et al. (2014).

Table 11 shows that for DR11 post-reconstruction the variations $\Delta\alpha \leq 0.002$ and $\Delta\epsilon \leq 0.004$ between variations of Multipoles fitting method (including using De-Wiggled Template, $P_{\rm pt}$ Template, and MCMC). However, Table 11 reveals that the DR11 post-reconstruction Multipoles (RPT) and Wedges results disagree by nearly to 1σ: $\alpha_{\|,\,\rm Mult} = 0.952 \pm 0.031$, $\alpha_{\|,\,\rm Wedges} = 0.982 \pm 0.031$; $\alpha_{\perp,\,\rm Mult} = 1.051 \pm 0.012$, $\alpha_{\perp,\,\rm Wedges} = 1.038 \pm 0.012$. The difference in $\alpha_{\|}$ is 0.030.

We then turn to the galaxy mock catalogues to see whether this behaviour is common. In 39 cases out of 600, the same or larger differences are produced between the two methods. The mean difference is 0.005 with an rms of 0.016, implying that this difference is at 1.9σ level. The difference in $\alpha_{\perp}$ is 0.013; 45 out of 600 cases show the same or larger differences between the two methods. The mean difference found in the mocks is 0.001 and the rms is 0.008, suggesting that the difference is a 1.6σ event. Table 11 indicates that this difference is primarily driven by differences in ϵ fitted results, as the α's from both methodologies only differ by 0.2 per cent, while ϵ changes by 1.5 per cent. This is comparable to the 1σ error on ϵ. We therefore turn to a discussion using α–ϵ parametrization.

Pre-reconstruction the Wedges and Multipoles measurements in α and ϵ differ by less than 0.25σ, as shown in Table 11. Fig. 13 shows that as reconstruction tightens the constraints from both methods the central values have shifted slightly along the axis of constant α. The discrepancy in the measurements is best quantified as a 1.5 per cent difference in ϵ. When we examine this comparison in our mocks, we find an rms difference in ϵ fits of 0.007, indicating that the data are a 2.004σ outlier. A total of 27 of 600 mocks have differences more extreme than ± 0.015; the other 3 cases (DR10 and DR11 pre-reconstruction) show smaller variations. We conclude that this event is consistent with normal scatter of the two estimators.

We briefly discuss the DR10 fitting results, as the differences between methodologies are small compared to the errors, and the best-fitting results in all parameterizations are consistent with each other. The only point of interest is in DR10 post-reconstruction, $\Delta\epsilon \approx 0.014$ in the Wedges and Multipoles (for all three variations) comparisons. This variation level is also observed in 81 out of 600 mocks, thus indicating that this is a 1.4σ event. Otherwise,these differences are in agreement with those obtained with the mocks.

8.3 Combining results from different methodologies

The tests on our fitting methodology, presented for the mock samples in Section 6 and on the DR11 data in Section 8.1, suggest that no systematic issue is causing the observed discrepancies in data. Thus, we combine results produced from the Multip. Grid and Wedges measurements to create our consensus anisotropic BAO measurement shown in Table 11. To combine results from Clustering Wedges

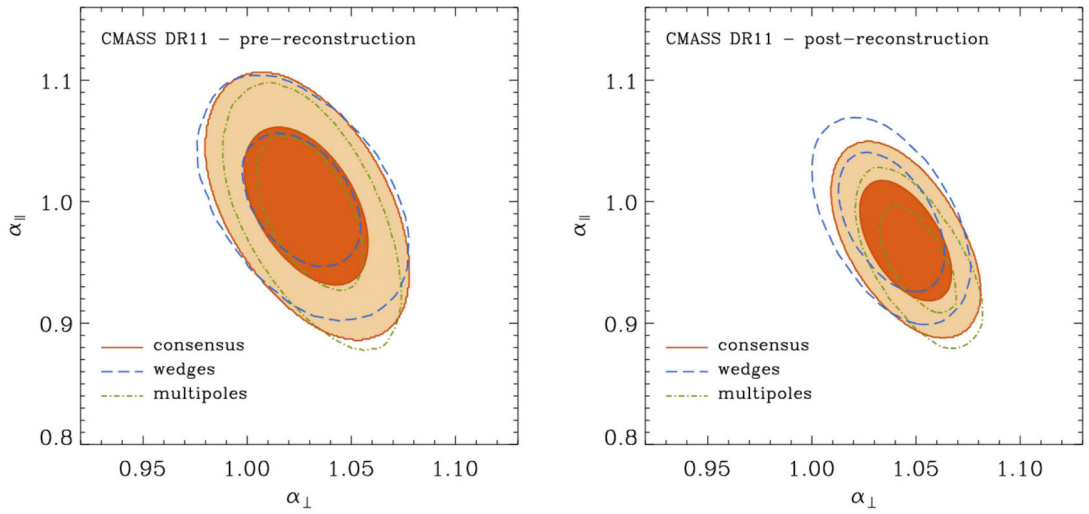

Figure 13. Comparison of the 68 and 95 per cent constraints in the $D_A - H(z)$ plane scaled by (r^{fid}/r_d) obtained from Multip. Grid analysis [blue short-dashed line] and Wedges [green long-dashed line], for DR11 pre-reconstruction[right] and post-reconstruction [left]. The solid contours are the consensus values issues from combining the $\log(\chi^2)$ from both approaches. The Multipoles provide slightly tighter constraints; the consensus contours follow a more elongated form aligned with the axis of constant α.

with Multipoles, we average the likelihood distributions recovered from the Multipoles and Wedges. We add the systematic errors to the consensus anisotropic BAO results. Although the marginalized constraints on $\alpha_\perp$ and $\alpha_{||}$ include covariance correction factors to account for the noise in our covariance matrix, this correction was not included in the full 2D posteriors that we combine to get the consensus result. We include an extra factor of $\sqrt{(m1)}$ centred at the corresponding best-fitting point. These dilations were applied to the posteriors from Wedges and Multipoles before averaging them to get the consensus constraints.

We include additional uncorrelated systematic error terms on α and ϵ of $\sigma_{\alpha_{sys}} = \sqrt{0.003^2 + 0.003^2}$ and $\sigma_{\epsilon_{sys}} = 0.003$. Translated into systematic errors on $\alpha_\perp$ and $\alpha_{||}$, these values correspond to $\sigma_{\perp_{sys}} = 0.005$ and $\sigma_{||_{sys}} = 0.007$ with a small correlation factor. To include these systematics in the consensus posterior a convolution with the Gaussian describing the systematic errors was performed.

Fig. 13 displays the comparison of the 68 and 95 per cent constraints in the $\alpha_\perp$ and $\alpha_{||}$ plane using the two methods: Multip. Grid (our fiducial methodology) and Wedges. The size of the contours from both methods agree well, with a more elongated contour from Multipoles. Post-reconstruction, we observe that the Multipoles method favours smaller values of $\alpha_{||}$ in both data releases while Wedges tends to higher values. However, the contours show a fairly good agreement between the two methodologies. Pre-reconstruction contours are well matched one to the other.

The solid contours are the consensus values from combining the $\log(\chi^2)$ from both approaches. The consensus anisotropic contours are larger than each of the individual methods (Multipoles and Wedges); this is due to the fact that there is slight difference in the central values of the contours fit by Multipoles and Wedges, thus enlarging the consensus contour. This effect can be clearly seen in Fig. 13.

8.4 Isotropic versus anisotropic results

We find consistent results between isotropic and anisotropic fitting results for all data sets (DR10, DR11) pre- and post-reconstruction as described in Table 11. Post-reconstruction, the central values of α measured from isotropic and anisotropic clustering are consistent to well within 1σ. Pre-reconstruction, the fits to the isotropic correlation function are approximately 1σ higher than the joint fits to both the monopole and quadrupole, for both DR10 and DR11. Part of this difference can be explained by the different correlation function templates used for the isotropic and anisotropic analyses. The isotropic fitting uses a non-linear power spectrum 'De-Wiggled template' (Anderson et al. 2012, 2013), while the anisotropic fitting uses $P_{pt}(k)$ as described in equation (17).

While the isotropic fits yield α measurements that agree with the correlation function anisotropic fits, they are in general higher than the anisotropic consensus value, and the effect of this is noticeable when the measurements are combined with the CMB data and turned into cosmological constraints (see Fig. 14).

Finally, we compare the anisotropic and isotropic clustering by examining the 68 and 95 per cent constraints in the $D_A(z = 0.57)(r_d^{fid}/r_d) - H(z = 0.57)(r_d/r_d^{fid})$ plane from CMASS consensus anisotropic [orange] and isotropic [grey] BAO constraints in Fig. 14. In general, the isotropic and anisotropic central values align well (along the constant α axis), but anisotropic clustering has a smaller contour. It provides constraints in both perpendicular and parallel to LOS direction. Also shown in Fig. 14 are the flat ΛCDM, $\sum m_\nu = 0.06$ eV predictions from the ePlanck and e*WMAP* CMB data sets detailed in Anderson et al. (2014). Our 68 and 95 per cent constraints in the $D_A(z = 0.57)(r_d^{fid}/r_d) - H(z = 0.57)(r_d/r_d^{fid})$ plane from CMASS consensus anisotropic measurements are highlighted in orange in Fig. 14. The grey are 1D 1σ–2σ contours of our consensus isotropic BAO fit (which is a combination of $P(k)$ fits and correlation function fits). This figure illustrates the 0.5 per cent increase in the best-fitting α from the anisotropic fits compared with the isotropic ones. The CMASS isotropic BAO constraints are consistent with both CMB predictions shown here, while the anisotropic constraints show more overlap with Planck, indicating a mild preference for higher values of $\Omega_c h^2$ preferred by Planck.

9 DISCUSSION AND CONCLUSIONS

We test the multipoles fitting methodology with mock catalogues and data for DR10/DR11 CMASS galaxy catalogues. The

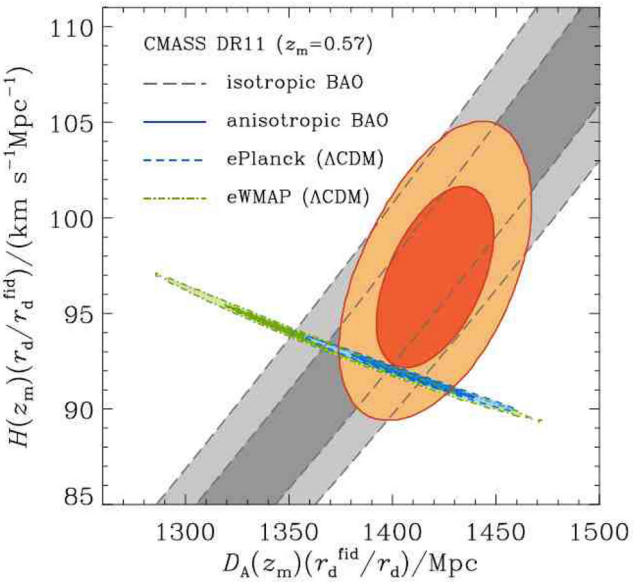

Figure 14. Comparison of the 68 and 95 per cent constraints in the $D_A(z=0.57)(r_d^{fid}/r_d)-H(z=0.57)(r_d^{fid}/r_d)$ plane from CMASS consensus anisotropic and isotropic BAO constraints. The Planck contours correspond to Planck+WMAP polarization (WP) and no lensing. The green contours show the constraints from *WMAP*9.

methodological changes tested are enumerated in Section 4. We summarize and discuss our findings in this section.

(i) With a large array of robustness tests, our fiducial methodology shows a maximum shift of 0.5 per cent in best-fitting α value and 0.3 per cent in best-fitting ϵ value pre-reconstruction. Post-reconstruction, the maximum shifts are further reduced to $\leq$0.1 per cent in α and remains $\leq$0.3 per cent in ϵ.

(ii) We list methodology changes that give the largest variations pre-reconstruction: (a) changing De-Wiggled Template to P_{pt} template (0.5 per cent in best-fitting α) ; (b) changing the fitting range from [50, 200] h^{-1} Mpc to [30, 200] h^{-1} Mpc (0.3 per cent in best-fitting α); (c) changing $\Sigma_{||,\perp}$ to $\Sigma_{||}=\Sigma_{\perp}=8.0$ Mpc h^{-1} (0.3 per cent in best-fitting ϵ).

(iii) Post-reconstruction, the variations in α and ϵ are impressively small, in all cases $\Delta\alpha$, $\Delta\epsilon \leq 0.1$ per cent except when we use polynomials of lower/higher order than the fiducial case to describe the broad-band terms, we observe changes of in $\Delta\epsilon \approx 0.2-0.3$ per cent.

(iv) A large array of robustness tests show only small effects in σ_α (a maximum shift of 0.1 per cent), while the various changes in the methodology mostly affect σ_ϵ (a maximum shift of 0.2 per cent) pre-reconstruction, if at all. Post-reconstruction, the errors have similar shifts as pre-reconstruction. However, there is significant scatter in the mocks when we do not include any priors on B_0, β in both pre- and post-reconstruction, while allowing the integration interval to calculate the errors to exceed the physical range that is used actually to fit the data.

(v) The effects of priors are stronger when the integration interval is not limited (which we use to calculate the errors) to a fixed $\alpha-\epsilon$ range. The range is chosen so that are not explored regions in $\alpha-\epsilon$ space that do not correspond to any physical ranges used to fit data.

We discuss the following changes in the fitting methodology that cause changes in the best-fitting values.

(i) *Templates*. The choice of templates affects mostly the best-fitting values and has a small effect on the fitted errors. In addition, the bias related to the De-Wiggled template is in the opposite direction to the biased shift when we use the RPT-inspired $P_{pt}(k)$ template. This inverted trend observed in pre-reconstruction data generates quite different results in term of $\alpha_{||}-\alpha_\perp$ parametrization, as the de-wiggled result becomes heavily biased, reaching a 0.9–1.2 per cent shift in $\alpha_{||}$ and a 0.2 per cent shift in $\alpha_\perp$. In the case of RPT, the shift in the parallel direction is only 0.2 per cent, while it is a little bit larger for the perpendicular direction, 0.2–0.3 per cent. After reconstruction, for both DR10/DR11 consistent results are obtained using either templates, the shift on α reduces to $\leq$1 per cent, and when we consider ϵ there is a slightly larger bias with the de-wiggled template of 0.1 per cent, compared to no bias for the $P_{pt}(k)$ template. This result is a reason why we choose to adopt the $P_{pt}(k)$ template in Anderson et al. (2014) as the fiducial template.

(ii) *Priors*. The elimination of priors produces a large effect pre- and post-reconstruction when a physically meaningful integration interval is not applied to the calculation of errors for α and ϵ. These changes do not actually affect the cosmological constraints provided by the anisotropic clustering measurement, as cosmological constraints are derived directly from using the full likelihood surface, and thus are not affected by the integration interval we adopt when we calculate the error on α or ϵ. These large variation in the σ's are related to non-zero likelihood at extreme ϵ. These cases correspond to situations where the acoustic peak along the LOS has been shifted out of the 50–200 Mpc fitting range. A prior on ϵ of 0.15 corresponds to a maximum dilation of $\alpha_{||}$ of $0.85^{-3}=1.63$, which should force the peak to be contained within our domain. Constraining the grid to be in the ϵ range $[-0.15,0.15]$ avoids these unphysical tails at low ϵ values.

We find the following when we compare significantly different methodologies (Multip. Grid, Multip. MCMC, Clustering Wedges), we switch to $\alpha_{||}-\alpha_\perp$ for the discussion and we concentrate on DR11 for ease of discussion.

(i) There is agreement between the MCMC and the Grid version when we use Multipoles, though there is a small level of scatter. The median difference pre-reconstruction for DR10/DR11 is $|\widetilde{\alpha_{||,\perp}}| \leq -0.3$ per cent. The median difference post-reconstruction reduces to $|\widetilde{\alpha_{||,\perp}}| \leq -0.1$ per cent.

(ii) The fitted errors are well correlated for the two methodologies (Multip. MCMC and Multip. Grid) with a small level of dispersion. The variation post-reconstruction is $|\widetilde{\sigma_{\alpha_{||}}}|=0.2$ per cent and $|\widetilde{\sigma_{\alpha_\perp}}|=0.1$ per cent. The dispersion is mostly observed in the parallel direction and decreases significantly post-reconstruction.

(iii) We compare Multip. Gridded against Clustering Wedges. There are small variations in the bias between methodologies but we do not find any indication that any methodology is more biased with respect to the others. The median differences in the best-fitting values are small. With pre-reconstructed mocks, we find $\Delta\alpha_{||}=0.7$ per cent, $\Delta\alpha_\perp=0.4$ per cent; post-reconstruction the discrepancies are even smaller, $\Delta\alpha_{||,\perp}=0.3, 0.1$ per cent.

(iv) When fitting using Multip. Gridded and Clustering Wedges, the differences in fitted errors are also small: $\Delta\sigma_{\alpha_{||}}=0.8$ per cent, $\Delta\sigma_{\alpha_\perp}=0.3$ per cent. Post-reconstruction the discrepancies are even smaller $\Delta\sigma_{\alpha_{||,\alpha_\perp}} \leq 0.5$ per cent. The errors are well correlated between both methodologies.

(v) The results suggests that there are two components in the median variation and dispersions of the fitted values and corresponding errors. The variation is produced by the estimator itself (wedges versus multipoles), and from the different implementations.

To conclude, we demonstrate the robustness of the multipoles fitting method at the 0.1–0.2 per cent level in α and ϵ. We quote a systematic error from these fitting techniques of 0.2 per cent + 0.2 per cent in quadrature, which is 0.3 per cent. Being more conservative, since we have only shown the result of one variation direction at a time; adding several uncertainties in quadrature could accumulate slightly more error. We highlight, however, that given the current precision on the measurements, and assuming the mean error in α and ϵ characterizes the full error budget, any variation observed in the α's lies perfectly within this error. There are possible systematics beyond this study, e.g. due to possible imperfections in the mocks: light cone effects, incorrect cosmology, incorrect dynamics in the mocks, and incorrect galaxy assignment model. The impacts of these issues are harder to assess, but might be at the 0.2–0.3 per cent level in ϵ. These are however beyond the scope of our current paper. We can conclude that for the current and near future data sets, the fitting model is still robust against changes in the methodology.

ACKNOWLEDGEMENTS

SH is partially supported by the New Frontiers in Astronomy and Cosmology programme at the John Templeton Foundation and was partially supported by RESCEU fellowship, and the Seaborg and Chamberlain Fellowship (via Lawrence Berkeley National Laboratory) during the preparation of this manuscript.

Numerical computations for the PTHalos mocks were done on the Sciama High Performance Compute (HPC) cluster which is supported by the ICG, SEPNet and the University of Portsmouth

Funding for SDSS-III has been provided by the Alfred P. Sloan Foundation, the Participating Institutions, the National Science Foundation, and the US Department of Energy.

AGS acknowledges support from the Trans-regional Collaborative Research Centre TR33 'The Dark Universe' of the German Research Foundation (DFG).

SDSS-III is managed by the Astrophysical Research Consortium for the Participating Institutions of the SDSS-III Collaboration including the University of Arizona, the Brazilian Participation Group, Brookhaven National Laboratory, University of Cambridge, Carnegie Mellon University, University of Florida, the French Participation Group, the German Participation Group, Harvard University, the Instituto de Astrofisica de Canarias, the Michigan State/Notre Dame/JINA Participation Group, Johns Hopkins University, Lawrence Berkeley National Laboratory, Max Planck Institute for Astrophysics, Max Planck Institute for Extraterrestrial Physics, New Mexico State University, New York University, Ohio State University, Pennsylvania State University, University of Portsmouth, Princeton University, the Spanish Participation Group, University of Tokyo, University of Utah, Vanderbilt University, University of Virginia, University of Washington, and Yale University.

REFERENCES

Abazajian K. N. et al., 2009, ApJS, 182, 543
Ahn C. et al., 2013, ApJS, 211, 17
Aihara H. et al., 2011, ApJS, 193, 29
Alcock C., Paczynski B., 1979, Nature, 281, 358
Anderson L. et al., 2012, MNRAS, 427, 3435
Anderson L. et al., 2013, MNRAS, 439, 83
Anderson L. et al., 2014, MNRAS, 441, 24
Beutler F. et al., 2011, MNRAS, 416, 3017
Blake C., Collister A., Bridle S., Lahav O., 2007, MNRAS, 374, 1527
Blanton M., Lin H., Lupton R. H., Maley F. M., Young N., Zehavi I., Loveday J., 2003, AJ, 125, 2276
Bolton A. et al., 2012, AJ, 144, 144
Crocce M., Scoccimarro R., 2008, Phys. Rev. D, 77, 023533
Dawson K. et al., 2012, AJ, 145, 10
Doi M. et al., 2010, AJ, 139, 1628
Dodelson S., Schneider M., 2013, Phys. Rev. D, 88, 063537
Eisenstein D. J., Hu W., 1998, ApJ, 496, 605
Eisenstein D. J., Seo H.-J., White M., 2007, ApJ, 664, 660
Eisenstein D. J. et al., 2011, AJ, 142, 72
Fukugita M., Ichikawa T., Gunn J. E., Doi M., Shimasaku K., Schneider D. P., 1996, AJ, 111, 1748
Gunn J. E. et al., 1998, AJ, 116, 3040
Gunn J. E. et al., 2006, AJ, 131, 233
Hartlap J., Simon P., Schneider P., 2007, A&A, 464, 399
Kaiser N., 1987, MNRAS, 227, 1
Kazin E. et al., 2010, ApJ, 710, 1444
Kazin E., Sanchez A. G., Blanton M. R., 2012, MNRAS, 419, 3223
Kazin E. et al., 2013, MNRAS, 435, 64
Landy S. D., Szalay A. S., 1993, ApJ 412, 64
Lupton R., Gunn J. E., Ivezić Z., Knapp G., Kent S., 2001, in Harnden F. R., Jr, Primini F. A., Payne H. E., eds, ASP Conf. Ser. Vol. 238, Astronomical Data Analysis Software and Systems X. Astron. Soc. Pac., San Francisco, p. 269
Manera M., Scoccimarro R., Percival W. J. et al., 2013, MNRAS, 428, 1036
Meiksin A., White M., Peacock J. A., 1999, MNRAS 304, 851
Noh Y., White M., Padmanabhan N., 2009, Phys. Rev. D, 80, 123501
Okumura T., Matsubara T., Eisenstein D. J., Kayo I., Hikage C., Szalay A. S., Schneider D. P., 2008, ApJ, 676, 889
Padmanabhan N., White M., 2009, Phys. Rev. D, 80, 063508
Padmanabhan N., Xu X., Eisenstein D. J., Scalzo R., Cuesta A. J., Mehta K. T., Kazin E., 2012, MNRAS, 427, 2132
Peacock J. A., Dodds S. J., 1994, MNRAS, 267, 1020
Percival W. J. et al., 2014, MNRAS, 439, 2531
Pier J. R., Munn J. A., Hindsley R. B., Hennessy G. S., Kent S. M., Lupton R. H., Ivezić Ž., 2003, AJ, 125, 1559
Sanchez A. G., Baugh C. M., Angulo R., 2008, 390, 1470
Sanchez A. G. et al., 2012, MNRAS, 425, 415
Sánchez A. G. et al., 2014, MNRAS, 440, 2692
Scoccimarro R., Sheth R. K., 2002, MNRAS, 329, 629
Smee S. et al., 2013, AJ, 146, 32
Smith J. A. et al., 2002, AJ, 123, 2121
Taylor A., Joachimi B., Kitching T., 2013, MNRAS, 432, 1928
White M. et al., 2011, ApJ, 728, 126
Xu X., Padmanabhan N., Eisenstein D. J., Mehta K. T., Cuesta A. J., 2012, MNRAS, 427, 2146
Xu X., Cuesta A. J., Padmanabhan N., Eisenstein D. J., McBride C. K., 2013, MNRAS, 431, 2834
York D. G. et al., 2000, AJ, 120, 1579

APPENDIX A: DR11 VERSUS DR10 MOCKS

A1 DR11 versus DR10 mocks

The results for DR10 are shown in Tables A1, and A2 for the best-fitting values, pre- and post-reconstruction and in Tables A3, and A4 for the uncertainties pre- and post-reconstruction. For the best-fitting values we observe the same trends in both data releases; however, we can notice two differences: the median α's in DR11 are for the most part lower by 0.001–0.002 in $\alpha_\parallel$ and $\alpha_\perp$ (with four cases showing a difference 0.003). This differences in the bias could be associated with the correlation between mocks generated by the overlapping regions. This correlation is larger in DR11 is $r = 0.49$ while in DR10, $r = 0.33$. The second difference is the dispersion, quantified by the percentiles of the distributions of the best-fitting values and their uncertainties, which for all cases is lower

Table A1. Fitting results fof mocks with numerous variations of our fiducial fitting methodology for DR10 mock galaxy catalogues pre-reconstruction without covariance corrections for the overlapping mock regions. First line shows the median and 16th and 84th percentiles for the α, ϵ, $\alpha_{||,\perp}$. The rest of the lines show the median bias and median variations $\Delta v = v_i - v_f$ with their corresponding 16th and 84th percentiles. The median bias $\widetilde{b}$, median variations $\widetilde{\Delta v}$, and percentiles are multiplied by 100.

Model	$\widetilde{\alpha}$	–	$\widetilde{\epsilon}$	–	$\widetilde{\alpha_\parallel}$	–	$\widetilde{\alpha_\perp}$	–
				DR10 Pre-reconstruction				
Fiducial	$1.0033^{+0.0186}_{-0.0177}$	–	$0.0029^{+0.0201}_{-0.0239}$	–	$1.0092^{+0.0469}_{-0.0512}$	–	$1.0022^{+0.026}_{-0.026}$	–
Model	$\widetilde{b_\alpha}$	$\widetilde{\Delta\alpha}$	$\widetilde{b_\epsilon}$	$\widetilde{\Delta\epsilon}$	$\widetilde{b_\parallel}$	$\widetilde{\Delta\alpha_\parallel}$	$\widetilde{b_\perp}$	$\widetilde{\Delta\alpha_\perp}$
$30 < r < 200\,\mathrm{Mpc}\,h^{-1}$	$-5\mathrm{e}{-3}^{+1.96}_{-1.73}$	$-0.29^{+0.25}_{-0.30}$	$-0.10^{+2.01}_{-2.52}$	$-0.20^{+0.20}_{-0.25}$	$0.16^{+4.63}_{-4.89}$	$-0.70^{+0.57}_{-0.73}$	$0.16^{+2.63}_{-2.62}$	$-0.06^{+0.20}_{-0.22}$
Two−term $A_\ell(r)$	$0.26^{+1.88}_{-1.68}$	$-0.01^{+0.16}_{-0.18}$	$-0.28^{+1.95}_{-2.27}$	$0.01^{+0.31}_{-0.28}$	$0.79^{+4.66}_{-4.60}$	$4\mathrm{e}{-3}^{+0.77}_{-0.71}$	$0.23^{+2.41}_{-2.53}$	$-0.02^{+0.14}_{-0.17}$
Four−term $A_\ell(r)$	$0.32^{+1.83}_{-1.89}$	$-0.04^{+0.18}_{-0.19}$	$-0.30^{+1.97}_{-2.44}$	$-0.03^{+0.23}_{-0.26}$	$0.87^{+4.70}_{-5.23}$	$-0.09^{+0.54}_{-0.59}$	$0.21^{+2.61}_{-2.55}$	$-0.03^{+0.26}_{-0.19}$
$\Sigma_\parallel = \Sigma_\perp = 8\,\mathrm{Mpc}\,h^{-1}$	$0.32^{+1.88}_{-1.65}$	$2\mathrm{e}{-3}^{+0.26}_{-0.28}$	$-0.03^{+2.03}_{-2.56}$	$-0.30^{+0.35}_{-0.35}$	$0.35^{+5.00}_{-5.30}$	$-0.57^{+0.86}_{-0.82}$	$0.57^{+2.67}_{-2.61}$	$0.32^{+0.34}_{-0.37}$
$\Sigma_s \rightarrow 3.0\,\mathrm{Mpc}\,h^{-1}$	$0.38^{+1.87}_{-1.75}$	$0.04^{+0.05}_{-0.05}$	$-0.37^{+2.03}_{-2.45}$	$0.06^{+0.07}_{-0.08}$	$1.04^{+4.86}_{-5.08}$	$0.17^{+0.18}_{-0.20}$	$0.23^{+2.59}_{-2.56}$	$-0.02^{+0.04}_{-0.04}$
No priors	$0.43^{+1.96}_{-1.87}$	$0.04^{+0.19}_{-0.11}$	$-0.29^{+2.04}_{-2.40}$	$-0.01^{+0.35}_{-0.33}$	$0.97^{+4.95}_{-5.12}$	$-0.02^{+0.73}_{-0.52}$	$0.21^{+2.79}_{-2.51}$	$0.02^{+0.47}_{-0.33}$
Only $\log(B_0^2)$ prior	$0.36^{+1.98}_{-1.73}$	$0.01^{+0.16}_{-0.05}$	$-0.27^{+2.04}_{-2.34}$	$-5\mathrm{e}{-3}^{+0.32}_{-0.30}$	$0.87^{+4.96}_{-5.14}$	$-0.01^{+0.59}_{-0.50}$	$0.21^{+2.61}_{-2.52}$	$2\mathrm{e}{-3}^{+0.43}_{-0.34}$
Only β prior	$0.36^{+1.93}_{-1.80}$	$4\mathrm{e}{-3}^{+0.13}_{-0.07}$	$-0.29^{+2.00}_{-2.37}$	$-5\mathrm{e}{-4}^{+0.07}_{-0.06}$	$0.96^{+4.75}_{-5.01}$	$0.01^{+0.20}_{-0.15}$	$0.27^{+2.63}_{-2.52}$	$0.01^{+0.12}_{-0.06}$
$P_{\rm pt}(k)$ floating β	$-0.24^{+1.90}_{-1.71}$	$-0.58^{+0.21}_{-0.18}$	$-0.26^{+2.05}_{-2.41}$	$-0.04^{+0.25}_{-0.21}$	$0.25^{+4.80}_{-4.96}$	$-0.70^{+0.58}_{-0.43}$	$-0.31^{+2.68}_{-2.51}$	$-0.54^{+0.32}_{-0.26}$
$P_{\rm pt}(k)\,\beta = 0.0$	$-0.25^{+1.90}_{-1.71}$	$-0.58^{+0.22}_{-0.18}$	$-0.25^{+2.06}_{-2.52}$	$-0.07^{+0.25}_{-0.25}$	$0.17^{+4.85}_{-5.11}$	$-0.74^{+0.59}_{-0.48}$	$-0.27^{+2.75}_{-2.58}$	$-0.51^{+0.36}_{-0.30}$
FoG model → exp	$0.33^{+1.87}_{-1.77}$	$-0.01^{+0.01}_{-0.01}$	$-0.28^{+2.02}_{-2.40}$	$-0.01^{+0.01}_{-0.01}$	$0.91^{+4.68}_{-5.09}$	$-0.02^{+0.03}_{-0.03}$	$0.22^{+2.61}_{-2.56}$	$2\mathrm{e}{-3}^{+0.01}_{-0.01}$
FoG model → Gauss	$0.33^{+1.86}_{-1.77}$	$1\mathrm{e}{-4}^{+2\mathrm{e}-4}_{-2\mathrm{e}-4}$	$-0.29^{+2.01}_{-2.39}$	$1\mathrm{e}{-4}^{+3\mathrm{e}-4}_{-3\mathrm{e}-4}$	$0.92^{+4.69}_{-5.12}$	$3\mathrm{e}{-4}^{+1\mathrm{e}-3}_{-\mathrm{e}-3}$	$0.22^{+2.62}_{-2.57}$	$-1\mathrm{e}{-4}^{+2\mathrm{e}-4}_{-1\mathrm{e}-4}$

Table A2. Fitting results of mocks with numerous variations of our fiducial fitting methodology for DR10 mock galaxy catalogues post-reconstruction, without covariance corrections for the overlapping mock regions. First line shows the median and 16th and 84th percentiles for the α, ϵ, $\alpha_{||,\perp}$. The rest of the lines show the median bias and median variations $\Delta v = v_i - v_f$ with their corresponding 16th and 84th percentiles. The median bias $\widetilde{b}$, median variations $\widetilde{\Delta v}$, and percentiles are multiplied by 100.

Model	$\widetilde{\alpha}$	–	$\widetilde{\epsilon}$	–	$\widetilde{\alpha_\parallel}$	–	$\widetilde{\alpha_\perp}$	–
				DR10 Post-reconstruction				
Fiducial	$1.0012^{+0.0123}_{-0.0121}$	–	$0.0007^{+0.0154}_{-0.0138}$	–	$1.0021^{+0.0367}_{-0.0283}$	–	$1.0000^{+0.020}_{-0.019}$	–
Model	$\widetilde{b_\alpha}$	$\widetilde{\Delta\alpha}$	$\widetilde{b_\epsilon}$	$\widetilde{\Delta\epsilon}$	$\widetilde{b_\parallel}$	$\widetilde{\Delta\alpha_\parallel}$	$\widetilde{b_\perp}$	$\widetilde{\Delta\alpha_\perp}$
$30 < r < 200\,\mathrm{Mpc}\,h^{-1}$	$0.28^{+1.25}_{-1.19}$	$0.15^{+0.17}_{-0.14}$	$-0.12^{+1.48}_{-1.39}$	$0.02^{+0.15}_{-0.10}$	$0.49^{+3.40}_{-2.65}$	$0.17^{+0.40}_{-0.26}$	$0.13^{+1.97}_{-1.92}$	$0.10^{+0.16}_{-0.14}$
Two−term $A_\ell(r)$	$0.06^{+1.22}_{-1.15}$	$-0.05^{+0.07}_{-0.10}$	$-0.33^{+1.49}_{-1.24}$	$0.27^{+0.19}_{-0.17}$	$0.73^{+3.34}_{-2.72}$	$0.47^{+0.35}_{-0.28}$	$-0.33^{+1.85}_{-1.79}$	$-0.32^{+0.19}_{-0.29}$
Four−term $A_\ell(r)$	$-0.04^{+1.23}_{-1.18}$	$-0.14^{+0.14}_{-0.15}$	$0.05^{+1.62}_{-1.39}$	$-0.12^{+0.14}_{-0.15}$	$-0.09^{+3.43}_{-3.02}$	$-0.39^{+0.36}_{-0.35}$	$0.02^{+1.97}_{-1.89}$	$-0.01^{+0.15}_{-0.17}$
$\Sigma_\parallel = 4$ & $\Sigma_\perp = 2$	$0.12^{+1.24}_{-1.24}$	$-0.01^{+0.04}_{-0.04}$	$-0.13^{+1.53}_{-1.40}$	$0.05^{+0.06}_{-0.06}$	$0.30^{+3.56}_{-2.82}$	$0.09^{+0.11}_{-0.12}$	$-0.06^{+2.07}_{-1.89}$	$-0.06^{+0.07}_{-0.07}$
$\Sigma_s \rightarrow 3.0\,\mathrm{M\,pc}\,h^{-1}$	$0.15^{+1.20}_{-1.15}$	$0.04^{+0.06}_{-0.05}$	$-0.15^{+1.57}_{-1.41}$	$0.07^{+0.09}_{-0.08}$	$0.33^{+3.72}_{-2.81}$	$0.18^{+0.21}_{-0.22}$	$-0.02^{+2.02}_{-1.90}$	$-0.03^{+0.05}_{-0.05}$
No priors	$0.15^{+1.24}_{-1.22}$	$0.01^{+0.07}_{-0.05}$	$-0.06^{+1.60}_{-1.43}$	$-0.02^{+0.25}_{-0.19}$	$0.26^{+3.82}_{-3.00}$	$-0.05^{+0.53}_{-0.37}$	$0.02^{+2.12}_{-1.93}$	$2\mathrm{e}{-3}^{+0.22}_{-0.20}$
Only B_0prior	$0.15^{+1.25}_{-1.20}$	$0.01^{+0.06}_{-0.02}$	$-0.07^{+1.57}_{-1.43}$	$-0.02^{+0.24}_{-0.17}$	$0.25^{+3.76}_{-2.89}$	$-0.04^{+0.49}_{-0.32}$	$0.01^{+2.11}_{-1.91}$	$0.01^{+0.21}_{-0.20}$
Only β prior	$0.12^{+1.22}_{-1.22}$	$-0.02^{+0.04}_{-0.03}$	$-0.07^{+1.58}_{-1.41}$	$<1\mathrm{e}{-4}^{+0.03}_{-0.04}$	$0.21^{+3.75}_{-2.93}$	$-3\mathrm{e}{-3}^{+0.07}_{-0.09}$	$-3\mathrm{e}{-3}^{+2.04}_{-1.88}$	$-5\mathrm{e}{-3}^{+0.04}_{-0.05}$
$P_{\rm pt}(k)$floating β	$0.14^{+1.23}_{-1.23}$	$0.01^{+0.04}_{-0.04}$	$-0.05^{+1.54}_{-1.37}$	$-0.02^{+0.05}_{-0.06}$	$0.26^{+3.63}_{-3.00}$	$-0.02^{+0.13}_{-0.14}$	$0.03^{+2.02}_{-1.87}$	$0.03^{+0.05}_{-0.05}$
$P_{\rm pt}(k)\,\beta = 0.0$	$0.12^{+1.25}_{-1.25}$	$-1\mathrm{e}{-3}^{+0.05}_{-0.05}$	$-0.05^{+1.54}_{-1.36}$	$-0.01^{+0.09}_{-0.11}$	$0.28^{+3.55}_{-2.98}$	$-0.02^{+0.19}_{-0.25}$	$0.01^{+2.04}_{-1.89}$	$0.02^{+0.11}_{-0.10}$
FoG model → exp	$0.11^{+1.23}_{-1.21}$	$-0.01^{+0.01}_{-0.01}$	$-0.06^{+1.55}_{-1.38}$	$-0.01^{+0.01}_{-0.01}$	$0.20^{+3.68}_{-2.88}$	$-0.02^{+0.04}_{-0.04}$	$4\mathrm{e}{-3}^{+2.03}_{-1.87}$	$5\mathrm{e}{-3}^{+0.01}_{-0.01}$
FoG model → Gauss	$0.12^{+1.23}_{-1.21}$	$1\mathrm{e}{-4}^{+5\mathrm{e}-4}_{-5\mathrm{e}-4}$	$-0.07^{+1.54}_{-1.38}$	$3\mathrm{e}{-4}^{+1\mathrm{e}-3}_{-1\mathrm{e}-3}$	$0.22^{+3.67}_{-2.83}$	$1\mathrm{e}{-3}^{+3\mathrm{e}-3}_{-2\mathrm{e}-3}$	$5\mathrm{e}{-3}^{+2.02}_{-1.88}$	$-2\mathrm{e}{-4}^{+5\mathrm{e}-4}_{-5\mathrm{e}-4}$

in DR11. The percentiles are also more symmetric for $\alpha_\parallel$ and $\alpha_\perp$. The dispersion reduction is related to the signal to noise increase with the larger volume covered by DR11. Concerning the best-fitting values, pre-reconstruction we observe two cases that appears only in one data release: (1) a $\Delta\alpha = 0.1$ per cent is observed in DR11 when using second-order polynomials that is not observed in DR10; (2) a $\Delta\epsilon = 0.1$ per cent is observed in DR10 using smaller bins that is not observed in DR11. Post-reconstruction two cases shows a $\Delta\alpha = 0.1$ per cent in DR10 that is not reproduced in DR11: using 4-Mpc bins and using higher order polynomials. One case in DR11 shows $\Delta\epsilon = 0.1$ per cent that is non observed in DR10: the larger fitting range.

For the uncertainties, we expect that the mean error decreases for DR11 compared with DR10 results because the increasing volume surveyed. The DR11 fiducial case show median uncertainty of $\widetilde{\sigma_{||}} = 0.044$ compared with DR10 $\widetilde{\sigma_{||}} = 0.057$. For the perpendicular direction $\widetilde{\sigma_\perp} = 0.021$ compared with $\widetilde{\sigma_\perp} = 0.027$. Post-reconstruction, $\widetilde{\sigma_{||}} = 0.036 \rightarrow 0.028$ and $\widetilde{\sigma_\perp} = 0.019 \rightarrow 0.015$.

In the case of the errors there are also some differences between data releases. Pre-reconstruction, two cases shows a

Table A3. Fitted errors of mocks with numerous variations of our fiducial fitting methodology for DR10 mock galaxy catalogues pre-reconstruction, without covariance corrections for the overlapping mock regions. The columns show the median and 16th and 84th percentiles of the $\sigma_{\alpha,\epsilon,||,\perp}$ and variations $\Delta v = v_i - v_f$. Except for the fiducial case all quantities are multiplied by 100.

Model	$\widetilde{\sigma_\alpha}$	$\widetilde{\Delta\sigma_\alpha}$	$\widetilde{\sigma_\epsilon}$	$\widetilde{\Delta\sigma_\epsilon}$	$\widetilde{\sigma_{\alpha_\parallel}}$	$\widetilde{\Delta\sigma_{\alpha_\parallel}}$	$\widetilde{\sigma_{\alpha_\perp}}$	$\widetilde{\Delta\sigma_{\alpha_\perp}}$
				DR10 Pre-reconstruction				
Fiducial	$0.0196^{+0.0066}_{-0.0037}$	–	$0.0249^{+0.0100}_{-0.0048}$	–	$0.0574^{+0.0271}_{-0.0127}$	–	$0.0269^{+0.0059}_{-0.0034}$	–
$30 < r < 200\,\mathrm{Mpc}\,h^{-1}$	$2.00^{+0.82}_{-0.40}$	$0.02^{+0.15}_{-0.08}$	$2.59^{+1.22}_{-0.52}$	$0.06^{+0.29}_{-0.13}$	$6.08^{+3.00}_{-1.45}$	$0.15^{+0.77}_{-0.37}$	$2.72^{+0.58}_{-0.39}$	$5\mathrm{e}{-3}^{+0.08}_{-0.05}$
Two−term $A_\ell(r)$	$1.95^{+0.63}_{-0.33}$	$1\mathrm{e}{-3}^{+0.08}_{-0.09}$	$2.39^{+0.94}_{-0.43}$	$-0.07^{+0.08}_{-0.16}$	$5.47^{+2.63}_{-1.10}$	$-0.16^{+0.18}_{-0.39}$	$2.66^{+0.55}_{-0.35}$	$-0.03^{+0.07}_{-0.10}$
Four−term $A_\ell(r)$	$1.95^{+0.69}_{-0.36}$	$0.01^{+0.05}_{-0.06}$	$2.54^{+1.03}_{-0.49}$	$0.05^{+0.12}_{-0.10}$	$5.85^{+2.73}_{-1.31}$	$0.08^{+0.28}_{-0.19}$	$2.72^{+0.60}_{-0.35}$	$0.03^{+0.06}_{-0.05}$
$\Sigma_\parallel = \Sigma_\perp = 8\,\mathrm{Mpc}\,h^{-1}$	$1.89^{+0.64}_{-0.33}$	$-0.04^{+0.07}_{-0.09}$	$2.38^{+1.10}_{-0.48}$	$-0.09^{+0.17}_{-0.14}$	$5.19^{+2.93}_{-1.25}$	$-0.52^{+0.38}_{-0.38}$	$2.93^{+0.65}_{-0.36}$	$0.23^{+0.14}_{-0.09}$
$\Sigma_s \to 3.0\,\mathrm{Mpc}\,h^{-1}$	$1.99^{+0.68}_{-0.37}$	$0.03^{+0.02}_{-0.01}$	$2.57^{+1.00}_{-0.49}$	$0.07^{+0.04}_{-0.03}$	$5.94^{+2.69}_{-1.26}$	$0.20^{+0.11}_{-0.07}$	$2.70^{+0.59}_{-0.35}$	$0.02^{+0.02}_{-0.02}$
No priors	$2.68^{+1.69}_{-0.81}$	$0.60^{+1.19}_{-0.44}$	$3.41^{+2.19}_{-1.12}$	$0.74^{+1.21}_{-0.53}$	$7.54^{+6.87}_{-2.80}$	$1.40^{+3.97}_{-1.25}$	$3.19^{+1.93}_{-0.67}$	$0.42^{+1.28}_{-0.31}$
Only $\log(B_0^2)$ prior	$2.38^{+1.30}_{-0.60}$	$0.31^{+0.77}_{-0.22}$	$3.07^{+1.80}_{-0.87}$	$0.48^{+0.87}_{-0.33}$	$6.60^{+5.67}_{-1.99}$	$0.78^{+2.52}_{-0.78}$	$3.01^{+1.36}_{-0.58}$	$0.27^{+0.92}_{-0.22}$
Only β prior	$2.19^{+1.41}_{-0.57}$	$0.17^{+0.67}_{-0.16}$	$2.78^{+1.82}_{-0.70}$	$0.18^{+0.87}_{-0.15}$	$6.61^{+5.14}_{-1.99}$	$0.53^{+2.63}_{-0.44}$	$2.77^{+0.79}_{-0.39}$	$0.08^{+0.20}_{-0.05}$
$P_{\rm pt}(k)$ floating β	$1.90^{+0.59}_{-0.34}$	$-0.05^{+0.07}_{-0.09}$	$2.46^{+1.01}_{-0.46}$	$-0.02^{+0.11}_{-0.12}$	$5.47^{+2.72}_{-1.21}$	$-0.24^{+0.28}_{-0.34}$	$2.83^{+0.60}_{-0.36}$	$0.12^{+0.10}_{-0.10}$
$P_{\rm pt}(k)$ $\beta = 0.0$	$1.88^{+0.57}_{-0.33}$	$-0.06^{+0.07}_{-0.10}$	$2.42^{+0.98}_{-0.45}$	$-0.05^{+0.10}_{-0.13}$	$5.38^{+2.57}_{-1.16}$	$-0.33^{+0.24}_{-0.41}$	$2.82^{+0.59}_{-0.36}$	$0.11^{+0.10}_{-0.11}$
FoG model → exp	$1.96^{+0.65}_{-0.37}$	$-4\mathrm{e}{-3}^{+2\mathrm{e}-3}_{-3\mathrm{e}-3}$	$2.47^{+1.01}_{-0.47}$	$-0.01^{+5\mathrm{e}-3}_{-0.01}$	$5.71^{+2.71}_{-1.27}$	$-0.03^{+0.01}_{-0.01}$	$2.69^{+0.59}_{-0.35}$	$-3\mathrm{e}{-3}^{+3\mathrm{e}-3}_{-2\mathrm{e}-3}$
FoG model → Gauss	$1.96^{+0.66}_{-0.37}$	$<1\mathrm{e}{-4}^{+1\mathrm{e}-4}_{-1\mathrm{e}-4}$	$2.49^{+1.00}_{-0.48}$	$1\mathrm{e}{-4}^{+1\mathrm{e}-4}_{-1\mathrm{e}-4}$	$5.74^{+2.71}_{-1.27}$	$3\mathrm{e}{-4}^{+4\mathrm{e}-4}_{-4\mathrm{e}-4}$	$2.69^{+0.59}_{-0.34}$	$<1\mathrm{e}{-4}^{+<1\mathrm{e}-4}_{-1\mathrm{e}-4}$

Table A4. We show the fitting errors from DR10 mock galaxy catalogues post-reconstruction for variations of the fiducial models, without covariance corrections for the overlapping mock regions. The columns show the median and 16th and 84th percentiles of the $\sigma_{\alpha,\epsilon,||,\perp}$ and variations $\Delta v = v_i - v_f$. Except for the fiducial case all quantities are multiplied by 100.

Model	$\widetilde{\sigma_\alpha}$	$\widetilde{\Delta\sigma_\alpha}$	$\widetilde{\sigma_\epsilon}$	$\widetilde{\Delta\sigma_\epsilon}$	$\widetilde{\sigma_{\alpha_\parallel}}$	$\widetilde{\Delta\sigma_{\alpha_\parallel}}$	$\widetilde{\sigma_{\alpha_\perp}}$	$\widetilde{\Delta\sigma_{\alpha_\perp}}$
				DR10 Post-reconstruction				
Fiducial	$0.0126^{+0.0028}_{-0.0019}$	–	$0.0162^{+0.0045}_{-0.0024}$	–	$0.0361^{+0.0127}_{-0.0068}$	–	$0.0191^{+0.0035}_{-0.0019}$	–
$30 < r < 200\,\mathrm{Mpc}\,h^{-1}$	$1.26^{+0.24}_{-0.19}$	$-0.01^{+0.03}_{-0.04}$	$1.61^{+0.40}_{-0.22}$	$-0.01^{+0.05}_{-0.08}$	$3.60^{+1.08}_{-0.63}$	$-0.01^{+0.16}_{-0.24}$	$1.89^{+0.36}_{-0.20}$	$-0.01^{+0.03}_{-0.03}$
Two−term $A_\ell(r)$	$1.27^{+0.25}_{-0.19}$	$0.02^{+0.02}_{-0.04}$	$1.54^{+0.33}_{-0.21}$	$-0.07^{+0.06}_{-0.13}$	$3.51^{+0.97}_{-0.62}$	$-0.09^{+0.16}_{-0.35}$	$1.82^{+0.29}_{-0.20}$	$-0.07^{+0.04}_{-0.07}$
Four−term $A_\ell(r)$	$1.27^{+0.33}_{-0.21}$	$-2\mathrm{e}{-3}^{+0.05}_{-0.02}$	$1.67^{+0.52}_{-0.27}$	$0.03^{+0.13}_{-0.05}$	$3.67^{+1.52}_{-0.73}$	$0.03^{+0.33}_{-0.13}$	$1.94^{+0.36}_{-0.20}$	$0.03^{+0.04}_{-0.03}$
$\Sigma_\parallel = 4$ & $\Sigma_\perp = 2$	$1.27^{+0.28}_{-0.20}$	$3\mathrm{e}{-3}^{+0.02}_{-0.01}$	$1.63^{+0.45}_{-0.24}$	$0.01^{+0.02}_{-0.02}$	$3.67^{+1.30}_{-0.68}$	$0.07^{+0.06}_{-0.05}$	$1.87^{+0.35}_{-0.20}$	$-0.03^{+0.02}_{-0.02}$
$\Sigma_s \to 3.0\,\mathrm{Mpc}\,h^{-1}$	$1.29^{+0.27}_{-0.20}$	$0.02^{+0.02}_{-0.01}$	$1.69^{+0.46}_{-0.24}$	$0.07^{+0.04}_{-0.03}$	$3.83^{+1.28}_{-0.70}$	$0.21^{+0.10}_{-0.08}$	$1.92^{+0.34}_{-0.20}$	$0.02^{+0.02}_{-0.02}$
No priors	$3.02^{+4.33}_{-1.58}$	$1.69^{+4.25}_{-1.40}$	$3.63^{+5.69}_{-1.86}$	$2.03^{+5.15}_{-1.70}$	$9.68^{+15.99}_{-5.75}$	$6.06^{+14.76}_{-5.21}$	$2.24^{+0.94}_{-0.37}$	$0.30^{+0.71}_{-0.17}$
Only $\log(B_0^2)$ prior	$1.71^{+2.30}_{-0.51}$	$0.40^{+2.05}_{-0.33}$	$2.22^{+3.08}_{-0.72}$	$0.55^{+2.60}_{-0.48}$	$5.25^{+9.29}_{-2.19}$	$1.57^{+7.67}_{-1.54}$	$2.09^{+0.54}_{-0.28}$	$0.16^{+0.27}_{-0.09}$
Only β prior	$2.53^{+3.87}_{-1.24}$	$1.19^{+3.79}_{-1.05}$	$3.18^{+4.98}_{-1.52}$	$1.48^{+4.54}_{-1.29}$	$8.33^{+14.16}_{-4.47}$	$4.60^{+12.88}_{-3.95}$	$2.05^{+0.78}_{-0.29}$	$0.07^{+0.52}_{-0.06}$
$P_{\rm pt}(k)$ floating β	$1.26^{+0.27}_{-0.20}$	$-0.01^{+0.01}_{-0.01}$	$1.57^{+0.46}_{-0.24}$	$-0.05^{+0.02}_{-0.02}$	$3.49^{+1.33}_{-0.68}$	$-0.11^{+0.06}_{-0.05}$	$1.88^{+0.35}_{-0.19}$	$-0.03^{+0.02}_{-0.01}$
$P_{\rm pt}(k)$ $\beta = 0.0$	$1.22^{+0.24}_{-0.19}$	$-0.03^{+0.01}_{-0.04}$	$1.52^{+0.38}_{-0.21}$	$-0.09^{+0.04}_{-0.10}$	$3.38^{+0.94}_{-0.56}$	$-0.21^{+0.14}_{-0.34}$	$1.86^{+0.33}_{-0.19}$	$-0.05^{+0.04}_{-0.04}$
FoG model → exp	$1.26^{+0.27}_{-0.19}$	$-3\mathrm{e}{-3}^{+2\mathrm{e}-3}_{-3\mathrm{e}-3}$	$1.61^{+0.45}_{-0.24}$	$-0.01^{+0.01}_{-0.01}$	$3.58^{+1.29}_{-0.67}$	$-0.03^{+0.02}_{-0.01}$	$1.90^{+0.35}_{-0.19}$	$-3\mathrm{e}{-3}^{+3\mathrm{e}-3}_{-3\mathrm{e}-3}$
FoG model → Gauss	$1.26^{+0.28}_{-0.19}$	$1\mathrm{e}{-4}^{+1\mathrm{e}-4}_{-1\mathrm{e}-4}$	$1.62^{+0.45}_{-0.24}$	$2\mathrm{e}{-4}^{+3\mathrm{e}-4}_{-4\mathrm{e}-4}$	$3.61^{+1.26}_{-0.68}$	$1\mathrm{e}{-3}^{+1\mathrm{e}-3}_{-1\mathrm{e}-3}$	$1.91^{+0.35}_{-0.19}$	$<1\mathrm{e}{-4}^{+1\mathrm{e}-4}_{-2\mathrm{e}-4}$

variation $\Delta\sigma_\alpha = 0.001$ in DR11 that is not observed in DR10: using 4 Mpc h^{-1} bins and using second-order polynomials. Also a $\Delta\sigma_\alpha = 0.001$ is observed in DR10 when using RPT templates with fixed β that is not reproduced in DR11. For σ_ϵ, there are three cases showing a 0.001 difference in DR10 that is not observed in DR11: large fitting range, two-order polynomials and RPT templates with fixed β. Post-reconstruction, we observe $\Delta\sigma_\alpha$, $\Delta\sigma_\epsilon = 0.001$ when using the RPT template with floating β in DR11 that is not observed in DR10 and vice-versa, we observe a $\Delta\sigma_\epsilon = 0.001$ in DR10 that is not observed in DR11 when using 2-order polynomials.

This paper has been typeset from a TEX/LATEX file prepared by the author.